

Superradiance and its implementation in cold atoms inside a hollow-core waveguide

by

Zhengkao Ding

A thesis
presented to the University of Waterloo
in fulfillment of the
thesis requirement for the degree of
Masters of Science
in
Physics (Quantum Information)

Waterloo, Ontario, Canada, 2019

© Zhengkao Ding 2019

I hereby declare that I am the sole author of this thesis. This is a true copy of the thesis, including any required final revisions, as accepted by my examiners.

I understand that my thesis may be made electronically available to the public.

Abstract

In this thesis, I am intending to understand the cooperative effect of an ensemble of quantum emitters, which constitutes the preliminary elements of our current experimental investigations towards realization of an ultra-narrow linewidth superradiant laser ¹. In the first part of the thesis, I investigate the basics of the theory of superradiance (SR), which includes the full derivation of the Hamiltonian and the Lindblad equation for an ensemble of two-level atoms in both free-space and a single-mode waveguide. In addition, I construct the simulations for observing the transition from single-atom uncorrelated spontaneous emission to superradiance in various physical settings, as well as a simulation for the understanding of the cooperative effects of an ensemble of two-level atoms inside an optical cavity. Then, in the second part of the thesis, I introduce the experimental progress we have been making to observe SR with an ensemble of laser-cooled Cs atoms inside a hollow-core photonic crystal fiber (HCPCF). In our experiment, the Cs atoms, initially cooled using a magneto-optical trap (MOT), are guided and confined inside a short piece of HCPCF with a magic-wavelength dipole trap. Currently we have successfully implemented a novel detection methods for studying superradiance.

¹This work has been supported by Industry Canada, NSERC Discovery grant, Ontario's Early Researcher Award, and by Transformative Quantum Technologies (TQT).

Acknowledgements

First, I would like to thank Prof. Michal Bajcsy for providing me with the opportunity of doing my Masters studies at the Institute for Quantum Computing (IQC) at the University of Waterloo. Also, I would like to express my sincere gratitude towards Prof. Martin Houde from University of Western Ontario and Dr. Laurin Ostermann from University of Innsbruck, who unselfishly and patiently provided me with their guidance and help for the theory part of my thesis work over many Friday visits and Skype calls. In addition, I would like to thank Dr. Fereshteh Rajabi for her help on my understanding of the theory of superradiance, as well as Dr. Taehyun Yoon for the experimental support and Jeremy Flannery, Rubayet Al Maruf, Sheng-Xiang Lin, Cameron Vickers, Supratik Sarkar, Vinodh Raj Rajagopal Muthu, Jackson Qiu, Behrooz Semnani, Jinjin Du, Wenfang Li, Sreesh Venuturumilli, Brian Duong, Paul Anderson and the rest of the IQC members for all the inspiring conversations and the emotional support. My gratitudes are also due to my roommates, Brendan Bramman and Noah Greenberg, and our cat Willow, with whom I made some of my most treasured memories in Canada. I would also like to acknowledge all the help and support from Steve Weiss and his team, as well as Prof. Gabe Spalding from Illinois Wesleyan University, my undergraduate honors thesis advisor. Steve and Gabe are like my second fathers to me, and will always be there for me during the good and bad times. During my Masters studies, I spent an amazing summer at the University of Vienna in Austria as a visiting student. I would like to express my gratitudes towards Dr. Nikolai Kiesel and Prof. Markus Aspelmeyer for this amazing opportunity and for their help and guidance, as well as Markus Rademacher, Dr. Maxime Debiossac, Dr. Mario Ciampini, Stefan Lindner, David Grass, Tobias Wenzl and Patrick Fraser for helping me with research and life in Vienna. Last but not least, I would like to thank all of my friends across the world, and most importantly, my family, who provided me with support from the other side of the earth. I could not be who I am without them.

Dedication

I would like to dedicate this thesis to all my hard days at the University of Waterloo.

Table of Contents

List of Figures	ix
1 Introduction	1
1.1 An introduction to the study of superradiance	1
1.2 A brief introduction to quantum dynamics and open quantum system	4
1.2.1 Heisenberg's picture vs Schrödinger's picture	4
1.2.2 Von Neumann equation	5
1.2.3 the quantum Master equation	6
1.3 Atoms inside an optical cavity	7
1.3.1 A cavity with no atoms	7
1.3.2 A single atom inside a cavity	8
2 Single atom spontaneous emission	11
2.1 Rate equation model	11
2.1.1 Stimulated absorption (absorption)	12
2.1.2 Stimulated emission	13
2.1.3 Spontaneous emission	13
2.1.4 Rate equation model	15
2.2 The Weisskopf-Wigner theory	16

3	Theory of Superradiance	20
3.1	Two-level atoms in a 1-D lattice in free space	20
3.1.1	Deriving the Lindblad equation for superradiance	20
3.1.2	Dissipative coupling and coherent energy exchange	30
3.2	Simulation: Two-level atoms in a 1-D lattice	34
3.2.1	Two-level atoms in free space	34
3.2.2	Two-level atoms in an ideal single-mode fiber	37
3.2.3	Two-level atoms in a leaky single-mode fiber	40
3.3	Two atom cooperative emissions	42
3.4	Simulation: Three-level atoms in a 1-D lattice	49
3.4.1	Three-level atoms in free space	49
3.4.2	Three-level atoms in an ideal single-mode fiber	52
3.4.3	Three-level atoms in a leaky single-mode fiber	54
4	Superradiant laser	57
4.1	A quick introduction to lasers	57
4.2	Introduction to steady-state superradiant lasers	59
4.3	A simple superradiant laser simulation	60
5	Experiment: Observation of spontaneous Raman emission in cold atoms inside a hollow-core waveguide	63
5.1	Introduction	63
5.2	Experimental setup	65
5.3	Experimental procedure	68
5.4	Experimental results	69
6	Conclusion	73
	References	75

APPENDICES	79
A Julia codes for the simulations	80
A.1 Two-level atoms in a 1-D lattice	80
A.1.1 Two-level atoms in a 1-D lattice in free space in the Lamb-Dicke regime	80
A.1.2 Two-level atoms in a 1-D lattice in free space in the extended ensemble regime	82
A.1.3 Two-level atoms in a 1-D lattice in an ideal single-mode fiber	83
A.1.4 Two-level atoms in a 1-D lattice in a leaky single-mode fiber	85
A.2 Three-level atoms in a 1-D lattice	87
A.2.1 Three-level atoms in a 1-D lattice in free space	87
A.2.2 Three-level atoms in a 1-D lattice in an ideal single-mode fiber	89
A.2.3 Three-level atoms in a 1-D lattice in a leaky single-mode fiber	91
A.3 Superradiant laser simulation	92
B AOM setup	95
B.1 AOM principle	95
B.2 AOM driver	96
B.3 AOM testing	97
C 935 nm laser setup	98
D PID circuit design	99

List of Figures

1.1	Superradiance	1
1.2	A graphic illustration of open quantum systems. Ω is the coherent energy exchange rate and Γ is the dissipative coupling rate.	6
1.3	A graphic illustration of cavity quantum electrodynamics.	9
2.1	Stimulated absorption for a single atom	12
2.2	Stimulated emission for a single atom	13
2.3	Spontaneous emission for a single atom	13
2.4	Uncorrelated spontaneous emission for an ensemble of atoms. (a). the normalized intensity of light from the ensemble as a function of time; (b). the population of atoms in their ground state, normalized by the total number of atoms.	14
2.5	Understanding the angles and the dot product	19
3.1	Energy exchange between the atom ensemble and the vacuum mode. The atom-atom interaction is mediated by the common mode with which they are interacting.	29
3.2	Energy exchange between the atom ensemble and the vacuum mode.	32
3.3	Energy exchange between the atom ensemble and the fiber mode	33
3.4	Couplings of two-level atoms in free space	34
3.5	Cooperative emission for 1-D atom lattice in free space in the Lamb-Dicke regime.	36
3.6	Cooperative emission for 1-D 5-atom lattice in free space in the extended ensemble regime	37

3.7	Couplings of two-level atoms in an ideal single-mode fiber	38
3.8	Cooperative emission for a 1-D atom lattice in a single-mode fiber in the Lamb-Dicke regime	39
3.9	Cooperative emission for a 1-D 4-atom lattice in a single-mode fiber in the extended ensemble regime	40
3.10	Couplings of two-level atoms in a leaky single-mode fiber	40
3.11	Cooperative emission for a 1-D 4 2-level atom lattice in a leaky single-mode fiber in the extended ensemble regime	42
3.12	Eigenstates and their corresponding energy eigenvalues for a two-atom en- semble	45
3.13	Transitions in a two-atom cooperative emission system	48
3.14	Variations of the transition paths with different atom separations. The thickness of the arrows indicates the transition strengths.	49
3.15	Couplings of three-level atoms in free space	50
3.16	Raman scheme for implementing superradiance as an effective two-level system	50
3.17	Cooperative emission for a 1-D three 3-level atom lattice in free space in the extended ensemble regime	52
3.18	Couplings of three level atoms in an ideal single-mode fiber	53
3.19	Cooperative emission for a 1-D 3 3-level atom lattice in an ideal fiber in the extended ensemble regime	54
3.20	Couplings of three-level atoms in a leaky single-mode fiber	54
3.21	Cooperative emission for a 1-D 3 3-level atom lattice in a leaky fiber in the extended ensemble regime	56
4.1	Principle of a laser	57
4.2	The diagram of a normal laser	59
4.3	The diagram of a superradiant laser	60
4.4	Steady state superradiant laser linewidth change with population	62
5.1	Spontaneous Raman emission in cold atoms inside a hollow-core photonic crystal fiber	63

5.2	(a) Schematics of Raman transition in a Λ -type three level system and the corresponding effective two level system. (b) The normalized intensity of the emitted light and (c) the atomic population in the ground state as a function of time for an exponential decay in a two level system.	64
5.3	(a) The glass cell containing the MOT and the hollow-core fiber and a detail of the fiber mounting structure. (b) Schematic of the overall experimental setup. (c) Microscope image of the cross section of the hollow-core fiber. (d) Absorption image of the atomic cloud right after polarization gradient cooling. The fiber tip can be seen at the bottom. (e) Time sequence of our experimental procedure. This figure is from ref.[45]	66
5.4	Connections between the controll and the experimental apparatus	67
5.5	(a) Schematics of the experiment with an inset showing a microscope image of the cross section of the hollow-core fiber. (b) Time sequence of the experimental procedure. (c) Diagram of the cesium energy levels involved in detection of atoms. (d) Histograms of the probe photon counts with and without atoms inside the fiber. The figure is from Fig.2 of ref.[46].	68
5.6	(a) Measured data on the ground state population versus the pump duration. The dashed line is a fit of Eq.5.2 with Γ_R as the fitting parameter found to be $2\pi \times 18.4$ kHz. The inset shows the counts of the transmitted probe photons vs. time during the measurement process. The colored markers indicate the atom numbers that are derived from each shape- and color-matched plot in the inset. The decay rates, Γ_R , obtained from the fits at (b) different pump powers and (c) different pump detunings. Solid lines in (b) and (c) are fits of Eq.5.4 , with Γ_{sg} and the atoms' distribution factor μ being the fitting parameters. This figure is from Fig.3 of ref.[46].	70
B.1	AOM principle	95
B.2	AOM driver structure	96
B.3	AOM efficiency testing optical layout	97
B.4	AOM efficiency test result	97
C.1	935 nm laser optical scheme	98
D.1	PID conceptual diagram	99
D.2	PID circuit design layout	100

Chapter 1

Introduction

1.1 An introduction to the study of superradiance

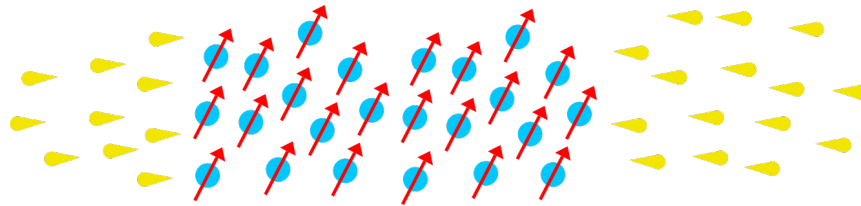


Figure 1.1: Superradiance

In 1905, Einstein was the first to propose a quantum theory of light [8]. Then in 1916, he introduced the elementary light-matter interaction processes, namely absorption, stimulated emission and spontaneous emission [10]. [9]. In his paper, Einstein quantitatively analyzed all three processes using the rate equation model, but he did not provide a full explanation for the mechanism of spontaneous emission, as it could not be completely understood using classical electrodynamics. The work was completed by Paul Dirac [7], as well as Weisskopf and Wigner [43] [44] in the 1920s and 30s with the development of quantum electrodynamics. They proposed that an excited atom in free space would couple to the modes generated by the vacuum fluctuation and make the transition to the ground state whilst emitting a photon of random polarization and direction. This later became known as the Weisskopf-Wigner theory.

However, Robert Dicke proposed in 1954 [6] that the radiation pattern of atoms would

change if there are more than one atom in free space interacting with the same mode of field. He argued that this interaction will result in correlation between the atom dipole moments, which would create a macroscopic atomic polarization [3]. For maximum polarization, the macroscopic dipole moment would be proportional to the number of atoms in the ensemble. As a result, the peak intensity of the radiation will be proportional to the population squared. This is known as superradiance, as proposed in the paper, which is one of the phenomena of cooperative emission processes. In general, when atoms in an ensemble are interacting with a common field, the radiation from them would either constructively or destructively interfere with each other, resulting in superradiance or subradiance, respectively. However, in the first model proposed in Dicke's paper, the atoms are packed into an ensemble with a size much smaller than the wavelength of the radiation [6]. This was later known as the Lamb-Dicke regime, which is an ideal theoretical scenario. Since the 1954 paper, superradiance had been under intense theoretical studies. For example, a full treatment of an extended, optically thick ensemble was proposed by MacGillivray and Feld in 1976 [24], and a full understanding of the collective Lamb-shift in single-photon superradiance was proposed by Scully in 2009 [39].

In 1973, a pioneer work by Skribanowitz *et al* at the MIT spectroscopy laboratory turned superradiance from a theoretical fantasy to an experimental observation [40] [3]. They have observed the superradiant signal in an optically-pumped HF gas and the ringing signal, which is a signature of superradiance in an extended ensemble. Then, a trail of experimental observations follow: Gross *et al* [19] observed near-infrared superradiance in cascading transitions in atomic sodium in 1976; Gibbs *et al* [16] observed single-pulse superradiance in caesium in 1977; Flusberg *et al* [14] observed superradiance at $1.3\mu\text{m}$ in atomic thallium vapour in 1976; Carlson *et al* [5] observed triggered superradiance in caesium in 1980, and Moi *et al* [18] observed superradiance in Rydberg atom for the first time in 1983. Later on, superradiance was also observed in solid-state systems. For example, Schmid and colleagues did a series of experiments in KCl crystals to observe superradiance in the 1980s [12] [13] [35] [36] [37]. Furthermore, the transition from superradiance to amplified spontaneous emission was observed in a KCl crystal by Malcuit *et al* in 1987 [26]. In more recent years, superradiance was first realized in quantum dot systems by Scheibner *et al* in 2007 [34], and then in atoms trapped along a photonic crystal waveguide by Kimble's group in 2015 [17]. Superradiance collective Lamb shift was also observed by Röhlsberger *et al* in 2018 in resonant Fe nuclei excited with synchrotron radiation [32]. In 2016, as part of the effort of building a superradiant laser, Thompson's group at the University of Colorado, Boulder realized superradiance on the millihertz linewidth strontium clock transition [28].

Over the years there have been many comprehensive reviews on the study of superradi-

ance. There is the famous one by Gross and Haroche in 1982 [20], which serves almost as a textbook material for researchers interested in studying superradiance. Also, there is a review on collective nonclassical effects in two-atom systems by Ficek and Tanas in 2002 [11], which I have used for my two-atom superradiance section in my thesis. For a comprehensive summary of both the theory and the experimental work, there is a review written by Andreev *et al* in 1980 [2], and a nice book by Benedict *et al* [3] in 1996 that I have used for the introduction part of the thesis and the literature review. Last but not least, there is a short summary of superradiance by Scully and Svidzinsky in 2009 [38] discussing the properties of superradiance that I found very inspiring.

Initially, we started focusing on superradiance and its realization in cold Cs atoms inside a hollow-core waveguide because we were interested in realizing a steady-state superradiant laser, which was first proposed by Haake *et al* [21] in the 90s and more recently by Meiser *et al* in 2009 [27]. Also, there are some intriguing discussions and simulations for superradiant laser by Maier *et al* [25], from which I built my superradiant laser simulation in this thesis. It was first realized in experiment in Thompson's group at the University of Colorado, Boulder in 2012 [4]. In our experiments, we have developed a novel detection scheme for studying Raman superradiance and the result has been submitted to Optics Express in February, 2019. I was mainly in charge of data analysis for the project. In an effort to understand Superradiance and study the experimental signature of cooperative emission for our experimental setup and detection scheme, I have re-derived the superradiance Hamiltonian in full detail and set up simulations for free-space superradiance and superradiance in a single-mode fiber. I also have done studies on the properties of superradiant lasers and built a simple simulation on understanding the effect cooperative emission has on the linewidth of superradiant lasers.

In this thesis, the first chapter will be a brief introduction to some of the physics principles and formalisms we will be using in the thesis, including the Heisenberg equation of motion, the Von Neumann equation, the master equation and the Jaynes-Cummings Hamiltonian. In the second chapter, I would introduce the rate equation model proposed by Einstein and the Weisskopf-Wigner theory for calculating the single-atom spontaneous emission rate in free space. The third chapter would contain a full derivation of the Lindblad equation for free-space superradiance, simulations for two-level and three-level atom superradiance in both free space and a single-mode fiber, and a fully worked-out two-atom cooperative emission study. The fourth chapter would be a brief discussion on superradiant lasers, with a simple superradiant laser simulation, and the fifth chapter would be about the experiment we have performed in an effort of observing superradiance in cold atoms in a hollow-core waveguide.

1.2 A brief introduction to quantum dynamics and open quantum system

In this section, I will give a brief overview of quantum dynamics and the master equation, as we will be using them for later discussions on the theory of superradiance. Most of the materials presented here are intended to be a quick introduction instead of a exhaustive discussion. For more information on this subject, please check ref.[33], which was used as the main reference for this section.

1.2.1 Heisenberg's picture vs Schrödinger's picture

The dynamics of quantum systems are described using the time evolution operator,

$$\mathcal{U}(t) = e^{-\frac{iHt}{\hbar}}, \quad (1.1)$$

and it could be used to time-evolve both operators and state vectors. The evolution does not change the result of the inner products of the state vectors. To illustrate, assuming we are evolving a state vector $|\psi\rangle$, according to eq.1.1, we have

$$\begin{aligned} |\psi(t)\rangle &= \mathcal{U}(t)|\psi(0)\rangle \\ &= e^{-\frac{iHt}{\hbar}}|\psi(0)\rangle. \end{aligned} \quad (1.2)$$

Also, when we are time-evolving an observable A , we have

$$\begin{aligned} A(t) &= \mathcal{U}^\dagger A \mathcal{U} \\ &= e^{\frac{iHt}{\hbar}} A(0) e^{-\frac{iHt}{\hbar}}. \end{aligned} \quad (1.3)$$

We can demonstrate the time-invariance of the inner product between two state vectors: $|\psi\rangle$ and $|\phi\rangle$:

$$\begin{aligned} \langle\phi(t)|\psi(t)\rangle &= \langle\phi(0)|e^{\frac{iHt}{\hbar}} e^{-\frac{iHt}{\hbar}}|\psi(0)\rangle \\ &= \langle\phi(0)|\psi(0)\rangle. \end{aligned} \quad (1.4)$$

When we are calculating the expectation value of a given operator A :

$$\begin{aligned}\langle\psi(0)|A(t)|\psi(0)\rangle &= \langle\psi(0)|e^{\frac{iHt}{\hbar}}A(0)e^{-\frac{iHt}{\hbar}}|\psi(0)\rangle \\ &= \langle\psi(t)|A(0)|\psi(t)\rangle,\end{aligned}\tag{1.5}$$

Here, the mathematics provides us with two possible explanations. First, we can assume that the state vectors are time dependent and the operator is invariant, which gives us the Schrödinger's picture. More strictly speaking, this is a special version of Schrödinger's picture. In the more general definition for it, the operators could be time-variant as well. However, for our later calculations, we adopt the special version. The equation of motion describing the dynamics of the state vector is given by the Schroedinger equation,

$$i\hbar\frac{d|\psi(t)\rangle}{dt} = H|\psi(t)\rangle.\tag{1.6}$$

On the other hand, if we assume that the operator is time-dependent and the state vector is constant, we would arrive at the Heisenberg picture. The dynamics of the operator is determined by the Heisenberg equation of motion,

$$\begin{aligned}\frac{dA(t)}{dt} &= \frac{d}{dt}(\mathcal{U}^\dagger A(0)\mathcal{U}) \\ &= \frac{d}{dt}(e^{\frac{iHt}{\hbar}}A(0)e^{-\frac{iHt}{\hbar}}) \\ &= \partial_t(e^{\frac{iHt}{\hbar}})A(0)e^{-\frac{iHt}{\hbar}} + e^{\frac{iHt}{\hbar}}A(0)\partial_t e^{-\frac{iHt}{\hbar}} \\ &= -\frac{1}{i\hbar}[A, e^{\frac{iHt}{\hbar}}He^{-\frac{iHt}{\hbar}}] \\ &= -\frac{1}{i\hbar}[A, H].\end{aligned}\tag{1.7}$$

Both pictures are used in the discussion of the theory of superradiance. The Heisenberg picture is used for part of the derivation of the free space superradiance Hamiltonian, and the Schroedinger picture is mainly used for understanding the dynamics of two-atom superradiance.

1.2.2 Von Neumann equation

Here we introduce the density matrix formalism, which is an alternative and more general way of describing the evolution of quantum system. A density matrix of a given quantum state $|\psi\rangle$ is

$$\rho = |\psi\rangle\langle\psi|\tag{1.8}$$

Using the Schroedinger equation of motion, the time evolution of $\rho(t)$ is given by

$$\begin{aligned}
 \partial_t \rho(t) &= \partial_t (|\psi(t)\rangle\langle\psi(t)|) \\
 &= \partial_t (|\psi(t)\rangle)\langle\psi(t)| + |\psi(t)\rangle\partial_t \langle\psi(t)| \\
 &= \frac{1}{i\hbar} H|\psi\rangle\langle\psi| - \frac{1}{i\hbar} |\psi\rangle\langle\psi|H \\
 &= \frac{1}{i\hbar} [H, \rho],
 \end{aligned} \tag{1.9}$$

which is known as the Von Neumann equation. This equation will be used in the derivation of the free space Superradiance Hamiltonian.

1.2.3 the quantum Master equation

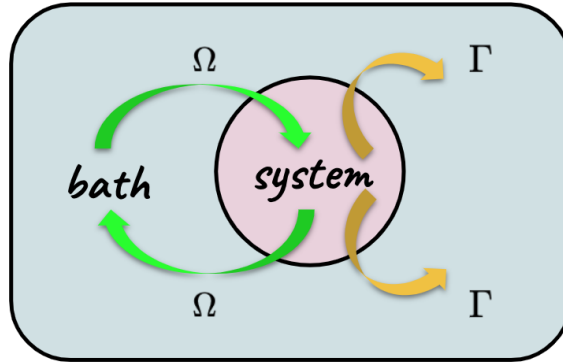


Figure 1.2: A graphic illustration of open quantum systems. Ω is the coherent energy exchange rate and Γ is the dissipative coupling rate.

One major advantage of the density matrix formalism is that we can use it to describe non-conservative processes, namely open quantum systems. Assume we have a quantum system that is coupled to a bath. If we trace out the bath part of the density matrix and focus on the system, we will get the quantum master equation,

$$\partial_t \rho = \frac{1}{i\hbar} [H, \rho] + \mathcal{L}[\rho] \tag{1.10}$$

where the Liouvillian superoperator $\mathcal{L}[\rho]$ describes the irreversible loss from the system to the bath and the Hamiltonian contains the coherent energy exchange between the system

and the bath. This process is illustrated in Fig.1.2. The Liouvillian usually has the following structure,

$$\mathcal{L}[\rho] = \frac{1}{2} \sum_{i,j} \Gamma_{ij} (2J_i^- \rho J_j^+ - J_i^+ J_j^- \rho - \rho J_i^+ J_j^-) \quad (1.11)$$

A detailed derivation of the master equation will be given in later part of the thesis discussing the superradiance Hamiltonian, which is a more specific case where the atom ensemble is coupled to a photon field bath. This equation will later be used in all the superradiance simulations.

1.3 Atoms inside an optical cavity

In this thesis, I will briefly discuss the prospect of building a superradiant laser, in which cavity-enhanced light-matter interactions will be used for building the simulation. As a result, I am giving a quick introduction to the physics of atoms inside a cavity, which is largely following the introduction part of Haruka Tanji's thesis in ref.[42].

1.3.1 A cavity with no atoms

An empty optical cavity supports light that forms a standing wave inside it, which implies that there is a numerical relationship between the wavelength of the light λ and the length of the cavity L ,

$$L = n \frac{\lambda_n}{2} (n = 1, 2, 3, \dots). \quad (1.12)$$

This implies that the frequencies of the modes inside the cavity is given by

$$f_n = n \frac{c}{2L} \quad (1.13)$$

where c is the speed of light. We define a quantity, the free spectrum range f_{FSR} to describe the frequency gap between two adjacent resonance peaks,

$$f_{FSR} = f_{n+1} - f_n = \frac{c}{2L}, \quad (1.14)$$

which happens to be the frequency at which the photon makes a round trip in the cavity. If we stop pumping the cavity, the loss of the photons inside will be exponential. Thus the power inside the cavity could be described as

$$\frac{dP}{dt} = -\kappa P \quad (1.15)$$

$$P(t) = P_0 e^{-\kappa t} \quad (1.16)$$

where κ is the loss rate of the cavity. The linewidth of the cavity is given by the FWHM of the Fourier transformation of $P(t)$, which would be $\frac{\kappa}{2\pi}$. If we want to calculate the loss rate of atoms in one trip, which is defined to be the total loss of the mirrors \mathcal{L}_t , we will need to multiple the rate of loss κ with the time for the photons to make a round trip inside the cavity $\frac{1}{f_{FSR}}$,

$$\mathcal{L}_t = \frac{\kappa}{f_{FSR}} \quad (1.17)$$

and the frequency of the total loss is defined to be the finesse of the cavity, \mathcal{F}

$$\mathcal{F} = \frac{2\pi}{\mathcal{L}_t}. \quad (1.18)$$

The average round trips a photon makes before leaving the cavity is given as

$$\begin{aligned} \langle N \rangle &= \sum_{N=1}^{\infty} N \mathcal{L}_t (1 - \mathcal{L}_t)^{N-1} \\ &= \sum_{N=1}^{\infty} N \frac{2\pi}{\mathcal{F}} \left(1 - \frac{2\pi}{\mathcal{F}}\right)^{N-1} \\ &= \frac{\frac{2\pi}{\mathcal{F}}}{1 - \frac{2\pi}{\mathcal{F}}} \sum_{N=1}^{\infty} N \left(1 - \frac{2\pi}{\mathcal{F}}\right)^N \\ &= \frac{\frac{2\pi}{\mathcal{F}}}{1 - \frac{2\pi}{\mathcal{F}}} \frac{1 - \frac{2\pi}{\mathcal{F}}}{\left(\frac{2\pi}{\mathcal{F}}\right)^2} \\ &= \frac{\mathcal{F}}{2\pi} \end{aligned} \quad (1.19)$$

1.3.2 A single atom inside a cavity

The dynamics of the cavity changes when we add a single atom inside the cavity. The Hamiltonian of the system is

$$H = H_A + H_F + H_{int} \quad (1.20)$$

where

$$\begin{aligned} H_A &= \hbar\omega_a \sigma^+ \sigma^- \\ H_F &= \hbar\omega_c a^\dagger a \\ H_{int} &= -\vec{d} \cdot \vec{E}. \end{aligned} \quad (1.21)$$

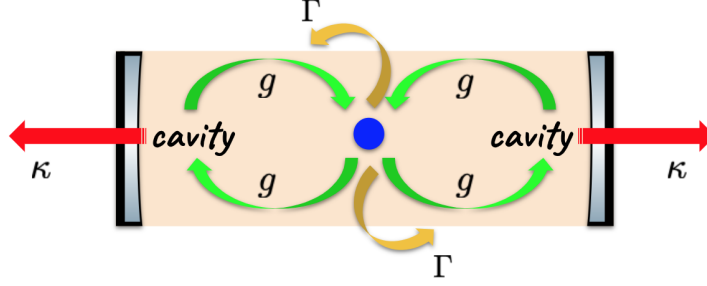


Figure 1.3: A graphic illustration of cavity quantum electrodynamics.

From the second quantization, the electric field could be expressed in terms of the raising and lowering operators as

$$\vec{E} = i\vec{E}_0(ae^{i\vec{k}\cdot\vec{r}} - a^\dagger e^{-i\vec{k}\cdot\vec{r}}) \quad (1.22)$$

where \vec{E}_0 is the electric field corresponding to the zero point energy [42]. The dipole moment term \vec{d} could be expressed as

$$\vec{d} = \vec{\mu}\sigma^+ + \vec{\mu}^\dagger\sigma^-. \quad (1.23)$$

As a result, the interaction Hamiltonian could be written as

$$H_{int} = -\hbar g(\sigma^+ - \sigma^-)(a - a^\dagger) \quad (1.24)$$

where for the field term we have applied the electric dipole approximation to get rid of the phase terms. Also, we defined the field-atom coupling strength $g := i/\hbar\vec{\mu} \cdot \vec{E}_0$. Now, we use the rotating wave approximation (RWA) to drop the fast rotating terms that violate energy conservation [42]. We will have

$$H_{int} = \hbar g(a\sigma^+ + a^\dagger\sigma^-), \quad (1.25)$$

and the entire Hamiltonian is

$$H = \hbar\omega_a\sigma^+\sigma^- + \hbar\omega_c a^\dagger a + \hbar g(a\sigma^+ + a^\dagger\sigma^-) \quad (1.26)$$

which is known as the Jaynes-Cummings Hamiltonian.

There are two major losses of the system, the cavity loss and the spontaneous emission loss. The Liouvillian terms for them can be expressed as

$$\begin{aligned} \mathcal{L}[\rho]_{sp} &= \frac{1}{2}\Gamma(2\sigma^-\rho\sigma^+ - \sigma^+\sigma^-\rho - \rho\sigma^+\sigma^-) \\ \mathcal{L}[\rho]_c &= \frac{1}{2}\kappa(2a\rho a^\dagger - a^\dagger a\rho - \rho a^\dagger a), \end{aligned} \quad (1.27)$$

and the entire atom-field interaction inside a cavity is illustrated in Fig.1.3.

Chapter 2

Single atom spontaneous emission

This chapter will give a short overview of the theories that describe single-atom light-matter interactions, which serves as a stepping stone to the study of superradiance in later chapters. We start with the traditional rate equation model, and then proceed to the full quantum picture, where we will take a closer look at the spontaneous emission process using the Weisskopf-Wigner theory. For more details on this topic, please refer to Daniel Steck's notes on quantum and atom optics [41].

2.1 Rate equation model

The rate equation model was first proposed by Albert Einstein in 1916 [10] [9]. It gives a phenomenological treatment to light-matter interactions. However, it is considered to be a rudimentary semi-classical model of light-matter interactions, as it does not take any coherence effects into consideration.

To start with, we assume that the light field is quantized, namely that given a specific monochromatic field with frequency ω_f can only contain energy

$$E = (n + \frac{1}{2})\hbar\omega_f, \tag{2.1}$$

where n is the number of photons in the field and $\hbar\omega_f$ is the energy of a single photon. Also, the electronic states are quantized as well. For simplicity reason, we assume that there are only two discrete electronic states in the atom: the ground state and the excited

state, with an energy difference of $\hbar\omega_a$ between them:

$$\Delta E = \hbar\omega_a = E_e - E_g. \quad (2.2)$$

Einstein proposed that there are three fundamental interactions between the two-level atoms and the photons: stimulated absorption (absorption), stimulated emission and spontaneous emission. These are the main processes that are responsible for the energy exchange between the external field and the atoms. In this discussion, we will derive the famous Einstein rate equation and find the relationship between the Einstein A and B coefficients. In the process, we assume that the photon field is on resonance with the two-level atoms, so that $\omega_f = \omega_a$.

2.1.1 Stimulated absorption (absorption)

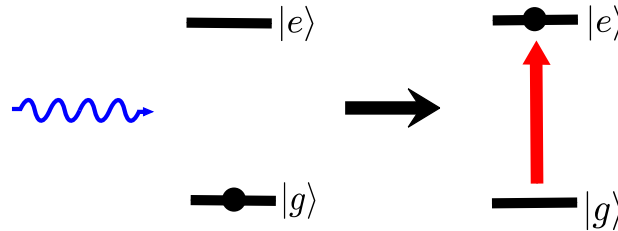


Figure 2.1: Stimulated absorption for a single atom

When two-level atoms in free space with an energy difference of $\hbar\omega$ between their ground and excited states are in their ground state, and they are interacting with incoming photons with energy $\hbar\omega$, they will absorb the photons and go to their excited state. This process is shown in Fig.2.1 The rate of this interaction is proportional to the population on the ground state and the energy density of the resonant field, $\rho(\omega)$. In mathematical language, this can be written as

$$\frac{dN_{e1}}{dt} = B_{ge}\rho(\omega)N_g. \quad (2.3)$$

In the equation, the coefficient B_{ge} is the rate at which population is transferred from the ground to the excited state by the incoming photons. dN_{e1} denotes that this is the population change of the excited state due to the first type of light-matter interaction process introduced above, the stimulated absorption.

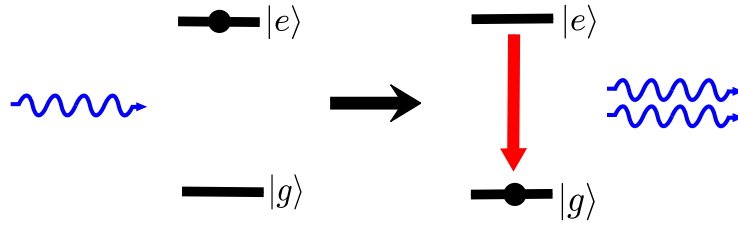


Figure 2.2: Stimulated emission for a single atom

2.1.2 Stimulated emission

Assuming that all the two-level atoms sitting in free space are in their excited states when they are exposed to the incoming resonant photons, the atom in the ensemble will emit a photon that is identical to the incoming photon and go to its ground state. This process is called stimulated emission and is illustrated in Fig.2.2 The emission rate is proportional to the population in the excited state and the energy density of the resonant field. In mathematical language, this can be written as

$$\frac{dN_{e2}}{dt} = -B_{eg}\rho(\omega)N_e, \quad (2.4)$$

in which B_{eg} denotes the rate at which population is transferred from the excited state to the ground state by the external field and dN_{e2} represents the population change in the excited state due to the stimulated emission process.

2.1.3 Spontaneous emission

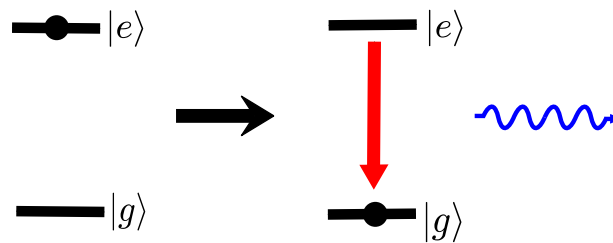


Figure 2.3: Spontaneous emission for a single atom

Besides the light-matter interaction processes mentioned above, Einstein also proposed a

third process, in which an excited atom in free space will spontaneously emit a photon with energy $\hbar\omega$ in a random direction and go to its ground state. The process is visualized in Fig.2.4 The full explanation of this process was proposed after the advent of quantum field theory, and a detailed explanation will be provided in the next section of this thesis. The mathematical expression of this interaction is

$$\frac{dN_{e3}}{dt} = -A_{eg}N_e, \quad (2.5)$$

in which A_{eg} is the rate of spontaneous emission, usually denoted as γ in modern literature. Note that the population change rate is only proportional to the population of the excited state, and it is not correlated with the energy density of a specific monochromatic field. In certain cases, which will be used in our later discussion of free-space superradiance, the photons produced by the ensemble of excited atoms leave immediately, and there will be no further energy exchange between the atoms and the photons. Then essentially only spontaneous emission is taking place, and we can solve eq.2.5 and get the population as a function of time:

$$N_e = N_0 e^{-A_{eg}t}, \quad (2.6)$$

which is an exponential decay. In the equation, N_0 denotes the initial excited population. As we will see in later discussions on superradiance, this describes the case where the emission events in the ensemble are not correlated. We will have a very different emission process if the atoms are cooperatively spontaneously emitting into the same field.

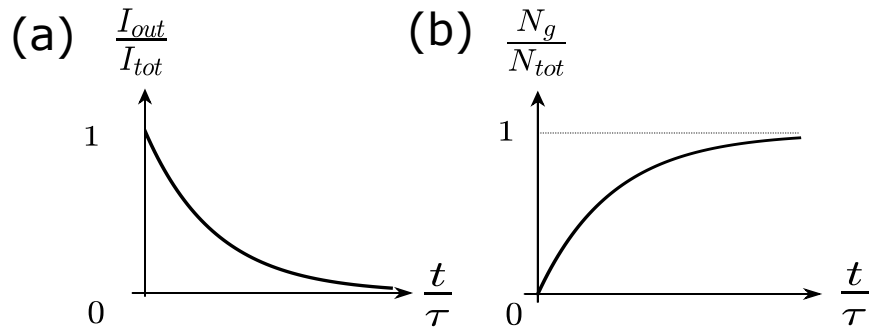


Figure 2.4: Uncorrelated spontaneous emission for an ensemble of atoms. (a). the normalized intensity of light from the ensemble as a function of time; (b). the population of atoms in their ground state, normalized by the total number of atoms.

2.1.4 Rate equation model

When we assume that all three different light-matter interactions are happening in the ensemble, to study the total interaction result, we need to add them all up. Basically, we have

$$\frac{dN_e}{dt} = \frac{dN_{e1}}{dt} + \frac{dN_{e2}}{dt} + \frac{dN_{e3}}{dt}. \quad (2.7)$$

We substitute eq.2.3, eq.2.4 and eq.2.5 into eq.2.7, and get

$$\frac{dN_e}{dt} = -A_{eg}N_e - B_{eg}\rho(\omega)N_e + B_{ge}\rho(\omega)N_g, \quad (2.8)$$

which is the rate equation. The A_{eg} , B_{eg} and B_{ge} are the Einstein A and B coefficients. To find the relationship between them, thereby studying the different interactions, we find the steady-state solution to eq.2.8:

$$\frac{N_e}{N_g} = \frac{B_{eg}\rho(\omega)}{A_{eg} + B_{eg}\rho(\omega)} \quad (2.9)$$

$$\rho(\omega) = \frac{A_{eg}}{B_{eg}} \frac{1}{\frac{B_{ge}N_g}{B_{eg}N_e} - 1} \quad (2.10)$$

Using classical thermodynamics, the population and the energy of the excited and ground state is given by the Boltzmann distribution:

$$\frac{N_e}{N_g} = \frac{g_e e^{-E_e/kT}}{g_g e^{-E_g/kT}} = \frac{g_e}{g_g} e^{-\hbar\omega/kT}, \quad (2.11)$$

in which k is the Boltzmann constant. If we substitute eq.2.11 into eq.2.9, we will have

$$\rho(\omega) = \frac{A_{eg}}{B_{eg}} \frac{1}{\frac{B_{ge}g_g}{B_{eg}g_e} e^{\hbar\omega/kT} - 1}. \quad (2.12)$$

If we compare eq.2.12 with the Planck black body distribution,

$$\rho(\omega) = \frac{8\pi\hbar}{\lambda^3} \frac{1}{e^{\hbar\omega/kT} - 1}, \quad (2.13)$$

we will have the following relationship between the Einstein A and B coefficients,

$$g_g B_{ge} = g_e B_{eg}, \quad (2.14)$$

$$\frac{A_{eg}}{B_{eg}} = \frac{8\pi\hbar}{\lambda^3}. \quad (2.15)$$

If we assume that the degeneracies of the ground and excited states are the same, then we have $B_{eg} = B_{ge}$, which shows that the stimulated emission and stimulated absorption are symmetric processes. However, the rate equation alone would not provide the expressions for the Einstein coefficients. In order to derive the mathematical expression for the single-atom spontaneous emission rate, we need to use the full quantum picture, which treats spontaneous emission as a process where the atom is coupled to the vacuum modes in free space.

2.2 The Weisskopf-Wigner theory

We use Fermi's Golden Rule to derive the spontaneous emission rate of a single atom. In order to do that, first we need to write down the full Hamiltonian of our system, which comprises of a single two-level atom in free space, all the electromagnetic modes available in vacuum, and the atom-field interaction term. The Hamiltonian is shown in eq.2.16.

$$\begin{aligned} H &= H_F + H_A + H_{int} \\ &= \sum_{\vec{k},\lambda} \hbar\omega_{\vec{k}} a_{\vec{k},\lambda}^\dagger a_{\vec{k},\lambda} + \hbar\omega_0 \sigma^\dagger \sigma - \vec{d} \cdot \vec{E}(\vec{r}) \end{aligned} \quad (2.16)$$

In eq.2.16, the interaction Hamiltonian is written in the form of a dipole-field interaction. If we take the second quantization, and express both the field and the atom in terms of raising and lowering operators, we will get

$$H_{int} = i \sum_{\vec{k},\lambda} \hbar g_{\vec{k},\lambda} (a_{\vec{k},\lambda} - a_{\vec{k},\lambda}^\dagger) (\sigma + \sigma^\dagger). \quad (2.17)$$

If we use the rotating wave approximation (RWA), we will get

$$H_{int} = i \sum_{\vec{k},\lambda} \hbar g_{\vec{k},\lambda} (a_{\vec{k},\lambda} \sigma^\dagger - a_{\vec{k},\lambda}^\dagger \sigma), \quad (2.18)$$

where we have

$$g_{\vec{k},\lambda} = \sqrt{\frac{\omega_{\vec{k}}}{2\epsilon_0 V}} \vec{e}_{\vec{k},\lambda} \cdot \vec{\mu}. \quad (2.19)$$

In eq.2.19, $\vec{e}_{\vec{k},\lambda}$ represents the polarization vector for the electromagnetic modes in vacuum, and $\vec{\mu}$ is the dipole matrix element of the two-level atom, e.g. $\vec{\mu} = \langle e|\vec{d}|g\rangle$.

With the final form of the interaction Hamiltonian, we can apply the Fermi's Golden Rule, shown in eq.2.20 to calculate the spontaneous emission rate of a single atom [41]. In the following discussions, we will switch to natural units, where $\hbar = 1$.

$$\Gamma = 2\pi \sum_{\vec{k},\lambda} |\langle f_{\vec{k},\lambda}|H_{int}|i\rangle|^2 \delta(\omega_i - \omega_f) \quad (2.20)$$

In Fermi's Golden Rule, the initial state is the excited atom with n photons in the field, which could be written as $|i\rangle = |g, n+1\rangle$, and the final state is the atom in its ground state with $n+1$ photons in the field, which could be written as $|f_{\vec{k},\lambda}\rangle = |e, n\rangle$ [41]. When we substitute eq.3.4 into eq.2.20, we have

$$\begin{aligned} \Gamma &= 2\pi \sum_{\vec{k},\lambda} |\langle g, n+1|(ig_{\vec{k},\lambda}(a_{\vec{k},\lambda}\sigma^\dagger - a_{\vec{k},\lambda}^\dagger\sigma))|e, n\rangle|^2 \delta(\omega_i - \omega_f) \\ &= 2\pi \sum_{\vec{k},\lambda} |\langle g, n+1|(-ig_{\vec{k},\lambda}a_{\vec{k},\lambda}^\dagger\sigma)|e, n\rangle|^2 \delta(\omega_i - \omega_f) \\ &= -2\pi \sum_{\vec{k},\lambda} g_{\vec{k},\lambda}^2 (n_{\vec{k},\lambda} + 1) \delta(\omega_i - \omega_f). \end{aligned} \quad (2.21)$$

Now, as we have the expression for $g_{\vec{k},\lambda}$ in eq.2.19, we can substitute eq.2.19 into eq.2.21 and get

$$\begin{aligned} \Gamma &= -2\pi \sum_{\vec{k},\lambda} \frac{\omega_k}{2\epsilon_0 V} |\vec{e}_{\vec{k},\lambda} \cdot \vec{\mu}|^2 (n_{\vec{k},\lambda} + 1) \delta(\omega_i - \omega_f) \\ &= -2\pi \sum_{\vec{k},\lambda} \frac{\omega_k}{2\epsilon_0 V} |\vec{e}_{\vec{k},\lambda} \cdot \vec{\mu}|^2 n_{\vec{k},\lambda} \delta(\omega_i - \omega_f) - 2\pi \sum_{\vec{k},\lambda} \frac{\omega_k}{2\epsilon_0 V} |\vec{e}_{\vec{k},\lambda} \cdot \vec{\mu}|^2 \delta(\omega_i - \omega_f). \end{aligned} \quad (2.22)$$

In the first term of the last line of eq.2.22, the decay rate is related to the number of photons in the environment with a specific polarization vector and wavelength. This term correspond to the stimulated emission process, where the second term is the expression for the spontaneous emission process [29].

In order to find an analytical expression for the second term in eq.2.22, first we need to understand the expression in the delta function. $\omega_i - \omega_f$ is related to the energy change of the system during the emission process. The initial energy of the system can be expressed as

$$\begin{aligned} E_i &= \omega_i \\ &= \omega_a + n_{\vec{k},\lambda} \omega_k, \end{aligned} \quad (2.23)$$

where ω_a is the frequency of the atom. The final energy can be written as

$$\begin{aligned} E_f &= \omega_f \\ &= \omega_k (n_{\vec{k},\lambda} + 1). \end{aligned} \quad (2.24)$$

Then the difference of the energy is

$$\begin{aligned} \Delta E &= E_i - E_f \\ &= \omega_i - \omega_f \\ &= \omega_a + n_{\vec{k},\lambda} \omega_k - \omega_k (n_{\vec{k},\lambda} + 1) \\ &= \omega_a - \omega_k. \end{aligned} \quad (2.25)$$

As a result, we have

$$\omega_i - \omega_f = \omega_a - \omega_k \quad (2.26)$$

When we substitute eq.2.26 into eq.2.22, and assume a continuous distribution of all available electromagnetic wave vector \vec{k} in free space by changing the summation into an integration, we will get

$$\begin{aligned} \Gamma &= 2\pi \frac{V}{(2\pi)^3} \int dk^3 \frac{\omega_k}{2\epsilon_0 V} |\vec{e}_{\vec{k},\lambda} \cdot \vec{\mu}|^2 \delta(\omega_a - \omega_k) \\ &= \frac{1}{8\pi^2 \epsilon_0} \int dk k^2 \int d\theta \sin \theta \int d\phi \omega_k |\vec{e}_{\vec{k},\lambda} \cdot \vec{\mu}|^2 \delta(\omega_a - \omega_k) \\ &= \frac{1}{8\pi^2 \epsilon_0 c^3} \int d\omega_k \omega_k^3 \delta(\omega_a - \omega_k) \int d\theta \sin \theta \int d\phi |\vec{e}_{\vec{k},\lambda} \cdot \vec{\mu}|^2 \\ &= \frac{\omega_0^3}{8\pi^2 \epsilon_0 c^3} \int d\theta \sin \theta \int d\phi |\vec{e}_{\vec{k},\lambda} \cdot \vec{\mu}|^2 \\ &= \frac{\omega_0^3}{8\pi^2 \epsilon_0 c^3} \int d\theta \sin \theta \int d\phi \sin^2 \theta \mu^2 \\ &= \frac{\omega_0^3 \mu^2}{8\pi^2 \epsilon_0 c^3} \int d\theta \sin^3 \theta \int d\phi \\ &= \frac{\omega_0^3 \mu^2}{3\pi \epsilon_0 c^3}, \end{aligned} \quad (2.27)$$

which gives us the spontaneous emission rate of a single atom in free space. In the derivation, we integrate over the angle θ , which is the angle between the direction of the atomic dipole moment $\vec{\mu}$ and the wave vector of the field \vec{k} . To calculate the dot product between the polarization vector and the atomic dipole moment, we first need to realize that the polarization vectors lies in the plane that is perpendicular to the wave vector \vec{k} . The plane is spanned by two basis, $\vec{e}_{\vec{k},\lambda}$ and $\vec{e}_{\vec{k},\lambda'}$, that are orthogonal to each other. We have the freedom to choose the orientation of these two vectors as long as the angle between them does not change, so we can rotate them so that one of the vectors, $\vec{e}_{\vec{k},\lambda}$ lies in the plane spanned by \vec{k} and $\vec{\mu}$, and the other one is perpendicular to it. The geometry is shown in Fig.2.5. Then, using simple trigonometry, it is easy to get that $\vec{e}_{\vec{k},\lambda} \cdot \vec{\mu} = \mu \sin \theta$, where μ is the magnitude of the dipole moment $\vec{\mu}$ [29].

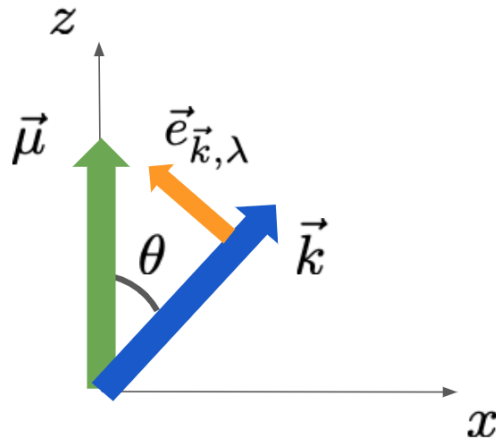


Figure 2.5: Understanding the angles and the dot product

Now, we have a reasonable understanding of single-atom spontaneous emission process. When an excited atom is sitting in free space, it will couple to the modes in vacuum and emit a photon. It could also be seen as that the atom undergoes stimulated emission by a virtual photon generated by random vacuum fluctuations. In later chapters we will see that the emission pattern of an atom will change if there are more emitters in the vicinity that are interacting with the same field.

Chapter 3

Theory of Superradiance

In this chapter, we will look into the spontaneous emission pattern of more than one atom in a lattice. First, we investigate the case for a 1-D ensemble of two level atoms in free space, and then we study in greater detail the super- and subradiance of two atoms, which can provide some intuition and insights for understanding cooperative spontaneous emission. Lastly, we present the simulation result for the three-level atom case, which is eventually what we will use in the actual experiments. All the simulation codes are written using the Julia QuantumOptics package [23], with very valuable help from Dr. Laurin Ostermann and David Plankensteiner at the University of Innsbruck. Most of the mathematical derivations are following Laurin's PhD thesis. I gratefully acknowledge all the valuable guidance from him when I was writing up this chapter.

3.1 Two-level atoms in a 1-D lattice in free space

3.1.1 Deriving the Lindblad equation for superradiance

Assuming we have a 1-D lattice of excited two level atoms in vacuum. The Hamiltonian for the system is

$$H = H_A + H_F + H_{int} \quad (3.1)$$

where we have

$$H_A = \omega_a \sum_{i=1}^N \sigma_i^+ \sigma_i^-, \quad (3.2)$$

$$H_F = \sum_{\vec{k}, \lambda} \omega_k a_{\vec{k}, \lambda}^\dagger a_{\vec{k}, \lambda}, \quad (3.3)$$

$$\begin{aligned} H_{int} &= - \sum_{i=1}^N \vec{d}_i \cdot \vec{E}(\vec{r}_i) \\ &= i \sum_{i=1}^N \sum_{\vec{k}, \lambda} g_{\vec{k}, \lambda} (a_{\vec{k}, \lambda} e^{i\vec{k}\vec{r}_i} - a_{\vec{k}, \lambda}^\dagger e^{-i\vec{k}\vec{r}_i}) (\sigma_i^+ + \sigma_i^-), \end{aligned} \quad (3.4)$$

in which we used the second quantization in eq.3.4. The coupling strength $g_{\vec{k}, \lambda}$ can be expressed as

$$g_{\vec{k}, \lambda} = \sqrt{\frac{\omega_k}{2\epsilon_0 V}} (\vec{e}_{\vec{k}, \lambda} \cdot \vec{\mu}) \quad (3.5)$$

In Heisenberg's picture, the density matrix is a constant in time. In order to analyze the dynamics of the system, we need to perform a substitution here, with $\rho \rightarrow \rho(t) = \rho + \epsilon O(t)$, with ϵ being an arbitrary mathematical constant and $O(t)$ being a random physical observable that is a function of time. As a result, we have

$$\partial_t \rho = i[H, \rho]. \quad (3.6)$$

If we substitute our Hamiltonian into eq.3.6, we will have

$$\begin{aligned} \partial_t \rho &= i[H_A + H_F + H_{int}, \rho] \\ &= i[H_A, \rho] + i[H_F, \rho] + i[H_{int}, \rho], \end{aligned} \quad (3.7)$$

in which we have

$$i[H_A, \rho] = i\omega_a \sum_{i=0}^N [\sigma_i^+ \sigma_i, \rho], \quad (3.8)$$

$$i[H_F, \rho] = i \sum_{\vec{k}, \lambda} \omega_k [a_{\vec{k}, \lambda}^\dagger a_{\vec{k}, \lambda}, \rho], \quad (3.9)$$

$$\begin{aligned} i[H_{int}, \rho] &= - \sum_{\vec{k}, \lambda} \sum_{i=0}^N g_{\vec{k}, \lambda} [(a_{\vec{k}, \lambda} e^{i\vec{k}\vec{r}_i} - a_{\vec{k}, \lambda}^\dagger e^{-i\vec{k}\vec{r}_i}) (\sigma_i^+ + \sigma_i^-), \rho] \\ &= - \sum_{\vec{k}, \lambda} \sum_{i=0}^N g_{\vec{k}, \lambda} ([\sigma_i^+ + \sigma_i^-, \rho] a_{\vec{k}, \lambda} e^{i\vec{k}\vec{r}_i} - a_{\vec{k}, \lambda}^\dagger [\sigma_i^+ + \sigma_i^-, \rho] e^{-i\vec{k}\vec{r}_i}), \end{aligned} \quad (3.10)$$

where in the last step we introduced normal ordering for the ladder operators.

The field operators $a_{\vec{k},\lambda}$ and $a_{\vec{k},\lambda}^\dagger$ are time-dependent and are correlated to atom operators. In order to study the time evolution of the system, we need to find the equation of motion for the field operators. Using Heisenberg's equation of motion, we get

$$\begin{aligned}\partial_t a_{\vec{k},\lambda} &= i[H, a_{\vec{k},\lambda}] \\ &= i[H_A + H_F + H_{int}, a_{\vec{k},\lambda}] \\ &= i[H_A, a_{\vec{k},\lambda}] + i[H_F, a_{\vec{k},\lambda}] + i[H_{int}, a_{\vec{k},\lambda}],\end{aligned}\tag{3.11}$$

where we have

$$\begin{aligned}i[H_A, a_{\vec{k},\lambda}] &= i\omega_a \sum_{i=0}^N [\sigma_i^+ \sigma_i, a_{\vec{k},\lambda}] \\ &= 0\end{aligned}\tag{3.12}$$

$$\begin{aligned}i[H_F, a_{\vec{k},\lambda}] &= i\omega_k [a_{\vec{k},\lambda}^\dagger a_{\vec{k},\lambda}, a_{\vec{k},\lambda}] \\ &= i\omega_k a_{\vec{k},\lambda}\end{aligned}\tag{3.13}$$

$$\begin{aligned}i[H_{int}, a_{\vec{k},\lambda}] &= -\sum_{i=0}^N g_{\vec{k},\lambda} [(a_{\vec{k},\lambda} e^{i\vec{k}\vec{r}_i} - a_{\vec{k},\lambda}^\dagger e^{-i\vec{k}\vec{r}_i})(\sigma_i^+ + \sigma_i^-), a_{\vec{k},\lambda}] \\ &= -\sum_{i=0}^N g_{\vec{k},\lambda} (\sigma_i^+ + \sigma_i^-) e^{-i\vec{k}\vec{r}_i}.\end{aligned}\tag{3.14}$$

Substituting into our equation of motion for the field operator, we have

$$\partial_t a_{\vec{k},\lambda} = i\omega_k a_{\vec{k},\lambda} - \sum_{i=0}^N g_{\vec{k},\lambda} (\sigma_i^+ + \sigma_i^-) e^{-i\vec{k}\vec{r}_i},\tag{3.15}$$

which could be solved using retarded Green function to get [\[29\]](#)

$$a_{\vec{k},\lambda}(t) = a_{\vec{k},\lambda}(t_0) e^{-i\omega_k(t-t_0)} - \sum_{i=0}^N g_{\vec{k},\lambda} \int_{t_0}^t dt' e^{-i\omega_k(t-t_0)} (\sigma_i^+ + \sigma_i^-) e^{-i\vec{k}\vec{r}_i}.\tag{3.16}$$

The raising operator as a function of time $a_{\vec{k},\lambda}^\dagger(t)$ is just the complex conjugate of eq.3.16. Once we obtain the equation of motion of the field operators, we can substitute them into

eq.3.10 and get

$$\begin{aligned}
i[H_{int}, \rho] &= - \sum_{\vec{k}, \lambda} \sum_{i=0}^N g_{\vec{k}, \lambda} \\
&\quad ([\sigma_i^+(t) + \sigma_i^-(t), \rho(t)] e^{i\vec{k}\vec{r}_i} \\
&\quad \cdot (a_{\vec{k}, \lambda}(t_0) e^{-i\omega_k(t-t_0)} - \sum_{j=0}^N g_{\vec{k}, \lambda} \int_{t_0}^t dt' e^{-i\omega_k(t-t')} (\sigma_j^+(t') + \sigma_j^-(t')) e^{-i\vec{k}\vec{r}_j}) \\
&\quad - (a_{\vec{k}, \lambda}^\dagger(t_0) e^{i\omega_k(t-t_0)} - \sum_{j=0}^N g_{\vec{k}, \lambda} \int_{t_0}^t dt' e^{i\omega_k(t-t')} (\sigma_j^+(t') + \sigma_j^-(t')) e^{i\vec{k}\vec{r}_j}) \\
&\quad \cdot [\sigma_i^+(t) + \sigma_i^-(t), \rho(t)] e^{-i\vec{k}\vec{r}_i}) \\
&= - \sum_{\vec{k}, \lambda} \sum_{i=0}^N g_{\vec{k}, \lambda} \\
&\quad \cdot ([\sigma_i^+(t) + \sigma_i^-(t), \rho(t)] a_{\vec{k}, \lambda}(t_0) e^{-i\omega_k(t-t_0) + i\vec{k}\cdot\vec{r}_i} \\
&\quad - a_{\vec{k}, \lambda}^\dagger(t_0) [\sigma_i^+(t) + \sigma_i^-(t), \rho(t)] e^{i\omega_k(t-t_0) - i\vec{k}\cdot\vec{r}_i}) \\
&\quad + \sum_{\vec{k}, \lambda} \sum_{i=0}^N (g_{\vec{k}, \lambda})^2 \\
&\quad \cdot (\sum_{i,j} \int_{t_0}^t dt' e^{-i\omega_k(t-t')} [\sigma_i^+(t) + \sigma_i^-(t), \rho(t)] (\sigma_j^+(t') + \sigma_j^-(t')) e^{i\vec{k}\vec{r}_{ij}} \\
&\quad - \sum_{i,j} \int_{t_0}^t dt' e^{i\omega_k(t-t')} (\sigma_j^+(t') + \sigma_j^-(t')) [\sigma_i^+(t) + \sigma_i^-(t), \rho(t)] e^{-i\vec{k}\vec{r}_{ij}}) \\
&= \mathcal{E}_{int} \\
&\quad + \sum_{\vec{k}, \lambda} \sum_{i=0}^N (g_{\vec{k}, \lambda})^2 \\
&\quad \cdot (\sum_{i,j} \int_{t_0}^t dt' e^{-i\omega_k(t-t')} [\sigma_i^+(t) + \sigma_i^-(t), \rho(t)] (\sigma_j^+(t') + \sigma_j^-(t')) e^{i\vec{k}\vec{r}_{ij}} \\
&\quad - \sum_{i,j} \int_{t_0}^t dt' e^{i\omega_k(t-t')} (\sigma_j^+(t') + \sigma_j^-(t')) [\sigma_i^+(t) + \sigma_i^-(t), \rho(t)] e^{-i\vec{k}\vec{r}_{ij}}),
\end{aligned} \tag{3.17}$$

where $r_{ij} := r_i - r_j$ and

$$\begin{aligned} \mathcal{E}_{int} = & - \sum_{\vec{k}, \lambda} \sum_{i=0}^N g_{\vec{k}, \lambda} \\ & \cdot ([\sigma_i^+(t) + \sigma_i^-(t), \rho(t)] a_{\vec{k}, \lambda}(t_0) e^{-i\omega_k(t-t_0) + i\vec{k} \cdot \vec{r}_i} \\ & - a_{\vec{k}, \lambda}^\dagger(t_0) [\sigma_i^+(t) + \sigma_i^-(t), \rho(t)] e^{i\omega_k(t-t_0) - i\vec{k} \cdot \vec{r}_i}), \end{aligned} \quad (3.18)$$

which describes the atom-photon interaction. Specifically, this term assumes that the field and the atoms have further exchange of energy since photon emission. However, in free space without a cavity, we assume that the photon leaves the ensemble immediately when emitted. As a result, we can discard this part of the interaction term and focus on the atom-atom interactions.

Now, we perform similar operations as we did for the single atom spontaneous emission analysis. Basically we assume that the distributions of \vec{k} and λ are continuous and turn the summations into integrals, namely $\sum_{\vec{k}} \rightarrow V/(2\pi)^2 \int d^3k$ [29]. Also, we substitute the expression for the coupling strength $g_{\vec{k}, \lambda}$ into the equation. Now, we have

$$\begin{aligned} i[H_{int}, \rho] = & \frac{V}{(2\pi)^3} \int d^3k \frac{\omega_k}{2\epsilon_0 V} \sum_{\lambda} |\vec{e}_{\vec{k}, \lambda} \cdot \vec{\mu}|^2 \\ & \cdot \left(\sum_{i,j} \int_{t_0}^t dt' e^{-i\omega_k(t-t')} [\sigma_i^+(t) + \sigma_i^-(t), \rho(t)] (\sigma_j^+(t') + \sigma_j^-(t')) e^{i\vec{k} \cdot \vec{r}_{ij}} \right. \\ & \left. - \sum_{i,j} \int_{t_0}^t dt' e^{i\omega_k(t-t')} (\sigma_j^+(t') + \sigma_j^-(t')) [\sigma_i^+(t) + \sigma_i^-(t), \rho(t)] e^{-i\vec{k} \cdot \vec{r}_{ij}} \right) \end{aligned} \quad (3.19)$$

and from fig.2.5, we can express the dot product $\sum_{\lambda} |\vec{e}_{\vec{k}, \lambda} \cdot \vec{\mu}|^2$ as [29]

$$\sum_{\lambda} |\vec{e}_{\vec{k}, \lambda} \cdot \vec{\mu}|^2 = \mu^2 (1 - (\vec{e}_{\vec{k}} \cdot \vec{e}_{\vec{\mu}})^2), \quad (3.20)$$

so we have

$$\begin{aligned}
i[H_{int}, \rho] &= \frac{V}{(2\pi)^3} \int d^3k \frac{\omega_k}{2\epsilon_0 V} \mu^2 (1 - (\vec{e}_{\vec{k}} \cdot \vec{e}_{\vec{\mu}})^2) \\
&\cdot \left(\sum_{i,j} \int_{t_0}^t dt' e^{-i\omega_k(t-t')} [\sigma_i^+(t) + \sigma_i^-(t), \rho(t)] (\sigma_j^+(t') + \sigma_j^-(t')) e^{i\vec{k}\vec{r}_{ij}} \right. \\
&- \sum_{i,j} \int_{t_0}^t dt' e^{i\omega_k(t-t')} (\sigma_j^+(t') + \sigma_j^-(t')) [\sigma_i^+(t) + \sigma_i^-(t), \rho(t)] e^{-i\vec{k}\vec{r}_{ij}} \Big) \\
&= \frac{\mu^2}{2\epsilon_0 (2\pi c)^3} \int d\omega_k \omega_k^3 \int_{\Omega} d\Omega_k (1 - (\vec{e}_{\vec{k}} \cdot \vec{e}_{\vec{\mu}})^2) \\
&\cdot \left(\sum_{i,j} \int_{t_0}^t dt' e^{-i\omega_k(t-t')} [\sigma_i^+(t) + \sigma_i^-(t), \rho(t)] (\sigma_j^+(t') + \sigma_j^-(t')) e^{i\vec{k}\vec{r}_{ij}} \right. \\
&- \sum_{i,j} \int_{t_0}^t dt' e^{i\omega_k(t-t')} (\sigma_j^+(t') + \sigma_j^-(t')) [\sigma_i^+(t) + \sigma_i^-(t), \rho(t)] e^{-i\vec{k}\vec{r}_{ij}} \Big),
\end{aligned} \tag{3.21}$$

Next, we apply the Markov approximation [29] [15]

$$\sigma_j^+(t') + \sigma_j^-(t') \rightarrow \sigma_j^+(t) e^{i\omega_a(t-t')} + \sigma_j^-(t) e^{-i\omega_a(t-t')}, \tag{3.22}$$

and get

$$\begin{aligned}
i[H_{int}, \rho] &= \frac{\mu^2}{2\epsilon_0 (2\pi c)^3} \int d\omega_k \omega_k^3 \int_{\Omega} d\Omega_k (1 - (\vec{e}_{\vec{k}} \cdot \vec{e}_{\vec{\mu}})^2) \\
&\cdot \left(\sum_{i,j} [\sigma_i^+(t) + \sigma_i^-(t), \rho(t)] e^{i\omega_k \vec{r}_{ij} \cdot \vec{e}_{\vec{k}}} \right. \\
&\cdot (\sigma_j^+(t) \int_{t_0}^t dt' e^{-i(\omega_k + \omega_a)(t-t')} + \sigma_j^-(t) \int_{t_0}^t dt' e^{-i(\omega_k - \omega_a)(t-t')}) \\
&- \sum_{i,j} (\sigma_j^+(t) \int_{t_0}^t dt' e^{i(\omega_k - \omega_a)(t-t')} + \sigma_j^-(t) \int_{t_0}^t dt' e^{i(\omega_k + \omega_a)(t-t')}) \\
&\cdot [\sigma_i^+(t) + \sigma_i^-(t), \rho(t)] e^{-i\omega_k \vec{r}_{ij} \cdot \vec{e}_{\vec{k}}}).
\end{aligned} \tag{3.23}$$

For the time integral in the expression in the last step of eq.3.23, we are re-expressing it as a Cauchy principle value with an additional Dirac delta distribution [29]. As an example, we have

$$\int_{t_0}^t dt' e^{-i(\omega_k + \omega_a)(t-t')} = -i\mathcal{P} \frac{1}{\omega_k + \omega_a} + \pi\delta(\omega_k + \omega_a). \tag{3.24}$$

So our expression for the dynamics of the interaction part of the Hamiltonian becomes

$$\begin{aligned}
i[H_{int}, \rho] &= \frac{\mu^2}{2\epsilon_0(2\pi c)^3} \int d\omega_k \omega_k^3 \int_{\Omega} d\Omega_k (1 - (\vec{e}_{\vec{k}} \cdot \vec{e}_{\vec{\mu}})^2) \\
&\cdot \left(\sum_{i,j} [\sigma_i^+(t) + \sigma_i^-(t), \rho(t)] e^{i\omega_k \vec{r}_{ij} \cdot \vec{e}_{\vec{k}}} \right. \\
&\cdot [\sigma_j^+(t) (-i\mathcal{P} \frac{1}{\omega_k + \omega_a} + \pi\delta(\omega_k + \omega_a)) + \sigma_j^-(t) (-i\mathcal{P} \frac{1}{\omega_k - \omega_a} + \pi\delta(\omega_k - \omega_a))] \\
&- \sum_{i,j} [\sigma_j^+(t) (i\mathcal{P} \frac{1}{\omega_k - \omega_a} + \pi\delta(\omega_k - \omega_a)) + \sigma_j^-(t) (i\mathcal{P} \frac{1}{\omega_k + \omega_a} + \pi\delta(\omega_k + \omega_a))] \\
&\cdot [\sigma_i^+(t) + \sigma_i^-(t), \rho(t)] e^{-i\omega_k \vec{r}_{ij} \cdot \vec{e}_{\vec{k}}}.
\end{aligned} \tag{3.25}$$

Now, if we define a coupling function [29] to be

$$F(kr) := \frac{3}{2} \int_{\Omega} \frac{d\Omega_k}{4\pi} (1 - (\vec{e}_{\vec{k}} \cdot \vec{e}_{\vec{\mu}})^2) e^{i\omega_k \vec{r}_{ij} \cdot \vec{e}_{\vec{k}}}, \tag{3.26}$$

and recall our final expression for the single-atom spontaneous emission rate to be

$$\Gamma = \frac{\omega_0^3 \mu^2}{3\pi\epsilon_0 c^3}, \tag{3.27}$$

then the dynamics of the interaction part of the Hamiltonian will become

$$\begin{aligned}
i[H_{int}, \rho] &= \sum_{i,j} \frac{\Gamma}{k_a^3} \int \frac{dk}{2\pi} k^3 F(kr_{ij}) \cdot [\sigma_i^+(t) + \sigma_i^-(t), \rho(t)] \\
&\cdot [\sigma_j^+(t) (-i\mathcal{P} \frac{1}{k + k_a} + \pi\delta(k + k_a)) + \sigma_j^-(t) (-i\mathcal{P} \frac{1}{k - k_a} + \pi\delta(k - k_a))] \\
&- \sum_{i,j} \frac{\Gamma}{k_a^3} \int \frac{dk}{2\pi} k^3 F(kr_{ij}) \\
&\cdot [\sigma_j^+(t) (i\mathcal{P} \frac{1}{k - k_a} + \pi\delta(k - k_a)) + \sigma_j^-(t) (i\mathcal{P} \frac{1}{k + k_a} + \pi\delta(k + k_a))] \\
&\cdot [\sigma_i^+(t) + \sigma_i^-(t), \rho(t)].
\end{aligned} \tag{3.28}$$

$$\begin{aligned}
i[H_{int}, \rho] &= \sum_{i,j} [\sigma_i^+(t) + \sigma_i^-(t), \rho(t)] \\
&\cdot [\sigma_j^+(t) (-i \frac{\Gamma}{k_a^3} \mathcal{P} \int \frac{dk}{2\pi} \frac{k^3 F(kr_{ij})}{k+k_a}) + \sigma_j^-(t) (-i \frac{\Gamma}{k_a^3} \mathcal{P} \int \frac{dk}{2\pi} \frac{k^3 F(kr_{ij})}{k-k_a} + \Gamma F(k_a r_{ij}))] \\
&- \sum_{i,j} [\sigma_j^+(t) (-i \frac{\Gamma}{k_a^3} \mathcal{P} \int \frac{dk}{2\pi} \frac{k^3 F(kr_{ij})}{k-k_a} + \Gamma F(k_a r_{ij})) \\
&+ \sigma_j^-(t) (-i \frac{\Gamma}{k_a^3} \mathcal{P} \int \frac{dk}{2\pi} \frac{k^3 F(kr_{ij})}{k+k_a})] [\sigma_i^+(t) + \sigma_i^-(t), \rho(t)].
\end{aligned} \tag{3.29}$$

Here, we definite two coupling rates, the dissipative coupling, Γ_{ij} and the coherent energy exchange coupling, Ω_{ij} , and they are expressed as the following [29],

$$\Gamma_{ij} := \Gamma F(k_a r_{ij}). \tag{3.30}$$

$$\Omega_{ij}^\pm := \frac{\Gamma}{k_a^3} \mathcal{P} \int \frac{dk}{2\pi} \frac{k^3 F(kr_{ij})}{k \pm k_a}. \tag{3.31}$$

Now, we can finally clean up our expression a little bit for the dynamics of the interaction part of the Hamiltonian and get

$$\begin{aligned}
i[H_{int}, \rho] &= \sum_{i,j} [\sigma_i^+(t) + \sigma_i^-(t), \rho(t)] [\sigma_j^+(t) (-i\Omega_{ij}^+) + \sigma_j^-(t) (-i\Omega_{ij}^- + \frac{\Gamma_{ij}}{2})] \\
&- \sum_{i,j} [\sigma_j^+(t) (i\Omega_{ij}^- + \frac{\Gamma_{ij}}{2}) + \sigma_j^-(t) (i\Omega_{ij}^+)] [\sigma_i^+(t) + \sigma_i^-(t), \rho(t)].
\end{aligned} \tag{3.32}$$

Then we apply the RWA to drop fast oscillating terms and we have

$$\begin{aligned}
i[H_{int}, \rho] &= \sum_{i,j} [[\sigma_i^-(t), \rho(t)] (-i\Omega_{ij}^+) \sigma_j^+(t) + [\sigma_i^+(t), \rho(t)] (-i\Omega_{ij}^- + \frac{\Gamma_{ij}}{2}) \sigma_j^-(t)] \\
&- \sum_{i,j} [(i\Omega_{ij}^- + \frac{\Gamma_{ij}}{2}) \sigma_j^+(t) [\sigma_i^-(t), \rho(t)] + (i\Omega_{ij}^+) \sigma_j^-(t) [\sigma_i^+(t), \rho(t)]] \\
&= \sum_i [(-i\Omega_{ii}^+) [\sigma_i^-(t) \sigma_i^+(t), \rho(t)] + (-i\Omega_{ii}^-) [\sigma_i^+(t) \sigma_i^-(t), \rho(t)]] \\
&+ \sum_{i \neq j} (-i\Omega_{ij}^+ - i\Omega_{ij}^-) [\sigma_i^+(t) \sigma_j^-(t), \rho(t)] \\
&+ \sum_{i,j} \frac{\Gamma_{ij}}{2} (2\sigma_i^+(t) \rho(t) \sigma_j^-(t) - \sigma_j^+(t) \sigma_i^-(t) \rho(t) - \rho(t) \sigma_i^+(t) \sigma_j^-(t))
\end{aligned} \tag{3.33}$$

We define $\Omega_{ij} = -i\Omega_{ij}^+ - i\Omega_{ij}^-$, and we substitute eq.3.33 into eq.3.6, ignoring the Hamiltonian of the field.

$$\begin{aligned}
\partial_t \rho &= i[H_A + H_F + H_{int}, \rho] \\
&= i[H_A, \rho] + i[H_F, \rho] + i[H_{int}, \rho] \\
&= \sum_i [(-i\Omega_{ii}^+)[\sigma_i^-(t)\sigma_i^+(t), \rho(t)] + (-i\Omega_{ii}^-)[\sigma_i^+(t)\sigma_i^-(t), \rho(t)]] \\
&+ \sum_i i\omega_a[\sigma_i^+(t)\sigma_i^-(t), \rho(t)] + \sum_{i \neq j} i\Omega_{ij}[\sigma_i^+(t)\sigma_j^-(t), \rho(t)] \\
&+ \sum_{i,j} \frac{\Gamma_{ij}}{2}(2\sigma_i^-(t)\rho(t)\sigma_i^+ + j(t) - \sigma_j^+(t)\sigma_i^-(t)\rho(t) - \rho(t)\sigma_i^+(t)\sigma_j^-(t)).
\end{aligned} \tag{3.34}$$

As we will see in the next section, when two atoms are infinitely close to each other, while the dissipative coupling rate approaches the spontaneous decay rate of a single atom, the coherent energy exchange rate goes to infinity, showing a breakdown of our theoretical model, as in real cases molecules will form if we put atoms close enough to each other so that their electronic wavefunctions overlap. As a result, we will discard the Ω_{ii}^+ and Ω_{ii}^- terms. This gives us

$$\begin{aligned}
\partial_t \rho &= \sum_i i\omega_a[\sigma_i^+(t)\sigma_i^-(t), \rho(t)] + \sum_{i \neq j} i\Omega_{ij}[\sigma_i^+(t)\sigma_j^-(t), \rho(t)] \\
&+ \sum_{i,j} \frac{\Gamma_{ij}}{2}(2\sigma_i^-(t)\rho(t)\sigma_j^+(t) - \sigma_j^+(t)\sigma_i^-(t)\rho(t) - \rho(t)\sigma_i^+(t)\sigma_j^-(t)).
\end{aligned} \tag{3.35}$$

Now, we go back to our substitution, where $\rho \rightarrow \rho(t) = \rho + \epsilon O(t)$. We take the limit where $\epsilon \rightarrow 0$, and then we compare this result with the Optical Bloch equation

$$\partial_t \rho = i[H, \rho] + \mathcal{L}[\rho], \tag{3.36}$$

we can extract a new Hamiltonian with the atom coherent dipole-dipole interaction term

$$H = \sum_i i\omega_a \sigma_i^+ \sigma_i^- + \sum_{i \neq j} i\Omega_{ij} \sigma_i^+ \sigma_j^-, \tag{3.37}$$

and the Liouvillian dissipative term

$$\mathcal{L}[\rho] = \sum_{i,j} \frac{\Gamma_{ij}}{2}(2\sigma_i^- \rho \sigma_j^+ - \sigma_j^+ \sigma_i^- \rho - \rho \sigma_i^+ \sigma_j^-). \tag{3.38}$$

The physical intuition of the Hamiltonian and the Liouvillian is quite straightforward. As is illustrated in Fig.3.1, the atom-atom interaction is mediated by a common field. The coherent energy exchange term describes the process where a photon is emitted into the field and is absorbed by another atom. In the end, the field remain the same, but the atoms have exchanged energy. The net effect is a atom-atom interaction. In the end, the total energy in the atomic ensemble is constant, and the coherence is maintained. At the same time, the dissipative coupling refers to an incoherent process where photons are irreversibly emitted into the field by the ensemble and the coherence is reduced. Thus, this term shows up as the Liouvillian dissipative term in the derivation. The first term of the Liouvillian describes a shuffling process, in which atoms with high and low energies are exchanged. The next two terms reduce the population at high energies and the coherence between the atoms in the ensemble.

We will be using the Hamiltonian and the Liouvillian derived in this section for our study on cooperative emission processes in later sections.

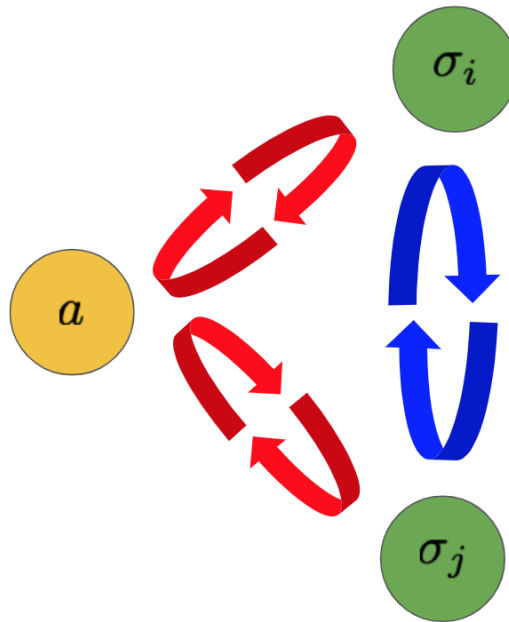


Figure 3.1: Energy exchange between the atom ensemble and the vacuum mode. The atom-atom interaction is mediated by the common mode with which they are interacting.

3.1.2 Dissipative coupling and coherent energy exchange

Free space coupling

We are now deriving the analytical expressions for the dissipative coupling Γ_{ij} and the coherent energy exchange rate Ω_{ij} . From the previous section, we defined them to be

$$\Gamma_{ij} = \Gamma F(k_a r_{ij}), \quad (3.39)$$

$$\Omega_{ij} = -\frac{\Gamma}{k_a^3} \mathcal{P} \int_0^\infty \frac{dk}{2\pi} \left(\frac{k^3 F(kr_{ij})}{k + k_a} + \frac{k^3 F(kr_{ij})}{k - k_a} \right), \quad (3.40)$$

in which we have

$$F(kr) = \frac{3}{2} \int_\Omega \frac{d\Omega_k}{4\pi} (1 - (\vec{e}_{\vec{k}} \cdot \vec{e}_{\vec{\mu}})^2) e^{i\vec{k} \cdot \vec{r}}. \quad (3.41)$$

Now we try to perform the integral

$$\begin{aligned} F(kr) &= \frac{3}{2} \int_\Omega \frac{d\Omega_k}{4\pi} (1 - (\vec{e}_{\vec{k}} \cdot \vec{e}_{\vec{\mu}})^2) e^{i\vec{k} \cdot \vec{r}} \\ &= \frac{3}{8\pi} (1 - (\vec{e}_{\vec{\mu}} \cdot \frac{\nabla_r}{k})^2) \int_\Omega d\Omega_k e^{i\vec{k} \cdot \vec{r}} \\ &= \frac{3}{8\pi} (1 - (\vec{e}_{\vec{\mu}} \cdot \frac{\nabla_r}{k})^2) \int_0^{2\pi} d\phi_k \int_0^\pi d\theta_k \sin \theta_k e^{ikr \cos \theta_k} \\ &= \frac{3}{4} (1 - (\vec{e}_{\vec{\mu}} \cdot \frac{\nabla_r}{k})^2) \int_0^\pi d(\cos \theta_k) e^{ikr(\cos \theta_k)}. \end{aligned} \quad (3.42)$$

The last line shows a Bessel's integral of the first kind [29]

$$J_n(x) = \frac{1}{2\pi} \int_{-\pi}^\pi d\tau e^{i(x \sin \tau - n\tau)}, \quad (3.43)$$

in which $\tau = \cos \theta_k$, $x = kr$ and $n = 0$. The solution to the integral is

$$\int_0^\pi d(\cos \theta_k) e^{ikr \cos \theta_k} = \frac{2 \sin(kr)}{kr}. \quad (3.44)$$

As a result,

$$\begin{aligned} F(kr) &= \frac{3}{2} (1 - (\vec{e}_{\vec{\mu}} \cdot \frac{\nabla_r}{k})^2) \frac{\sin(kr)}{kr} \\ &= \frac{3}{2} \left(\frac{\sin(kr)}{kr} - \frac{1}{k^2} (\vec{e}_{\vec{\mu}} \cdot \nabla_r)^2 \frac{\sin(kr)}{kr} \right). \end{aligned} \quad (3.45)$$

We can rotate the coordinate so that the dipole moment direction aligns with the \hat{z} direction, as is shown in Fig.2.5. Then we have

$$\begin{aligned}
F(kr) &= \frac{3}{2} \left[\frac{\sin(kr)}{kr} - \frac{1}{k^2} (\hat{z} \cdot \nabla_r)^2 \frac{\sin(kr)}{kr} \right] \\
&= \frac{3}{2} \left[\frac{\sin(kr)}{kr} - \frac{1}{k^2} (\hat{z} \cdot \nabla_r) (\hat{z} \cdot \hat{r} \partial_r) \frac{\sin(kr)}{kr} \right] \\
&= \frac{3}{2} \left[\frac{\sin(kr)}{kr} - \frac{1}{k^2} (\hat{z} \cdot \nabla_r) \cos \theta \cdot k \left(\frac{\cos(kr)}{kr} - \frac{\sin(kr)}{(kr)^2} \right) \right] \\
&= \frac{3}{2} \left[\frac{\sin(kr)}{kr} - \frac{1}{k} \hat{z} \cdot (\hat{r} \partial_r + \frac{\hat{\theta}}{r} \partial_\theta) \cos \theta \left(\frac{\cos(kr)}{kr} - \frac{\sin(kr)}{(kr)^2} \right) \right] \\
&= \frac{3}{2} \left[\frac{\sin(kr)}{kr} - \frac{1}{k} (\cos \theta \partial_r - \frac{\sin \theta}{r} \partial_\theta) \cos \theta \left(\frac{\cos(kr)}{kr} - \frac{\sin(kr)}{(kr)^2} \right) \right] \\
&= \frac{3}{2} \left[(1 - \cos^2 \theta) \frac{\sin(kr)}{kr} + (1 - 3 \cos^2 \theta) \left(\frac{\cos(kr)}{(kr)^2} - \frac{\sin(kr)}{(kr)^3} \right) \right]
\end{aligned} \tag{3.46}$$

For the free space coupling, we need to consider all the modes in the 3D space are available for our atomic ensemble, which is what we have performed for the calculation of $F(kr)$ above. Then we calculate the expression for the coherent energy exchange in free space,

$$\begin{aligned}
\Omega_{ij}^{3D} &= -\frac{\Gamma}{k_a^3} \mathcal{P} \int_0^\infty \frac{dk}{2\pi} \left(\frac{k^3 F(kr_{ij})}{k + k_a} + \frac{k^3 F(kr_{ij})}{k - k_a} \right) \\
&= -\frac{\Gamma}{k_a^3} \left[\int_0^\infty \frac{dk}{2\pi} k^3 \frac{F(kr_{ij})}{k - k_a} + \int_{-\infty}^0 \frac{dk}{2\pi} k^3 \frac{F(kr_{ij})}{k - k_a} \right] \\
&= -\frac{\Gamma}{(k_a r_{ij})^3} \int_{-\infty}^\infty \frac{d(kr_{ij})}{2\pi} (kr_{ij})^3 \frac{F(kr_{ij})}{(kr_{ij}) - (k_a r_{ij})},
\end{aligned} \tag{3.47}$$

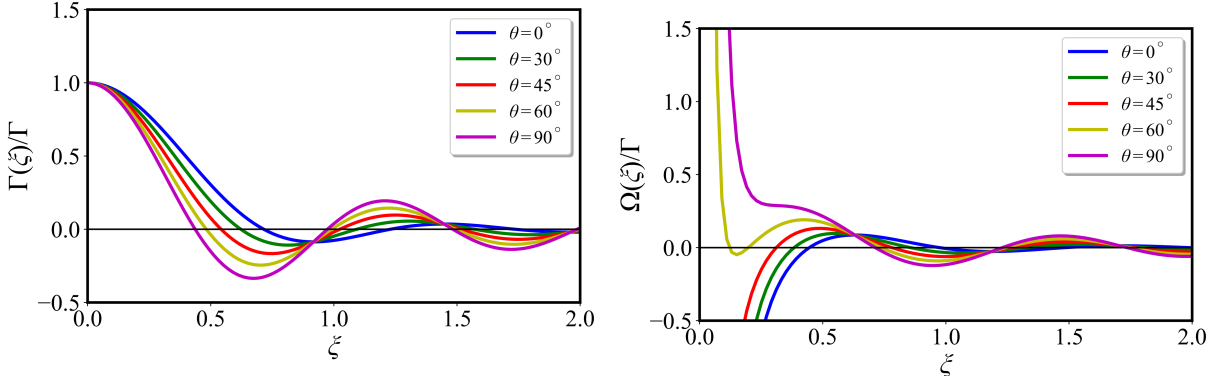
as $F(kr)$ is an even function. Now, we define $\xi := kr_{ij}$, so

$$\begin{aligned}
\Omega_{ij}^{3D} &= -\frac{\Gamma}{\xi_a^3} \int_{-\infty}^\infty \frac{d\xi}{2\pi} \xi^3 \frac{F(\xi)}{\xi - \xi_a} \\
&= -\frac{\Gamma}{\xi_a^3} \mathfrak{R} \left[\lim_{\epsilon \rightarrow 0} \oint \frac{d\xi}{2\pi} \frac{\xi^3}{\xi - i\epsilon - \xi_a} \right. \\
&\quad \cdot \left. \frac{3}{2} \left[(1 - \cos^2 \theta) \frac{e^{i\xi} - e^{-i\xi}}{2i\xi} + (1 - 3 \cos^2 \theta) \left(\frac{e^{i\xi} + e^{-i\xi}}{2i\xi^2} - \frac{e^{i\xi} - e^{-i\xi}}{2i\xi^3} \right) \right] \right] \\
&= -\frac{\Gamma}{\xi_a^3} \mathfrak{R} \left[\lim_{\epsilon \rightarrow 0} 2\pi i \cdot \frac{3}{2} \left[(1 - \cos^2 \theta) \frac{e^{i\xi}}{2i\xi} + (1 - 3 \cos^2 \theta) \left(\frac{e^{i\xi}}{2i\xi^2} - \frac{e^{i\xi}}{2i\xi^3} \right) \right] \Big|_{\xi=\xi_a+i\epsilon} \right] \\
&= -\frac{3}{4} \Gamma \left[(1 - \cos^2 \theta) \frac{\cos \xi}{\xi} + (1 - 3 \cos^2 \theta) \left(\frac{\sin \xi}{\xi^2} + \frac{\cos \xi}{\xi^3} \right) \right]
\end{aligned} \tag{3.48}$$

and the dissipative coupling in free space is

$$\Gamma_{ij}^{3D} = \frac{3}{2}\Gamma[(1 - \cos^2 \theta)\frac{\sin \xi}{\xi} + (1 - 3 \cos^2 \theta)(\frac{\cos \xi}{\xi^2} - \frac{\sin \xi}{\xi^3})]. \quad (3.49)$$

The dissipative coupling rate and the coherent energy exchange rate are plotted as functions of the distance in Fig.3.3 for different angles between the propagation direction of the radiation from one atom and the dipole orientation of another atom. For a fixed angle θ , when the atoms are very close to each other their collective dissipative coupling is approaching their individual spontaneous emission rate, while their coherent energy exchange rate is increasing to infinity. If we keep increasing the distance between them, the coupling rates would oscillate between positive and negative values around zero, and would eventually get damped away as the distance increases to infinity. This coincides with the physical intuition. The correlation between the emitters will weaken as they are moving away from each other. Eventually, the emission pattern of the ensemble will change from cooperative spontaneous emissions to uncorrelated single-atom spontaneous emissions.



(a) Dissipative coupling rate as a function of distance between the atoms. $\xi = kr$

(b) Coherent energy exchange rate

Figure 3.2: Energy exchange between the atom ensemble and the vacuum mode.

Coupling in an ideal single-mode fiber

Atoms couple to each other differently in the fiber, as there are less modes available. If we have a 1-D atomic lattice along an ideal single mode fiber, the atoms can only couple through the mode (\vec{k}_0, ω_0) along the fiber. In this case, the dissipative coupling rate and the coherent energy exchange rate can be calculated in a simpler way. In the derivation,

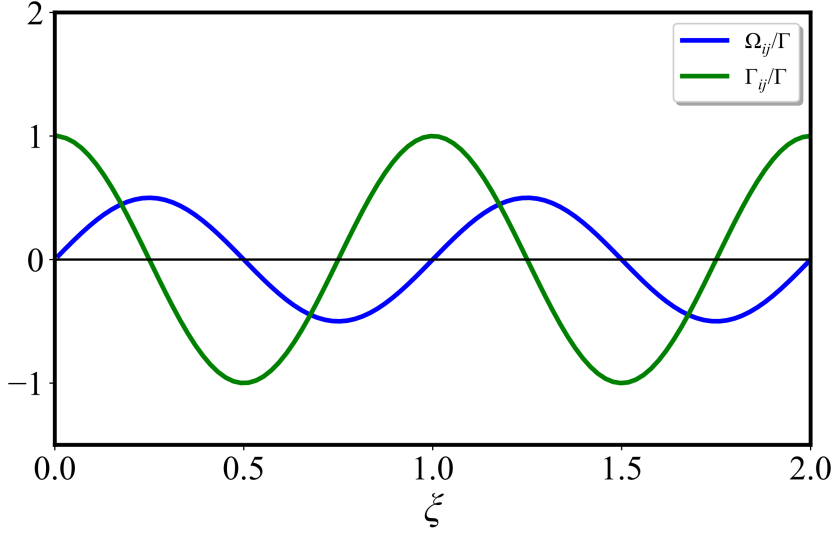


Figure 3.3: Energy exchange between the atom ensemble and the fiber mode

we assume the atoms are uniformly coupled to a single mode in the fiber. The spontaneous emission rate for an atom in a 1-D waveguide can be recalculated as

$$\begin{aligned}\Gamma^{1D} &= 2\pi \frac{L}{2\pi c} \int d\omega_k \frac{\omega_k}{2\epsilon_0 L} \mu^2 \delta(\omega_a - \omega_k) \\ &= \frac{\mu^2 \omega_a}{2\epsilon_0 c}\end{aligned}\tag{3.50}$$

From the derivation of the Hamiltonian in the last section, we have the integral form of the dissipative coupling rate. Here, we rewrite it for the 1-D case [30].

$$\begin{aligned}\frac{\Gamma_{ij}^{1D}}{2} &= \frac{\mu^2}{2\epsilon_0(2\pi c)} \int d\omega_k \omega_k \pi \delta(\omega_k - \omega_0) \cos(\omega_k r_{ij}) \\ &= \frac{\Gamma}{2} \cos(k_0 r_{ij})\end{aligned}\tag{3.51}$$

The coherent energy exchange rate as a function of distance along the fiber can be calculated as [30]

$$\begin{aligned}
\Omega_{ij}^{1D} &= -\Gamma \int_{-\infty}^{\infty} \frac{d(kr_{ij})}{2\pi} \frac{\cos(kr_{ij})}{kr_{ij} - k_0 r_{ij}} \\
&= -\Gamma \Re \left[\lim_{\epsilon \rightarrow 0} \oint \frac{d(kr_{ij})}{2\pi} \frac{1}{kr_{ij} + i\epsilon r_{ij} - k_0 r_{ij}} \frac{e^{ikr_{ij}} + e^{-ikr_{ij}}}{2i} \right] \\
&= -\Gamma \Re \left[\lim_{\epsilon \rightarrow 0} \frac{e^{-ikr_{ij}}}{2} \right]_{k=k_0 - i\epsilon} \\
&= -\frac{\Gamma}{2} \sin(k_0 r_{ij}),
\end{aligned} \tag{3.52}$$

Notice that in the case of a 1-D atom lattice inside a single-mode waveguide, the coupling rates are simply modulated by the changing distance instead of being attenuated, as was in the case of emissions in free space. However, in actual experimental settings, there will be 3-D modes available as well. The 1-D coupling and the 3-D coupling will be imposed on each other, and their relative magnitudes depend on the type of fibers used in the experiments. For our fiber simulations in later chapters, we would present both the idealized and the more realistic cases.

3.2 Simulation: Two-level atoms in a 1-D lattice

3.2.1 Two-level atoms in free space

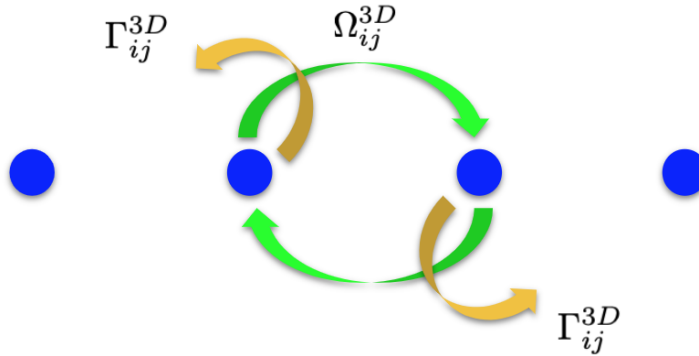


Figure 3.4: Couplings of two-level atoms in free space

In this section, we are applying the Liouvilian and the coupling rates we derived in previous sections to a physical setup. The simulation code was written in Julia using the QuantumOptics package [23] and is attached in the appendix. Assuming we have a 1-D excited two-level atom lattice in free space, the Hamiltonian for the system would be

$$H = \sum_i \omega_a \sigma_i^+ \sigma_i^- + \sum_{i \neq j} \Omega_{ij}^{3D} \sigma_i^+ \sigma_j^- \quad (3.53)$$

and the Optical Bloch equation would be

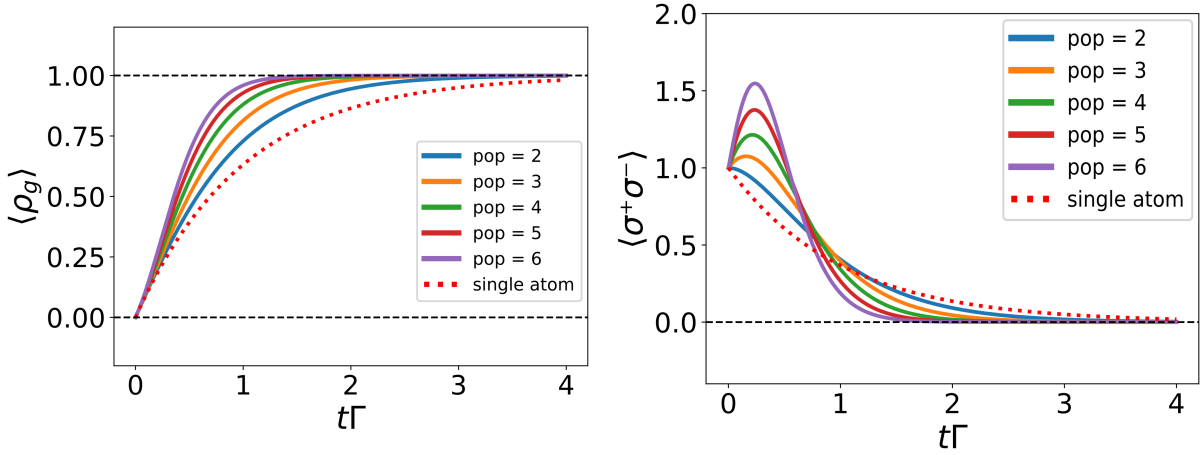
$$\partial_t \rho = i[H, \rho] + \mathcal{L}[\rho] \quad (3.54)$$

where the Lindblad superoperator is

$$\mathcal{L}[\rho] = \sum_{i,j} \frac{\Gamma_{ij}^{3D}}{2} (2\sigma_i^- \rho \sigma_j^+ - \sigma_j^+ \sigma_i^- \rho - \rho \sigma_i^+ \sigma_j^-). \quad (3.55)$$

The first simulation is performed where we assume there is no decoherence loss in the lattice. We increase the total population in the ensemble from one to six atoms, but we fix the distance between individual emitters to be in the Lamb-Dicke limit. We are measuring the ground state population and the total excitation, a.k.a, the light emitted by the ensemble. The code is attached in the appendix. The results are shown in Fig.3.5.

The Lamb-Dicke limit refers to the regime where the separation between the emitters are much smaller compared with the wavelength of their emitted photons, whilst assuming that the coherent energy exchange rate is not infinite. This model was first proposed by Robert Dicke in 1954 [6] as an ideal theoretical scenario to simplify the mathematics, as the emitters will see the field with the same phase. As is shown in Fig.3.5, when we are increasing the population in the ensemble, the decay rate increases while the maximum of the emission intensity increases as well. The emission gradually evolves into a burst as the population increases. This coincides with the traditional studies and understandings of superradiance established in the early days. However, this is more of a gedanken experiment, and would be improbable to realize in an actual experiment.



(a) The ground state population evolution

(b) Emission of the ensemble

Figure 3.5: Cooperative emission for 1-D atom lattice in free space in the Lamb-Dicke regime.

In the next part of the simulation, we fix the total population in the lattice and increase the distance between the atoms. As we are in free space, we would expect that the emission pattern would make the transition from cooperative spontaneous emission to single-atom spontaneous emission. The results are shown in Fig.3.6. The dissipative coupling rate and the coherent energy exchange rate for free space are shown below.

$$\begin{aligned}
 \Gamma_{ij}^{3D} &= \frac{3}{2}\Gamma[(1 - \cos^2 \theta) \frac{\sin \xi}{\xi} + (1 - 3 \cos^2 \theta) (\frac{\cos \xi}{\xi^2} - \frac{\sin \xi}{\xi^3})] \\
 \Omega_{ij}^{3D} &= -\frac{3}{4}\Gamma[(1 - \cos^2 \theta) \frac{\cos \xi}{\xi} + (1 - 3 \cos^2 \theta) (\frac{\sin \xi}{\xi^2} + \frac{\cos \xi}{\xi^3})]
 \end{aligned} \tag{3.56}$$

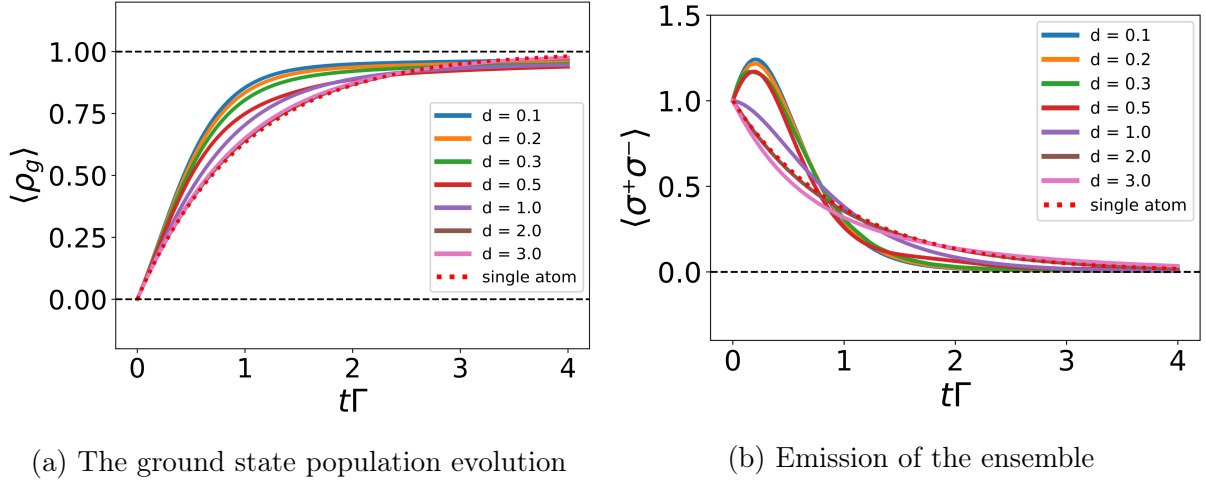


Figure 3.6: Cooperative emission for 1-D 5-atom lattice in free space in the extended ensemble regime

In the population evolution graph in Fig.3.6, we can see that the emission gradually changes from a faster superradiance burst into a single-atom spontaneous emission process, as we keep on increasing the distance. The change of the emission of the system is a little different. As was shown in Fig.3.3, the decay rate oscillates between negative values and positive values at small separations ($\sim \lambda$). This means that the emission pattern of the system will also oscillate between superradiance and subradiance before the distance becomes too large for the atoms to correlate with each other. This oscillatory behavior is better presented in a cartoon I made for the 2019 American Physical Society (APS) March Meeting presentation. In the graph presented in this thesis, however, the oscillatory behavior is still visible, as the radiation is further suppressed at $d = 3\lambda$ than $d = 2\lambda$. In the simulation, there are 5 atoms in the lattice, and the coupling rates are the ones derived from the previous section. All the curves in both graphs are normalized by their corresponding population.

3.2.2 Two-level atoms in an ideal single-mode fiber

When the 1-D atom lattice is put into a fiber, the available modes available for the atoms to couple to each other are limited. Thus their cooperative emission pattern is different, though the Hamiltonian has the exact same structure as the one used for 1-D lattice in

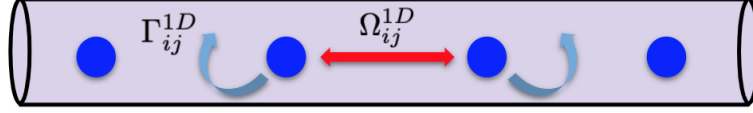


Figure 3.7: Couplings of two-level atoms in an ideal single-mode fiber

free space,

$$H = \sum_i \omega_a \sigma_i^+ \sigma_i^- + \sum_{i \neq j} \Omega_{ij}^{1D} \sigma_i^+ \sigma_j^-, \quad (3.57)$$

and the Optical Bloch equation would be

$$\partial_t \rho = i[H, \rho] + \mathcal{L}[\rho] \quad (3.58)$$

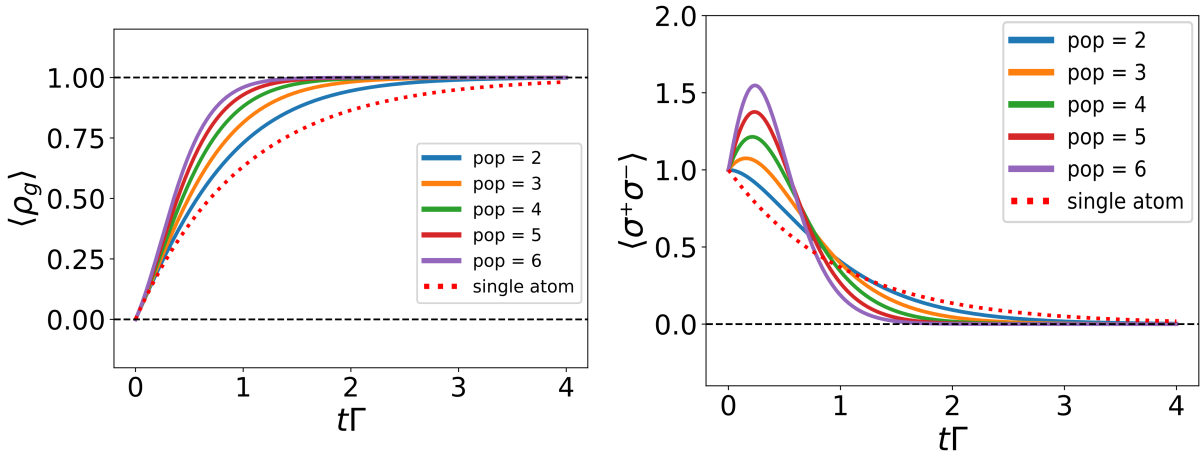
where the Lindblad superoperator is

$$\mathcal{L}[\rho] = \sum_{i,j} \frac{\Gamma_{ij}^{1D}}{2} (2\sigma_i^- \rho \sigma_j^+ - \sigma_j^+ \sigma_i^- \rho - \rho \sigma_i^+ \sigma_j^-). \quad (3.59)$$

From previous sections, we have derived the expressions for the dissipative coupling rate and the coherent energy exchange rate to be

$$\begin{aligned} \Omega_{ij}^{1D} &= \frac{\Gamma}{2} \sin(k_0 r_{ij}) \\ \Gamma_{ij}^{1D} &= \Gamma \cos(k_0 r_{ij}). \end{aligned} \quad (3.60)$$

The same set of simulations are performed for this physical setting. The program was written in Julia using QuantumOptics package [23] and is available in the appendix. First, we study the case for the Lamb-Dicke regime. The result is shown in Fig.3.8. There should be no difference between this simulation result and the one shown in Fig.3.5, as atoms are coupled to each other uniformly in Lamb-Dicke regime.



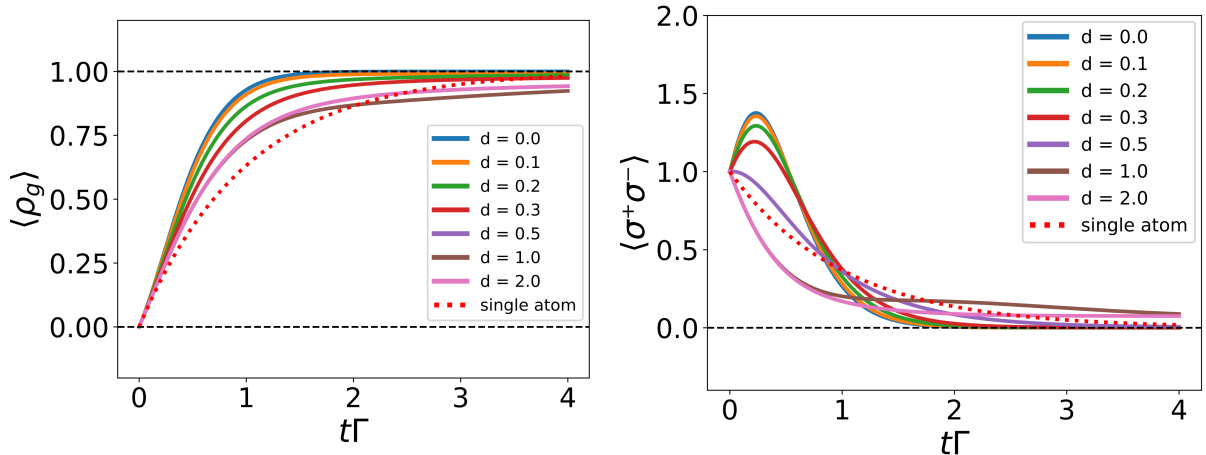
(a) The ground state population evolution

(b) Emission of the ensemble

Figure 3.8: Cooperative emission for a 1-D atom lattice in a single-mode fiber in the Lamb-Dicke regime

Interesting phenomena are happening if we keep stretching the ensemble, as is shown in Fig.3.9. From the coupling rate equations, we can predict that the evolution is going to display a periodic behavior. The figure showing the result is roughly one period of evolution of the curves before they rebound. From the simulation, at small separations ($\sim \lambda$), the emission and the population evolution are still similar to those of the Lamb-Dicke case. However, as the distance increases, the population and the emission curves are gradually morphing into the case of single-atom spontaneous emission, but as the coupling between the atoms is fundamentally different from the case of free space, the curves never fully make the transition from cooperative emission to the single-atom spontaneous emission. Then, as the system evolves, the curves bounce back to the initial emission pattern and restart the periodic dynamics.

Also, there are some interesting features about the population evolution curves displayed in Fig.3.9. Throughout the evolution, the decay rate of the cooperative emission is always higher than that of the single-atom spontaneous emission at the beginning of the process. Then as the distance increases, it takes longer time for the population to saturate. This is a feature that could be an experimental signature for cooperative emission, which would be discussed in the experimental part of the thesis.



(a) The ground state population evolution

(b) Emission of the ensemble

Figure 3.9: Cooperative emission for a 1-D 4-atom lattice in a single-mode fiber in the extended ensemble regime

3.2.3 Two-level atoms in a leaky single-mode fiber

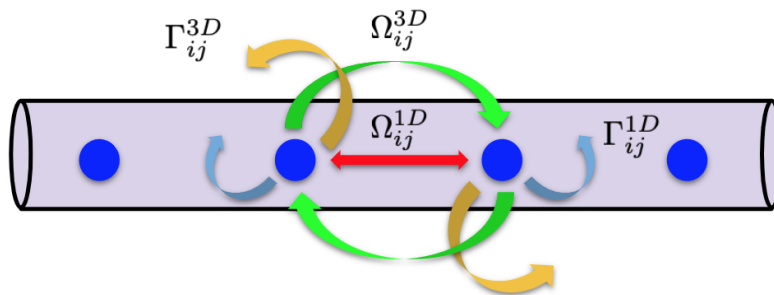


Figure 3.10: Couplings of two-level atoms in a leaky single-mode fiber

In a more realistic scenario, the atoms in a 1-D lattice inside a fiber will not only couple to each other through the fiber mode k_0 , but also through some other modes available in 3-D. Then, we will need to combine the Hamiltonians and the Liouvillians from the previous sections for a more generalized analysis.

$$H = \sum_i \omega_a \sigma_i^+ \sigma_i^- + \sum_{i \neq j} (\Omega_{ij}^{1D} \sigma_i^+ \sigma_j^- + \Omega_{ij}^{3D} \sigma_i^+ \sigma_j^-) \quad (3.61)$$

and the Optical Bloch equation would be

$$\partial_t \rho = i[H, \rho] + \mathcal{L}^{1D}[\rho] + \mathcal{L}^{3D}[\rho] \quad (3.62)$$

where the Lindblad superoperators are

$$\mathcal{L}^{1D}[\rho] = \sum_{i,j} \frac{\Gamma_{ij}^{1D}}{2} (2\sigma_i^- \rho \sigma_j^+ - \sigma_j^+ \sigma_i^- \rho - \rho \sigma_i^+ \sigma_j^-), \quad (3.63)$$

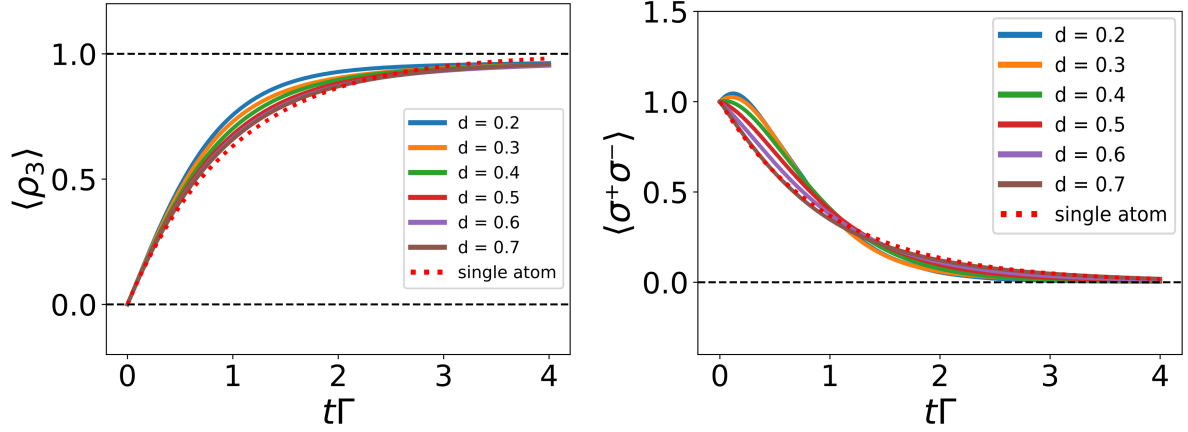
$$\mathcal{L}^{3D}[\rho] = \sum_{i,j} \frac{\Gamma_{ij}^{3D}}{2} (2\sigma_i^- \rho \sigma_j^+ - \sigma_j^+ \sigma_i^- \rho - \rho \sigma_i^+ \sigma_j^-), \quad (3.64)$$

with different coupling rates

$$\begin{aligned} \Omega_{ij}^{1D} &= \frac{\Gamma}{2} \sin(k_0 r_{ij}) \\ \Gamma_{ij}^{1D} &= \Gamma \cos(k_0 r_{ij}). \end{aligned} \quad (3.65)$$

$$\begin{aligned} \Gamma_{ij}^{3D} &= \frac{3}{2} \Gamma [(1 - \cos^2 \theta) \frac{\sin \xi}{\xi} + (1 - 3 \cos^2 \theta) (\frac{\cos \xi}{\xi^2} - \frac{\sin \xi}{\xi^3})] \\ \Omega_{ij}^{3D} &= -\frac{3}{4} \Gamma [(1 - \cos^2 \theta) \frac{\cos \xi}{\xi} + (1 - 3 \cos^2 \theta) (\frac{\sin \xi}{\xi^2} + \frac{\cos \xi}{\xi^3})] \end{aligned} \quad (3.66)$$

The program was written in Julia using QuantumOptics package [23] and is available in the appendix. In this simulation, we assume that the two ways of coupling are contributing equally to the decay and the energy exchange. For a more flexible simulation, however, scaling factors can be added in front of the 1-D and 3D coupling terms to adapt to the actual fiber parameters. The results are shown in Fig.3.11. The oscillatory behavior in the ideal fiber case has disappeared. As the distance increases, the emission pattern of the ensemble appears to be morphing into the single-atom spontaneous emission curve again. However, this is just one example of the possible parameters we could have chosen for our simulations. The code, which is attached in the appendix could be used for different fiber parameters and different experimental conditions.



(a) The ground state population evolution

(b) Emission of the ensemble

Figure 3.11: Cooperative emission for a 1-D 4 2-level atom lattice in a leaky single-mode fiber in the extended ensemble regime

3.3 Two atom cooperative emissions

Let's study the cooperative emission of a two-atom ensemble in greater detail in this section. The derivations shown in this section is a more detailed version of the two-atom superradiance studies in ref.[29] and ref.[11] for a better understanding of the concept of cooperative emission processes. Assuming the two atoms are the same, the Hamiltonian of the system could be written as

$$H = \omega_a(\sigma_1^z + \sigma_2^z) + \Omega(\sigma_1^+ \sigma_2^- + \sigma_1^- \sigma_2^+) \quad (3.67)$$

By using σ^z instead of $\sigma^+ \sigma^-$, we set the zero energy to be in the middle of the ground state and the excited state. This would simplify our expressions later on. For a two-atom ensemble, the bare atomic state can be presented as $|ee\rangle, |eg\rangle, |ge\rangle, |gg\rangle$. We can express the raising and lowering operators as

$$\begin{aligned} \sigma_1^+ &= |eg\rangle\langle gg| + |ee\rangle\langle ge| \\ \sigma_2^+ &= |ee\rangle\langle eg| + |ge\rangle\langle gg| \\ \sigma_1^- &= |gg\rangle\langle eg| + |ge\rangle\langle ee| \\ \sigma_2^- &= |eg\rangle\langle ee| + |gg\rangle\langle ge|, \end{aligned} \quad (3.68)$$

the Hamiltonian as

$$H = \hbar\omega_a(|ee\rangle - |gg\rangle) + \hbar\Omega\frac{1}{\sqrt{2}}(|eg\rangle + |ge\rangle) - \hbar\Omega\frac{1}{\sqrt{2}}(|eg\rangle - |ge\rangle). \quad (3.69)$$

and the Lindblad operator as

$$\mathcal{L}[\rho] = \mathcal{L}_1[\rho] + \mathcal{L}_2[\rho] + \mathcal{L}_{12}[\rho] + \mathcal{L}_{21}[\rho] \quad (3.70)$$

$$\begin{aligned} \mathcal{L}_1[\rho] &= \frac{\Gamma}{2}(2\sigma_1^- \rho \sigma_1^+ - \sigma_1^+ \sigma_1^- \rho - \rho \sigma_1^+ \sigma_1^-) \\ &= \frac{\Gamma}{2}[(|gg\rangle\langle eg| + |ge\rangle\langle ee|)\rho(|eg\rangle\langle gg| + |ee\rangle\langle ge|) \\ &\quad - \frac{1}{2}(|gg\rangle\langle eg| + |ge\rangle\langle ee|)(|eg\rangle\langle gg| + |ee\rangle\langle ge|)\rho \\ &\quad - \frac{1}{2}\rho(|gg\rangle\langle eg| + |ge\rangle\langle ee|)(|eg\rangle\langle gg| + |ee\rangle\langle ge|)] \end{aligned} \quad (3.71)$$

$$\begin{aligned} \mathcal{L}_2[\rho] &= \frac{\Gamma}{2}(2\sigma_2^- \rho \sigma_2^+ - \sigma_2^+ \sigma_2^- \rho - \rho \sigma_2^+ \sigma_2^-) \\ &= \frac{\Gamma}{2}[(|eg\rangle\langle ee| + |gg\rangle\langle ge|)\rho(|ee\rangle\langle eg| + |ge\rangle\langle gg|) \\ &\quad - \frac{1}{2}(|ee\rangle\langle eg| + |ge\rangle\langle gg|)(|eg\rangle\langle ee| + |gg\rangle\langle ge|)\rho \\ &\quad - \frac{1}{2}\rho(|ee\rangle\langle eg| + |ge\rangle\langle gg|)(|eg\rangle\langle ee| + |gg\rangle\langle ge|)] \\ &= \frac{\Gamma}{2}[(|eg\rangle\langle ee| + |gg\rangle\langle ge|)\rho(|ee\rangle\langle eg| + |ge\rangle\langle gg|) \\ &\quad - \frac{1}{2}(|ee\rangle\langle ee| + |ge\rangle\langle ge|)\rho - \frac{1}{2}\rho(|ee\rangle\langle ee| + |ge\rangle\langle ge|)] \end{aligned} \quad (3.72)$$

$$\begin{aligned}
\mathcal{L}_{12}[\rho] &= \frac{\gamma}{2}(2\sigma_1^- \rho \sigma_2^+ - \sigma_2^+ \sigma_1^- \rho - \rho \sigma_2^+ \sigma_1^-) \\
&= \frac{\gamma}{2}[(|gg\rangle\langle eg| + |ge\rangle\langle ee|)\rho(|ee\rangle\langle eg| + |ge\rangle\langle gg|) \\
&\quad - \frac{1}{2}(|ee\rangle\langle eg| + |ge\rangle\langle gg|)(|gg\rangle\langle eg| + |ge\rangle\langle ee|)\rho \\
&\quad - \frac{1}{2}\rho(|ee\rangle\langle eg| + |ge\rangle\langle gg|)(|gg\rangle\langle eg| + |ge\rangle\langle ee|)] \\
&= \frac{\gamma}{2}[(|gg\rangle\langle eg| + |ge\rangle\langle ee|)\rho(|ee\rangle\langle eg| + |ge\rangle\langle gg|) \\
&\quad - \frac{1}{2}|ge\rangle\langle eg|\rho - \frac{1}{2}\rho|ge\rangle\langle eg|]
\end{aligned} \tag{3.73}$$

$$\begin{aligned}
\mathcal{L}_{21}[\rho] &= \frac{\gamma}{2}(2\sigma_2^- \rho \sigma_1^+ - \sigma_1^+ \sigma_2^- \rho - \rho \sigma_1^+ \sigma_2^-) \\
&= \frac{\gamma}{2}[(|eg\rangle\langle ee| + |gg\rangle\langle ge|)\rho(|eg\rangle\langle gg| + |ee\rangle\langle ge|) \\
&\quad - \frac{1}{2}(|eg\rangle\langle gg| + |ee\rangle\langle ge|)(|eg\rangle\langle ee| + |gg\rangle\langle ge|)\rho \\
&\quad - \frac{1}{2}\rho(|eg\rangle\langle gg| + |ee\rangle\langle ge|)(|eg\rangle\langle ee| + |gg\rangle\langle ge|)] \\
&= \frac{\gamma}{2}[(|eg\rangle\langle ee| + |gg\rangle\langle ge|)\rho(|eg\rangle\langle gg| + |ee\rangle\langle ge|) \\
&\quad - \frac{1}{2}|eg\rangle\langle ge|\rho - \frac{1}{2}\rho|eg\rangle\langle ge|],
\end{aligned} \tag{3.74}$$

in which Γ is the single-atom spontaneous emission rate and γ is the cooperative dissipative coupling ($\Gamma F(\xi)$). From the single-atom Lindblad operators, $\mathcal{L}_1[\rho]$ and $\mathcal{L}_2[\rho]$, we can see that the first term $\sigma_i^- \rho_i^+$ drops population from higher energy levels to lower energy levels. Then when we subtract the second and the third terms, $\sigma_i^+ \sigma_i^- \rho$ and $\rho \sigma_i^+ \sigma_i^-$ from the expression, we effectively reduce the total population in the higher energy levels. As for the collective Lindblad terms, $\mathcal{L}_{12}[\rho]$ and $\mathcal{L}_{21}[\rho]$, the first term serves the same functionality as the first term in the single-atom Lindblad, but the second and the third terms are swapping the states between the atoms. Collectively, all of the Lindblad terms provide the system with incoherent energy loss.

We would use the bare states as our basis and we can write our Hamiltonian in the following matrix form [11].

$$H = \begin{bmatrix} \omega_a & 0 & 0 & 0 \\ 0 & 0 & \Omega & 0 \\ 0 & \Omega & 0 & 0 \\ 0 & 0 & 0 & -\omega_a \end{bmatrix} \tag{3.75}$$

The eigenstates and their corresponding eigenvalues are

$$\begin{aligned}
 |e\rangle &= |ee\rangle, E_e = \hbar\omega_a \\
 |s\rangle &= \frac{1}{\sqrt{2}}(|eg\rangle + |ge\rangle), E_s = \hbar\Omega \\
 |a\rangle &= \frac{1}{\sqrt{2}}(|eg\rangle - |ge\rangle), E_a = -\hbar\Omega \\
 |g\rangle &= |gg\rangle, E_g = -\hbar\omega_a
 \end{aligned} \tag{3.76}$$

and they are shown in Fig.3.12. The energy separation between the symmetric and the asymmetric states is the collective Lamb shift induced by the dipole-dipole interactions.

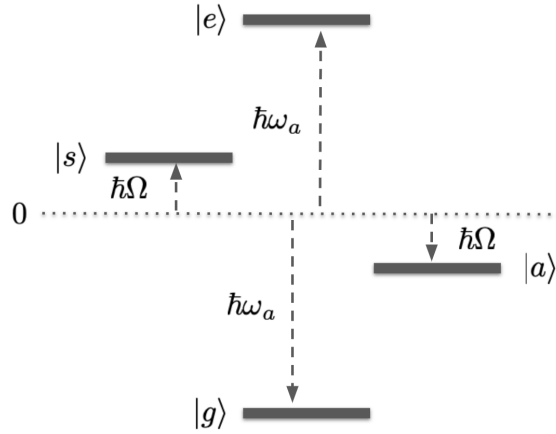


Figure 3.12: Eigenstates and their corresponding energy eigenvalues for a two-atom ensemble

Now, we can re-express our system using the eigenstates as our new basis. The raising and

lowering operators could be expressed as

$$\begin{aligned}
\sigma_1^+ &= \frac{1}{\sqrt{2}}[|e\rangle\langle s| - |e\rangle\langle a| + |s\rangle\langle g| + |a\rangle\langle g|] \\
\sigma_2^+ &= \frac{1}{\sqrt{2}}[|e\rangle\langle s| + |e\rangle\langle a| + |s\rangle\langle g| - |a\rangle\langle g|] \\
\sigma_1^- &= \frac{1}{\sqrt{2}}[|s\rangle\langle e| - |a\rangle\langle e| + |g\rangle\langle s| + |g\rangle\langle a|] \\
\sigma_2^- &= \frac{1}{\sqrt{2}}[|s\rangle\langle e| + |a\rangle\langle e| + |g\rangle\langle s| - |g\rangle\langle a|]
\end{aligned} \tag{3.77}$$

We can rewrite our Hamiltonian using the eigenstates of the system as

$$H = \hbar\omega_a(|e\rangle\langle e| - |g\rangle\langle g|) + \hbar\Omega(|s\rangle\langle s| - |a\rangle\langle a|), \tag{3.78}$$

and the Lindblad operator as

$$\mathcal{L}[\rho] = \mathcal{L}_1[\rho] + \mathcal{L}_2[\rho] + \mathcal{L}_{12}[\rho] + \mathcal{L}_{21}[\rho] \tag{3.79}$$

$$\begin{aligned}
\mathcal{L}_1[\rho] &= \frac{\Gamma}{2}(2\sigma_1^- \rho \sigma_1^+ - \sigma_1^+ \sigma_1^- \rho - \rho \sigma_1^+ \sigma_1^-) \\
&= \frac{\Gamma}{2}[(|s\rangle\langle e| - |a\rangle\langle e| + |g\rangle\langle s| + |g\rangle\langle a|) \rho (|e\rangle\langle s| - |e\rangle\langle a| + |s\rangle\langle g| + |a\rangle\langle g|) \\
&\quad - \frac{1}{2} (|e\rangle\langle s| - |e\rangle\langle a| + |s\rangle\langle g| + |a\rangle\langle g|) (|s\rangle\langle e| - |a\rangle\langle e| + |g\rangle\langle s| + |g\rangle\langle a|) \rho \\
&\quad - \frac{1}{2} \rho (|e\rangle\langle s| - |e\rangle\langle a| + |s\rangle\langle g| + |a\rangle\langle g|) (|s\rangle\langle e| - |a\rangle\langle e| + |g\rangle\langle s| + |g\rangle\langle a|)] \\
&= \frac{\Gamma}{2}[(|s\rangle\langle e| - |a\rangle\langle e| + |g\rangle\langle s| + |g\rangle\langle a|) \rho (|e\rangle\langle s| - |e\rangle\langle a| + |s\rangle\langle g| + |a\rangle\langle g|) \\
&\quad - \frac{1}{2} (2|e\rangle\langle e| + |s\rangle\langle s| + |a\rangle\langle a| + |s\rangle\langle a| + |a\rangle\langle s|) \rho \\
&\quad - \frac{1}{2} \rho (2|e\rangle\langle e| + |s\rangle\langle s| + |a\rangle\langle a| + |s\rangle\langle a| + |a\rangle\langle s|)]
\end{aligned} \tag{3.80}$$

$$\begin{aligned}
\mathcal{L}_2[\rho] &= \frac{\Gamma}{2}(2\sigma_2^- \rho \sigma_2^+ - \sigma_2^+ \sigma_2^- \rho - \rho \sigma_2^+ \sigma_2^-) \\
&= \frac{\Gamma}{2}[(|s\rangle\langle e| + |a\rangle\langle e| + |g\rangle\langle s| - |g\rangle\langle a|)\rho(|e\rangle\langle s| + |e\rangle\langle a| + |s\rangle\langle g| - |a\rangle\langle g|) \\
&\quad - \frac{1}{2}(|e\rangle\langle s| + |e\rangle\langle a| + |s\rangle\langle g| - |a\rangle\langle g|)(|s\rangle\langle e| + |a\rangle\langle e| + |g\rangle\langle s| - |g\rangle\langle a|)\rho \\
&\quad - \frac{1}{2}\rho(|e\rangle\langle s| + |e\rangle\langle a| + |s\rangle\langle g| - |a\rangle\langle g|)(|s\rangle\langle e| + |a\rangle\langle e| + |g\rangle\langle s| - |g\rangle\langle a|)] \quad (3.81) \\
&= \frac{\Gamma}{2}[(|s\rangle\langle e| + |a\rangle\langle e| + |g\rangle\langle s| - |g\rangle\langle a|)\rho(|e\rangle\langle s| + |e\rangle\langle a| + |s\rangle\langle g| - |a\rangle\langle g|) \\
&\quad - \frac{1}{2}(2|e\rangle\langle e| + |s\rangle\langle s| + |a\rangle\langle a| - |s\rangle\langle a| - |a\rangle\langle s|)\rho \\
&\quad - \frac{1}{2}\rho(2|e\rangle\langle e| + |s\rangle\langle s| + |a\rangle\langle a| - |s\rangle\langle a| - |a\rangle\langle s|)]
\end{aligned}$$

$$\begin{aligned}
\mathcal{L}_{12}[\rho] &= \frac{\gamma}{2}(2\sigma_1^- \rho \sigma_2^+ - \sigma_2^+ \sigma_1^- \rho - \rho \sigma_2^+ \sigma_1^-) \\
&= \frac{\gamma}{2}[(|s\rangle\langle e| - |a\rangle\langle e| + |g\rangle\langle s| + |g\rangle\langle a|)\rho(|e\rangle\langle s| + |e\rangle\langle a| + |s\rangle\langle g| - |a\rangle\langle g|) \\
&\quad - \frac{1}{2}(|e\rangle\langle s| + |e\rangle\langle a| + |s\rangle\langle g| - |a\rangle\langle g|)(|s\rangle\langle e| - |a\rangle\langle e| + |g\rangle\langle s| + |g\rangle\langle a|)\rho \\
&\quad - \frac{1}{2}\rho(|e\rangle\langle s| + |e\rangle\langle a| + |s\rangle\langle g| - |a\rangle\langle g|)(|s\rangle\langle e| - |a\rangle\langle e| + |g\rangle\langle s| + |g\rangle\langle a|)] \quad (3.82) \\
&= \frac{\gamma}{2}[(|s\rangle\langle e| - |a\rangle\langle e| + |g\rangle\langle s| + |g\rangle\langle a|)\rho(|e\rangle\langle s| + |e\rangle\langle a| + |s\rangle\langle g| - |a\rangle\langle g|) \\
&\quad - \frac{1}{2}(|s\rangle\langle s| - |a\rangle\langle s| + |s\rangle\langle a| - |a\rangle\langle a|)\rho - \frac{1}{2}\rho(|s\rangle\langle s| - |a\rangle\langle s| + |s\rangle\langle a| - |a\rangle\langle a|)]
\end{aligned}$$

$$\begin{aligned}
\mathcal{L}_{21}[\rho] &= \frac{\gamma}{2}(2\sigma_2^- \rho \sigma_1^+ - \sigma_1^+ \sigma_2^- \rho - \rho \sigma_1^+ \sigma_2^-) \\
&= \frac{\gamma}{2}[(|s\rangle\langle e| + |a\rangle\langle e| + |g\rangle\langle s| - |g\rangle\langle a|)\rho(|e\rangle\langle s| - |e\rangle\langle a| + |s\rangle\langle g| + |a\rangle\langle g|) \\
&\quad - \frac{1}{2}(|e\rangle\langle s| - |e\rangle\langle a| + |s\rangle\langle g| + |a\rangle\langle g|)(|s\rangle\langle e| + |a\rangle\langle e| + |g\rangle\langle s| - |g\rangle\langle a|)\rho \\
&\quad - \frac{1}{2}\rho(|e\rangle\langle s| - |e\rangle\langle a| + |s\rangle\langle g| + |a\rangle\langle g|)(|s\rangle\langle e| + |a\rangle\langle e| + |g\rangle\langle s| - |g\rangle\langle a|)] \\
&= \frac{\gamma}{2}[(|s\rangle\langle e| + |a\rangle\langle e| + |g\rangle\langle s| - |g\rangle\langle a|)\rho(|e\rangle\langle s| - |e\rangle\langle a| + |s\rangle\langle g| + |a\rangle\langle g|) \\
&\quad - \frac{1}{2}(|s\rangle\langle s| + |a\rangle\langle s| - |s\rangle\langle a| - |a\rangle\langle a|)\rho - \frac{1}{2}\rho(|s\rangle\langle s| + |a\rangle\langle s| - |s\rangle\langle a| - |a\rangle\langle a|)]. \quad (3.83)
\end{aligned}$$

Then we substitute these equations into the total Lindblad term and get

$$\begin{aligned}
\mathcal{L}[\rho] &= \frac{\Gamma + \gamma}{2} [2(|g\rangle\langle s| + |s\rangle\langle e|)\rho(|e\rangle\langle s| + |s\rangle\langle g|) - (|e\rangle\langle e| + |s\rangle\langle s|)\rho - \rho(|e\rangle\langle e| + |s\rangle\langle s|)] \\
&\quad + \frac{\Gamma - \gamma}{2} [2(|g\rangle\langle a| - |a\rangle\langle e|)\rho(|e\rangle\langle a| + |a\rangle\langle g|) - (|e\rangle\langle e| + |a\rangle\langle a|)\rho - \rho(|e\rangle\langle e| + |a\rangle\langle a|)] \\
&= \mathcal{L}_s[\rho] + \mathcal{L}_a[\rho],
\end{aligned} \tag{3.84}$$

with

$$\begin{aligned}
\mathcal{L}_s[\rho] &= \frac{\Gamma + \gamma}{2} [2(|g\rangle\langle s| + |s\rangle\langle e|)\rho(|e\rangle\langle s| + |s\rangle\langle g|) - (|e\rangle\langle e| + |s\rangle\langle s|)\rho - \rho(|e\rangle\langle e| + |s\rangle\langle s|)] \\
\mathcal{L}_a[\rho] &= \frac{\Gamma - \gamma}{2} [2(|g\rangle\langle a| - |a\rangle\langle e|)\rho(|e\rangle\langle a| + |a\rangle\langle g|) - (|e\rangle\langle e| + |a\rangle\langle a|)\rho - \rho(|e\rangle\langle e| + |a\rangle\langle a|)]
\end{aligned} \tag{3.85}$$

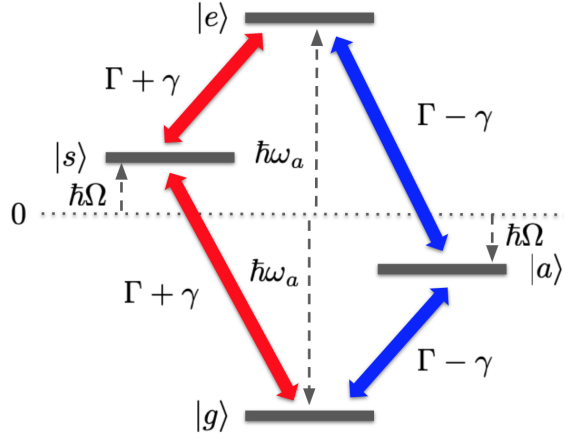


Figure 3.13: Transitions in a two-atom cooperative emission system

$\mathcal{L}_s[\rho]$ and $\mathcal{L}_a[\rho]$ describe the decays through the symmetric state ($\gamma_s = |e\rangle \rightarrow |s\rangle \rightarrow |g\rangle$) and the asymmetric state ($\gamma_a = |e\rangle \rightarrow |a\rangle \rightarrow |g\rangle$). The transition is described in Fig.3.13. There is no direct transition between the fully excited state and the ground state. The transitions γ_s and γ_a have different rates depending on the dipole separation, which is indicated by Fig.3.14. At the Lamb-Dicke limit, ignoring the dipole-dipole interaction, we

have $\Gamma = \gamma$ and the asymmetric state becomes a dark state, while γ_s is the superradiant transition. However, when $r \approx 0.6\lambda$, we have $\gamma < 0$. Then γ_a is the superradiant transition instead of γ_s . If the separation keeps increasing, eventually $\gamma \sim 0$ and all the decay rates will approach that of the single-atom spontaneous emission [29].

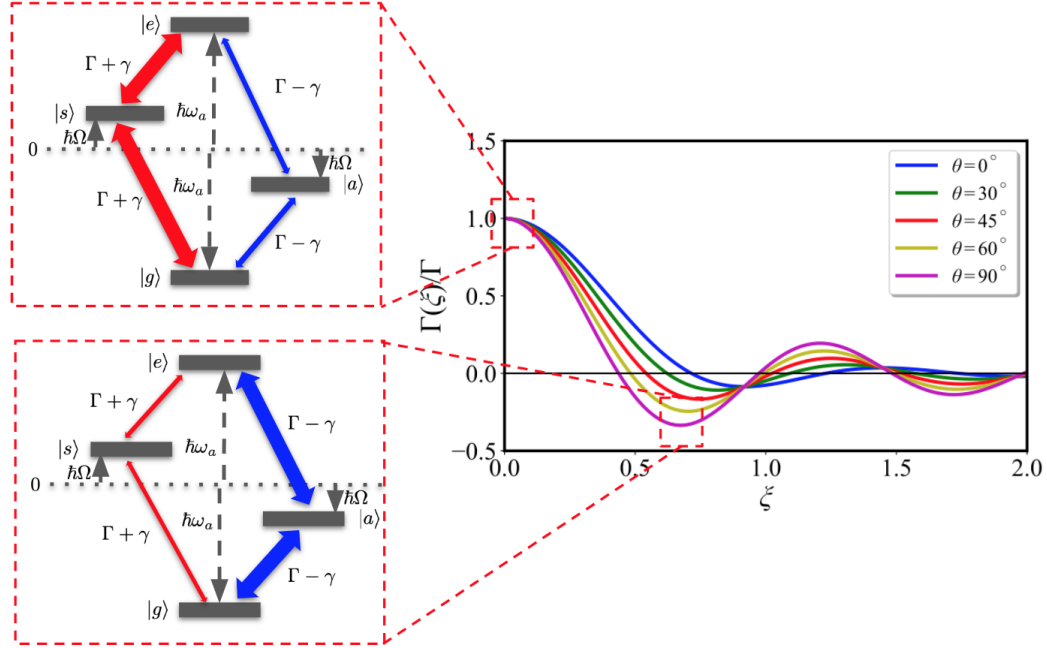


Figure 3.14: Variations of the transition paths with different atom separations. The thickness of the arrows indicates the transition strengths.

3.4 Simulation: Three-level atoms in a 1-D lattice

3.4.1 Three-level atoms in free space

In order to experimentally implement superradiance in an ensemble of cold atoms, it is conventional to adapt an effective two-level system instead of an actual two-level system. There are various reasons behind this decision. In the case of realizing a steady state laser, for example, it is impossible to achieve total population inversion. In our case, we would like to adopt a three-level Raman transition scheme, where all the population is prepared in the effective excited state, and will get transferred to the ground state via an intermediate

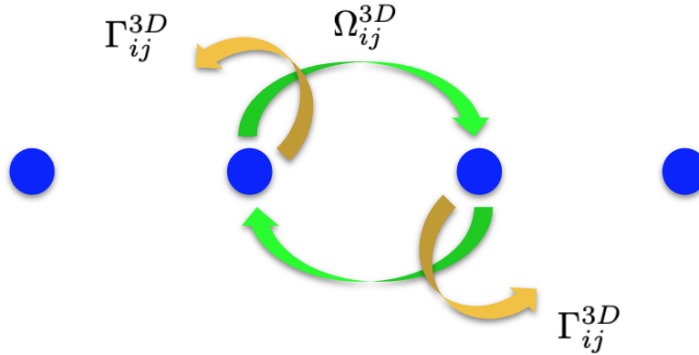


Figure 3.15: Couplings of three-level atoms in free space

state, as is shown in Fig.3.16. A coherent laser is pumping the population from the excited state $|e\rangle$ to the intermediate state $|s\rangle$, and then the population incoherently decay from the intermediate state to the ground state $|g\rangle$.

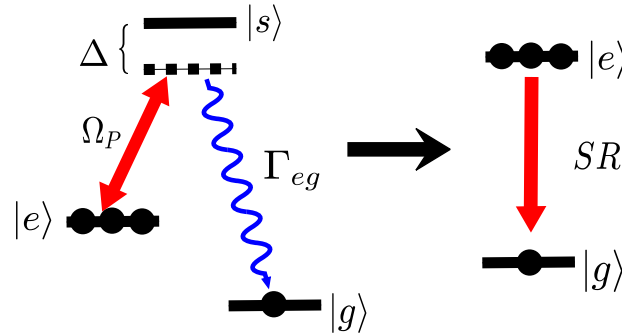


Figure 3.16: Raman scheme for implementing superradiance as an effective two-level system

There are several advantages to the Raman scheme. The transition rate could be controlled by tuning the pumping power and its detuning from the intermediate state, and the transition could be shut off completely once the pumping laser is turning off. This allows for a novel detection scheme for superradiance, which would be discussed in detail in later chapters.

The Hamiltonian for this system could be written as

$$H = \Delta_e \sum_i \sigma_{ee}^{(i)} + \Delta_s \sum_i \sigma_{ss}^{(i)} + \omega_p \sum_i (\sigma_{es}^{(i)} + \sigma_{se}^{(i)}) + \sum_{i,j} \Omega_{ij}^{3D} \sigma_{gs}^{(i)} \sigma_{sg}^{(j)}, \quad (3.86)$$

where Δ_s and Δ_e are the detunings, and ω_p is the strength of the pump between $|s\rangle$ and $|e\rangle$. The function Ω_{ij} is the coherent energy exchange function from previous sections. The dissipations of the system are the loss from spontaneous emission and incoherent pumping broadening,

$$\mathcal{L}_{sp}[\rho] = \frac{1}{2} \sum_{i,j} \Gamma_{ij}^{3D} \left(2\sigma_{32}^{(i)} \rho \sigma_{23}^{(j)} - \sigma_{23}^{(i)} \sigma_{32}^{(j)} \rho - \rho \sigma_{23}^{(i)} \sigma_{32}^{(j)} \right), \quad (3.87)$$

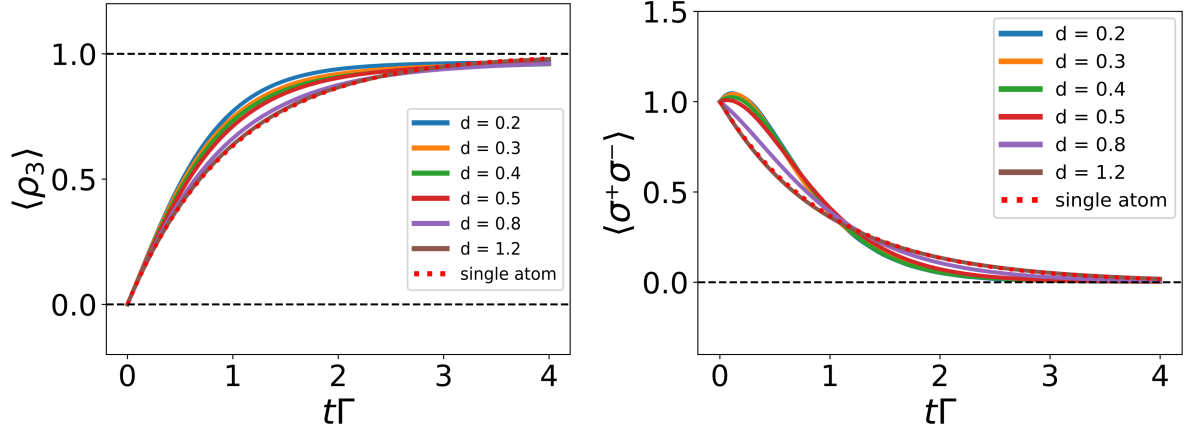
$$\mathcal{L}_p[\rho] = \frac{1}{2} \sum_i \Gamma_i \left(2\sigma_{23}^{(i)} \rho \sigma_{32}^{(i)} - \sigma_{23}^{(i)} \sigma_{32}^{(i)} \rho - \rho \sigma_{23}^{(i)} \sigma_{32}^{(i)} \right), \quad (3.88)$$

while the different coupling rates are giving as

$$\begin{aligned} \Gamma_{ij}^{3D} &= \frac{3}{2} \Gamma \left[(1 - \cos^2 \theta) \frac{\sin \xi}{\xi} + (1 - 3 \cos^2 \theta) \left(\frac{\cos \xi}{\xi^2} - \frac{\sin \xi}{\xi^3} \right) \right] \\ \Omega_{ij}^{3D} &= -\frac{3}{4} \Gamma \left[(1 - \cos^2 \theta) \frac{\cos \xi}{\xi} + (1 - 3 \cos^2 \theta) \left(\frac{\sin \xi}{\xi^2} + \frac{\cos \xi}{\xi^3} \right) \right] \end{aligned} \quad (3.89)$$

and Γ_i is a constant, as we assume that there is no collective incoherent broadening, and thus there is no cross-term in the Liouvillian for the incoherent pumping loss.

In our case, the pumping is incoherent, as the spontaneous emission from $|s\rangle$ to $|g\rangle$ is an incoherent process. As a result, in our simulation, we can set $\omega_p = 0$. The simulation results for 3 atoms are shown in Fig. 3.17. We can discover a familiar trend of the evolution of the system. It starts off with a faster decay than the single-atom spontaneous emission rate at a small separation, then gradually as the distance is increasing, the emission pattern morphs into the single-atom case. This is similar to the case of a 1-D lattice of two-level systems. The results shown here are just one example of the simulation parameter space. If an actual two-level system is used in the experiment, then we assume that there is no coherence loss due to pumping, and set $\Gamma_i^{3D} = 0$. The program was written in Julia using QuantumOptics package [23] and is available in the appendix.



(a) The ground state population evolution

(b) Emission of the ensemble

Figure 3.17: Cooperative emission for a 1-D three 3-level atom lattice in free space in the extended ensemble regime

3.4.2 Three-level atoms in an ideal single-mode fiber

Similar to the case of an ideal single-mode fiber with two-level atoms inside, we assume that the atoms are only coupled to each other through the only mode available in the fiber. The Hamiltonian of the system is

$$H = \Delta_e \sum_i \sigma_{ee}^{(i)} + \Delta_s \sum_i \sigma_{ss}^{(i)} + \omega_p \sum_i (\sigma_{es}^{(i)} + \sigma_{se}^{(i)}) + \sum_{i,j} \Omega_{ij}^{1D} \sigma_{gs}^{(i)} \sigma_{sg}^{(j)}, \quad (3.90)$$

and the Liouvillians are

$$\mathcal{L}_{sp}[\rho] = \frac{1}{2} \sum_{i,j} \Gamma_{ij}^{1D} \left(2\sigma_{32}^{(i)} \rho \sigma_{23}^{(j)} - \sigma_{23}^{(i)} \sigma_{32}^{(j)} \rho - \rho \sigma_{23}^{(i)} \sigma_{32}^{(j)} \right), \quad (3.91)$$

$$\mathcal{L}_p[\rho] = \frac{1}{2} \sum_i \Gamma_i \left(2\sigma_{23}^{(i)} \rho \sigma_{32}^{(i)} - \sigma_{23}^{(i)} \sigma_{32}^{(i)} \rho - \rho \sigma_{23}^{(i)} \sigma_{32}^{(i)} \right), \quad (3.92)$$

with the coupling rates for a 1-D case as

$$\begin{aligned} \Omega_{ij}^{1D} &= \frac{\Gamma}{2} \sin(k_0 r_{ij}) \\ \Gamma_{ij}^{1D} &= \Gamma \cos(k_0 r_{ij}). \end{aligned} \quad (3.93)$$

The program was written in Julia using QuantumOptics package [23] and is available in the appendix. Assuming that the \vec{k} of the mode is perpendicular to the dipole moment orientation of the chain of atoms, we get the results that are shown in Fig.3.19. In the simulation, there are three atoms in the lattice, and there is no detuning between the superradiance field and the $|s\rangle \rightarrow |g\rangle$ transition. This result is qualitatively similar to the ones shown in Fig.3.9, where they both have shown oscillatory behaviors in the ground state population evolution and the emission when the distance between the atoms is being changed. This is due to the fact that the atoms are only allowed to couple to each other through the only mode that is supported by the waveguide. Thus, the coherent energy exchange rate and the dissipative coupling rate are being modulated by distance, giving rise to the oscillatory behavior. In the plots shown in Fig.3.19, to avoid confusion, only curves in one oscillation period are shown.

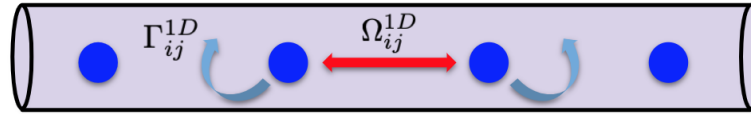
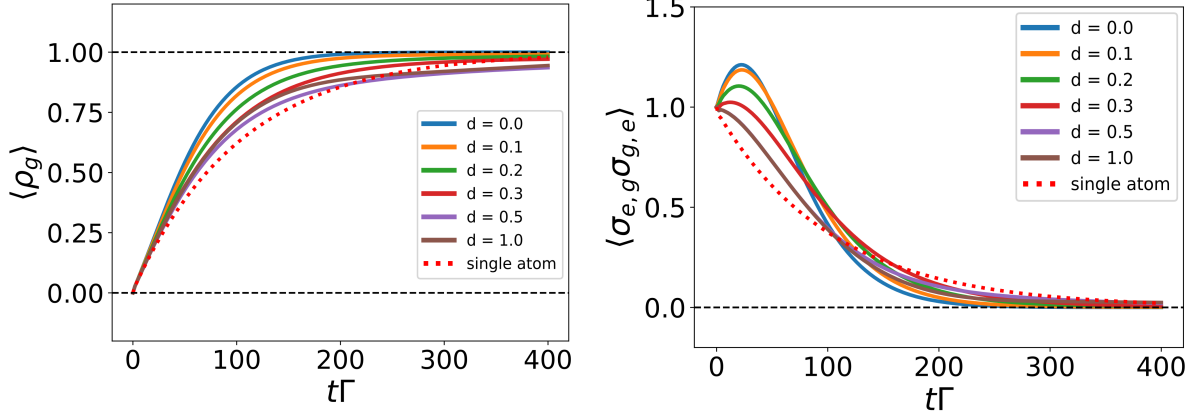


Figure 3.18: Couplings of three level atoms in an ideal single-mode fiber



(a) The ground state population evolution

(b) Emission of the ensemble

Figure 3.19: Cooperative emission for a 1-D 3-level atom lattice in an ideal fiber in the extended ensemble regime

3.4.3 Three-level atoms in a leaky single-mode fiber

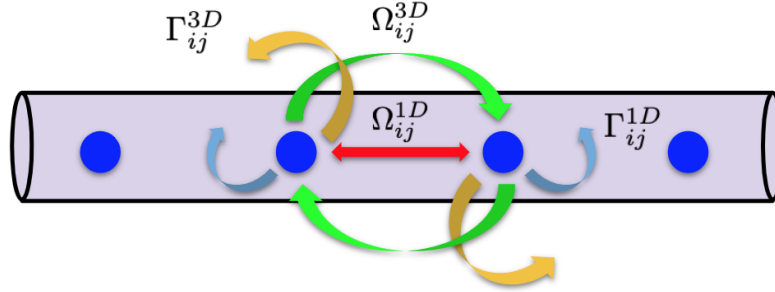


Figure 3.20: Couplings of three-level atoms in a leaky single-mode fiber

We are setting up our simulation similar to the case of two-level atoms in a leaky single-mode fiber, where our Hamiltonian is

$$H = \Delta_e \sum_i \sigma_{ee}^{(i)} + \Delta_s \sum_i \sigma_{ss}^{(i)} + \omega_p \sum_i (\sigma_{es}^{(i)} + \sigma_{se}^{(i)}) + \sum_{i,j} \Omega_{ij}^{1D} \sigma_{gs}^{(i)} \sigma_{sg}^{(j)} + \sum_{i,j} \Omega_{ij}^{3D} \sigma_{gs}^{(i)} \sigma_{sg}^{(j)}, \quad (3.94)$$

and the Optical Bloch equation would be

$$\partial_t \rho = i[H, \rho] + \mathcal{L}^{1D}[\rho] + \mathcal{L}^{3D}[\rho] + \mathcal{L}_p[\rho] \quad (3.95)$$

where the Lindblad superoperators are

$$\mathcal{L}_{sp}[\rho] = \frac{1}{2} \sum_{i,j} \Gamma_{ij}^{1D} \left(2\sigma_{32}^{(i)} \rho \sigma_{23}^{(j)} - \sigma_{23}^{(i)} \sigma_{32}^{(j)} \rho - \rho \sigma_{23}^{(i)} \sigma_{32}^{(j)} \right), \quad (3.96)$$

$$\mathcal{L}_{sp}[\rho] = \frac{1}{2} \sum_{i,j} \Gamma_{ij}^{3D} \left(2\sigma_{32}^{(i)} \rho \sigma_{23}^{(j)} - \sigma_{23}^{(i)} \sigma_{32}^{(j)} \rho - \rho \sigma_{23}^{(i)} \sigma_{32}^{(j)} \right), \quad (3.97)$$

$$\mathcal{L}_p[\rho] = \frac{1}{2} \sum_i \Gamma_i \left(2\sigma_{23}^{(i)} \rho \sigma_{32}^{(i)} - \sigma_{23}^{(i)} \sigma_{32}^{(i)} \rho - \rho \sigma_{23}^{(i)} \sigma_{32}^{(i)} \right), \quad (3.98)$$

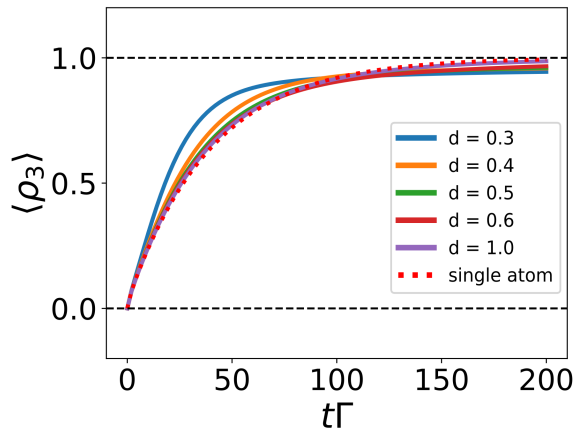
with different coupling rates

$$\Omega_{ij}^{1D} = \frac{\Gamma}{2} \sin(k_0 r_{ij}) \quad (3.99)$$

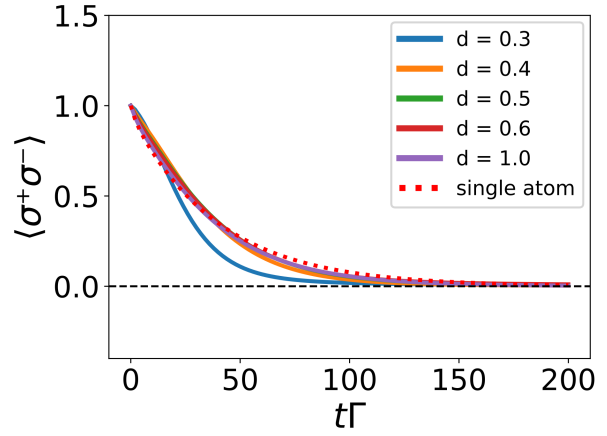
$$\Gamma_{ij}^{1D} = \Gamma \cos(k_0 r_{ij}).$$

$$\begin{aligned} \Gamma_{ij}^{3D} &= \frac{3}{2} \Gamma \left[(1 - \cos^2 \theta) \frac{\sin \xi}{\xi} + (1 - 3 \cos^2 \theta) \left(\frac{\cos \xi}{\xi^2} - \frac{\sin \xi}{\xi^3} \right) \right] \\ \Omega_{ij}^{3D} &= -\frac{3}{4} \Gamma \left[(1 - \cos^2 \theta) \frac{\cos \xi}{\xi} + (1 - 3 \cos^2 \theta) \left(\frac{\sin \xi}{\xi^2} + \frac{\cos \xi}{\xi^3} \right) \right] \end{aligned} \quad (3.100)$$

The program was written in Julia using QuantumOptics package [23] and is available in the appendix. The results are shown in Fig.3.21. The simulation was done with 3 atoms in a lattice. The couplings through 1-D mode and 3-D modes are equally weighted. At small separations between the atoms, we can see that the decay rate was fast at the beginning, given by the large distinction between the $d = 0.3$ curve and the single atom curve in the figure. However, as time progresses, it takes longer for the $d = 0.3$ curve to reach saturation. This has been observed in our experiment, where slight deviations have been seen in the fitting. This could be an experimental signal for correlated decays in an ensemble, which would be illustrated in detail in the experimental part of the thesis.



(a) The ground state population evolution



(b) Emission of the ensemble

Figure 3.21: Cooperative emission for a 1-D 3 3-level atom lattice in a leaky fiber in the extended ensemble regime

Chapter 4

Superradiant laser

4.1 A quick introduction to lasers

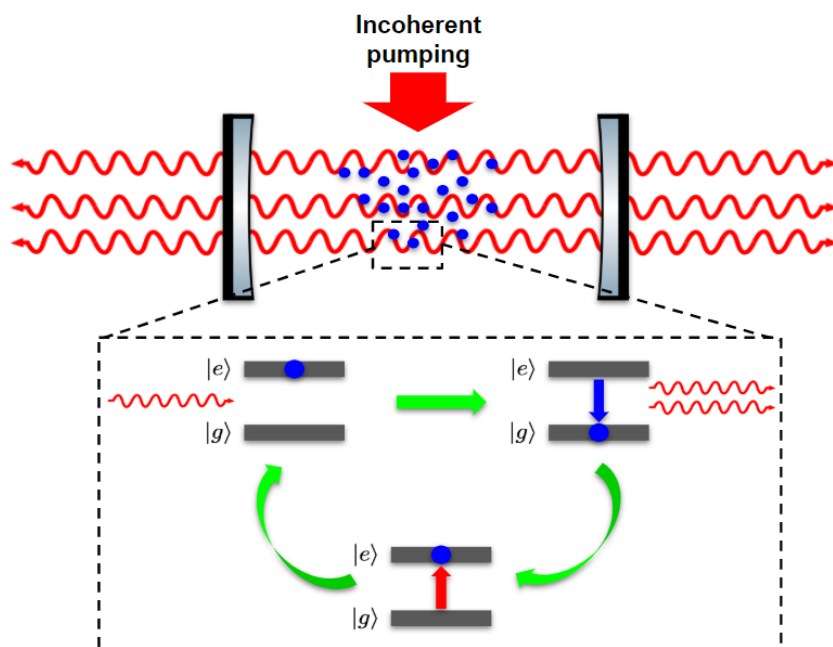


Figure 4.1: Principle of a laser

Before explaining how a steady-state superradiant laser works, I would like to give a quick introduction to the principle of an ordinary laser, focusing on the mechanism and the measurement of linewidth. This discussion is largely following the basic concept part of Christoph Hotter’s masters thesis in ref.[22].

The foundations of the laser are the three basic light-matter interactions discussed in Chapter 2: absorption, stimulated emission and spontaneous emission. The principle of a laser is illustrated in Fig.4.1. Assuming we have an atomic ensemble inside a good cavity. The population is being constantly incoherently pumped from the ground state to the excited state. Then through a seeding process, either a spontaneous emission event or a triggering pulse, a photon field is built up inside the cavity, bringing more stimulated emissions from the ensemble, resulting in a stronger field in the cavity. The incoherent pumping constantly feeds energy into the system by repumping the depleted atoms into its excited states, so the cycle could be continued. Eventually, the intensity would saturate to a maximum. [22] In this process, the key process is the stimulated emission, namely that the atoms are oscillating in phase driven by the field inside the cavity, where in superradiance, or as we will see, in a steady-state superradiant laser, the key process is spontaneous emission, which is a major distinction between these two lasers.

Usually to achieve lasing, the population inversion needs to be over 50%, which would be impossible for an actual steady-state two-level system. As a result, there are usually three or four energy levels in a laser transition scheme, and population is transferred to the effective excited state incoherently, hence the incoherent pump.

An important property of a laser is its linewidth, which could be measured using the correlation of the photons coming out of the cavity. The mathematical foundation of this method is the Wiener-Khintchine theorem [31] [22]:

$$S = 2\Re\left[\int_0^\infty d\tau g^{(1)}(\tau)e^{-i\omega\tau}\right] \quad (4.1)$$

where $g^{(1)}(\tau)$ is the first order correlation function

$$g^{(1)}(\tau) = \langle a^\dagger(\tau)a(0) \rangle. \quad (4.2)$$

The Fourier transform of the first order correlation function of the light coming out of the cavity provides us with the correlation spectrum of the laser. The FWHM of the spectrum is the linewidth of the laser. This method of linewidth measurement would be implemented in our simulation for steady-state superradiant laser [29].

4.2 Introduction to steady-state superradiant lasers

The prospect of building a superradiant laser was envisioned by Haake *et al* in 1993 [21] and Meiser *et al* in 2009. It was first realized using cold atoms by Thompson's group at the University of Colorado, Boulder in 2012, where they built a steady-state superradiant laser with less than one intracavity photon using strontium ultra-narrow clock transition [4].

Following the more modern meaning of the terminology, the basic idea behind a superradiant laser is that the coherence is stored in the atomic ensemble instead of the cavity, namely a superradiant laser is a laser operating in the bad cavity regime. In transitional lasers, as is demonstrated in Fig. 4.2, the cavity linewidth is much broader than that of the ensemble. Therefore, the cavity is responsible of maintaining the coherence of the system, making the linewidth of the laser sensitive to the technical noise of the cavity, including photon shot noise and thermal vibrations. Recent technological advances has pushed the transitional laser linewidth down to several Hz. However, that would still not meet the growing demand of a laser accurate enough to probe ultra-narrow atom clock transitions. For a superradiant laser, the linewidth of the ensemble is usually orders of magnitude higher than that of the cavity. As a result, the coherence is stored in the ensemble instead of the cavity, making the laser immune to the noise of the cavity, as is shown in Fig.4.3. Therefore, if an atomic clock transition were to be chosen as the laser transition, the superradiant laser would acquire an accuracy high enough to probe ultra-narrow linewidth transitions. However, in the 2009 proposal, the collective couplings between the atoms in the ensemble was not considered in the model. It was later modeled by Meiser *et al* in their 2009 paper, of which the result will be replicated in this part of the thesis.

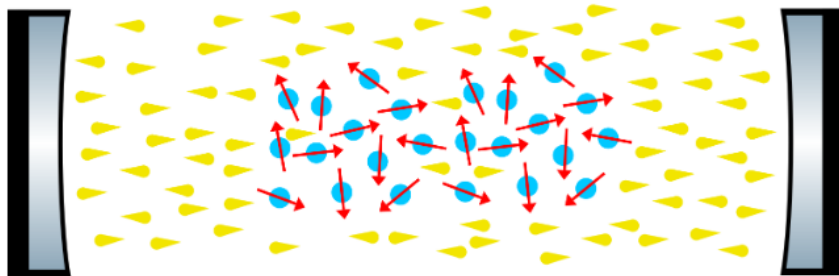


Figure 4.2: The diagram of a normal laser

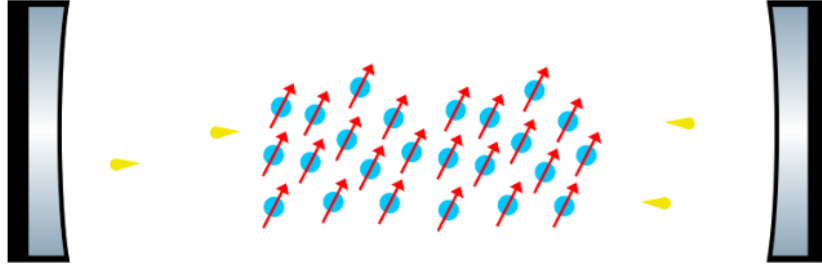


Figure 4.3: The diagram of a superradiant laser

In the original paper by Haake *et al*, it was proposed that the linewidth of the laser would be proportional to the inverse square of the population. This is derived roughly from the understanding that the number of photons from the superradiant process is proportional to the square of the number of atoms. As the linewidth is inversely related to the number of photons, the linewidth will go as inverse population squared. However, this simple derivation ignores the phase noise and the decoherence introduced by the collective couplings. When the laser is in the bad cavity regime, its linewidth would be sensitive to the noises in the collective atomic dipole. In the next section, I would try to build an intuitive understanding of the superradiant lasers by replicating one of the results of the 2009 paper by Meiser *et al*.

4.3 A simple superradiant laser simulation

This simulation is trying to replicate the result from ref.[25]. The program was written in Julia using QuantumOptics package [23] and is available in the appendix. The purpose of this simulation is to study the effect of the cooperative emission on the steady-state superradiance. To be more specific, we are changing the population of the Lamb-Dicke ensemble to see the change in the linewidth of the laser, which was a major unanswered question in our group before. Cooperative couplings would definitely have an impact on the properties of the laser. The intuition is that the superradiance effect, or the collective dissipative coupling would broaden the linewidth, as the dipole-dipole interaction and the dissipative couplings would introduce additional phase noise and decoherence of the collective atomic dipole [25] [29]. As a result, the more population we have in the ensemble, the broader the linewidth will be.

For a superradiant laser system, the Hamiltonian of the system is given by

$$H = H_0 + H_d + H_{AF} + H_p, \quad (4.3)$$

where the H_d term is the dipole interaction term, the H_{AF} term is the interaction between the atoms and the cavity field, and the H_p term is the coherent pump process. However, as discussed in the introduction part of this chapter, there will be no coherent pumping in the model, so we set $\omega_p = 0$.

$$H_0 = \sum_i \Delta_a \sigma_i^+ \sigma_i^- + \Delta_c a^\dagger a \quad (4.4)$$

$$H_d = \sum_{ij} \Omega_{ij} \sigma_i^+ \sigma_j^- \quad (4.5)$$

$$H_{AF} = \sum_i g(a^\dagger \sigma_i^- + a \sigma_i^+) \quad (4.6)$$

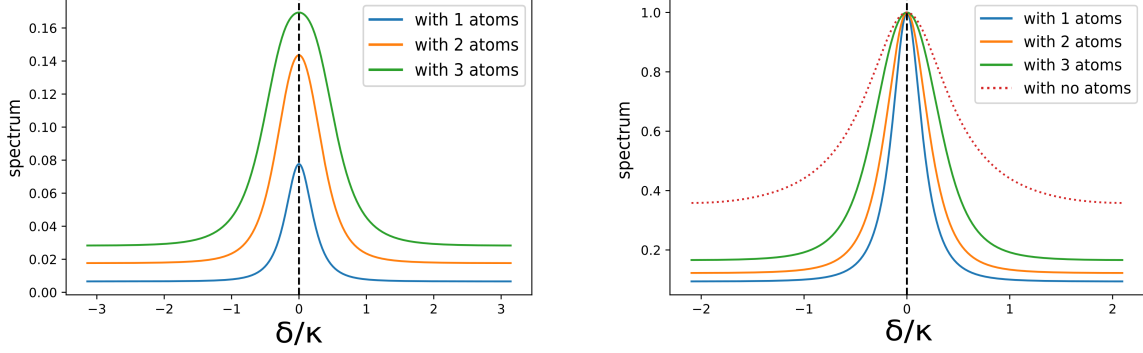
$$H_p = \sum_i \omega_p (\sigma_i^+ + \sigma_i^-). \quad (4.7)$$

Subsequently, we can represent the losses of the system by the Liouvillian operators. In our system, we have the cavity loss κ , the atomic spontaneous emission Γ , and the incoherent pumping broadening R . The Liouvillians of the system could be written as

$$\begin{aligned} \mathcal{L}_{sp}[\rho] &= \sum_{i,j} \frac{\Gamma_{ij}}{2} (2\sigma_i^- \rho \sigma_j^+ - \sigma_j^+ \sigma_i^- \rho - \rho \sigma_i^+ \sigma_j^-) \\ \mathcal{L}_c[\rho] &= \frac{\kappa}{2} (2a\rho a^\dagger - a^\dagger a \rho - \rho a^\dagger a) \\ \mathcal{L}_p[\rho] &= \sum_{i,j} \frac{R_{ij}}{2} (2\sigma_i^+ \rho \sigma_j^- - \sigma_j^- \sigma_i^+ \rho - \rho \sigma_i^- \sigma_j^+) \end{aligned} \quad (4.8)$$

In the simulation, we assume that the size of the ensemble is small compared with the size of the cavity and the wavelength of the mode, so that the atoms are uniformly coupled to the field inside the cavity, and we can apply the Lamb-Dicke regime approximation, which would simplify the simulation process. To get the linewidth of the superradiant laser, we need to calculate the first order correlation spectrum of the steady state of the system. Numerically, this could be done by first solving for the steady state using the master equation. Then we apply the annihilation operator a and evolve the state for time

τ . After that, we apply the creation operator $a^\dagger(\tau)$ and Fourier transform the result to get the first order correlation spectrum [25] [29]. The results are shown in Fig.4.4.



(a) Spectrum of the laser with different population
(b) Normalized spectrum of the laser with different population

Figure 4.4: Steady state superradiant laser linewidth change with population

From Fig.4.4, we can see that the intensity of the laser is nonlinearly increasing with the population. In addition, as we increase the population inside the cavity, the linewidth of the laser gets broader. This agrees with the result of the paper by Meiser *et al*, specifically Fig.3, where they are also investigating the linewidth change of the superradiant laser with increasing number of atoms. In my simulation, the ensemble, which consists of different numbers of two-level atoms is in the Lamb-Dicke regime. I assume that all the atoms are coupled to the cavity field uniformly. The cavity linewidth κ is 20 times the single-atom spontaneous emission rate Γ . The pumping broadening is incoherent and non-collective. The pumping rate is 8 times Γ . There is no detuning between the atom and the cavity, and between the pumping laser and the atomic transition. The atom-field coupling is chosen to be around the same order of magnitude as Γ . In the result shown in Fig.4.4, it was set to be 6Γ .

There are a lot of rooms to explore further in this project. For example, it would be interesting to look into the extended 1-D ensemble regime of the superradiant laser, which would be a nice simulation for the future experiments in this lab. Also, people can add broadening incoherent non-collective decay into the system to see the transition from a superradiant laser to a normal laser.

Chapter 5

Experiment: Observation of spontaneous Raman emission in cold atoms inside a hollow-core waveguide

5.1 Introduction

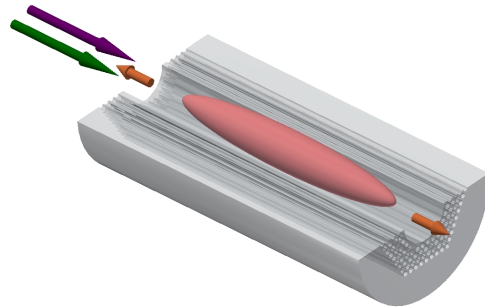


Figure 5.1: Spontaneous Raman emission in cold atoms inside a hollow-core photonic crystal fiber

In this chapter, I would like to discuss the experiment we carried out in the fall of 2017 where

we were trying to observe superradiance using our setup, which is cold cesium atoms inside a hollow-core photonic crystal fiber (HCPCF). We used the Raman three-level scheme for our superradiance transition. The project proceeded for almost four months, for which I was mainly performing data analysis and some experimental aid to the post doc, Taehyun Yoon, who built the main experimental setup. Eventually, using a novel detection scheme, we successfully observed spontaneous emission from the cold atom ensemble, where we measured the population evolution on the ground state instead of the light emitted from the ensemble. This technique, including the initial experimental results were submitted to Optics Express in February, 2019 [46], of which I am the second author.

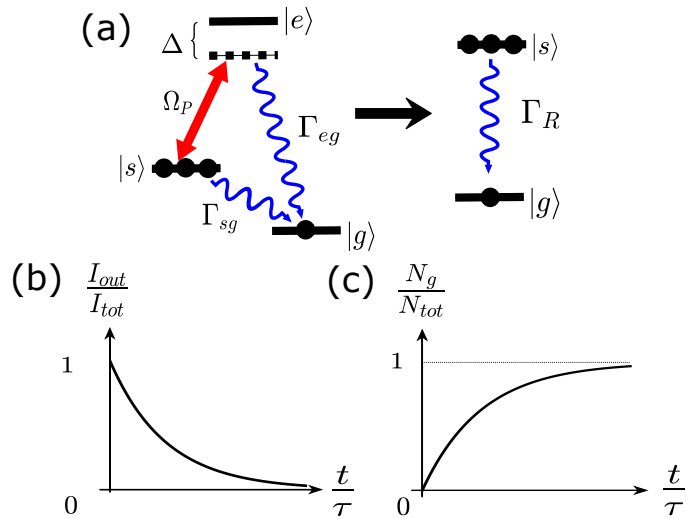


Figure 5.2: (a) Schematics of Raman transition in a Λ -type three level system and the corresponding effective two level system. (b) The normalized intensity of the emitted light and (c) the atomic population in the ground state as a function of time for an exponential decay in a two level system.

In this chapter, I would like to briefly introduce our experimental setup, which could be found in greater detail in ref.[45], and discuss the data analysis, which I was mainly responsible for. Some of my experimental contributions are discussed in the Appendix, including the PID circuit, the 795nm beam path and the AOM driver operating at 200MHz.

Laser-cooled atomic ensemble inside a HCPCF offers a hitherto untapped platform for experiments on potentially new regimes of superradiance phenomena, as HCPCF provides a much smaller mode area to enhance light-matter interaction rate compared to free-space

experiments and a more exotic ensemble geometry with extremely high ratio ($\sim 10^3 - 10^4$) between the diameter and the length of the cloud [45]. The three-level scheme used by the experiment was discussed in detail in the second chapter, where it is pointed out that this scheme offers full controllability over the transition. It is recapped in Fig.5.2, where the population is prepared in the metastable state $|s\rangle$, and is scattered to $|g\rangle$ through the excited state $|e\rangle$ using the pump laser Ω_P and spontaneous emission Γ_{eg} . This system can be viewed as an effective two-level system between $|s\rangle$ and $|g\rangle$, and the transition between them could be completely shut down when the pump is turned off [46]. As a result, the novel detection scheme for superradiance is to study the evolution of the population on the ground state by turning the pump laser on for increasingly longer durations. The population on the ground state is measured by blasting the system with a known amount of photons that scatters the ground state population to a dark state and measuring the number of lost photons at the other end of the ensemble. Then the number of atoms in the ground state would be correlated to the lost photons [46]. This technique was largely implemented in our experiment when we discovered that we have additional broadening in the atomic transitions that rendered the more traditional optical-depth measurement less accurate.

5.2 Experimental setup

The information provided in this chapter largely comes from ref.[45] and a group meeting presentation by Dr.Taehyun Yoon on February 8, 2018. I hereby express my gratitude towards him for providing me with these materials.

Fig.5.3(a) and (b) shows the experimental apparatus [45]. As an overview, the atoms are cooled inside the chamber and then loaded into the erected hollow-core fiber by gravity under the guidance of a dipole-trap laser. The fiber (HC-800-02, NKT Photonics) with an inner core of $\sim 5.5\mu m$ is vertically mounted in a ColdQuanta glass cell serves as an ultrahigh vacuum chamber ($\sim 10^{10}$ torr) maintained by nonevaporable getter pump and an ion pump. The whole vacuum system is mounted on a 1-m-long CNC rails so that the it would be easily moved out of the optics setup for fiber exchange with minimum experimental downtime and disruption. The 935 nm dipole trap laser is provided by a Ti:Sapphire laser (SolsTis by M Squared). The dipole trap laser is combined with a weak probe before being coupled into the fiber from the bottom of the cell by an aspherical lens ($f = 18$ mm) [45] outside the chamber at an efficiency of 40% – 50%. The beam is recollimated

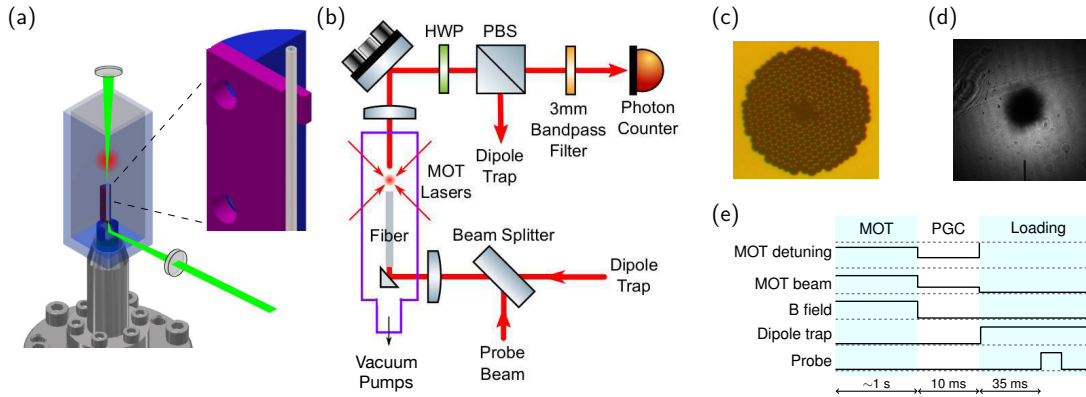


Figure 5.3: (a) The glass cell containing the MOT and the hollow-core fiber and a detail of the fiber mounting structure. (b) Schematic of the overall experimental setup. (c) Microscope image of the cross section of the hollow-core fiber. (d) Absorption image of the atomic cloud right after polarization gradient cooling. The fiber tip can be seen at the bottom. (e) Time sequence of our experimental procedure. This figure is from ref.[45]

by another aspheric lens at the top of the cell when it is coming out of the fiber. Then it is filtered out by a combination of a half-wave plate, a polarization beam splitter and a 3-nm-wide bandpass filter in front of the single photon module (Excelitas Technologies Corp, SPCM-AQRH-NIR). [45]

The control scheme is shown in Fig.5.4. The GUI program controlling the entire experimental setup is written in C/C++ using QT, and NI ANSI C/C++ libraries and is stored on a computer in the lab, which has an NI DAQ card (PCI-6259) plugged onto its mother board. The NI DAQ card has 32 analog inputs and 4 analog outputs controlling the laser power and the magnetic field used for laser cooling and trapping. Both of the inputs and the outputs have a resolution of 16 bits. There are 2 counters for photon detection with a TTL logic level and maximum source frequency of 80MHz. In addition, there are 48 digital IO ports on the board for switching and serial commands with a maximum clock rate of 10MHz. All of these connections are facilitated by an NI connector block and a BNC connection board, from which all the devices, including the laser systems and the acousto-optic modulator (AOM) drivers are talking to the NI DAQ card.

The laser systems consist of a Vescent laser system and a Ti:Sapphire laser. The Vescent laser system has a master laser and 3 slave lasers. The master laser is locked onto the Cs D_2 transition ($6^2S_{1/2} \rightarrow 6^2P_{3/2}$, 532nm) using saturation spectroscopy, while all the

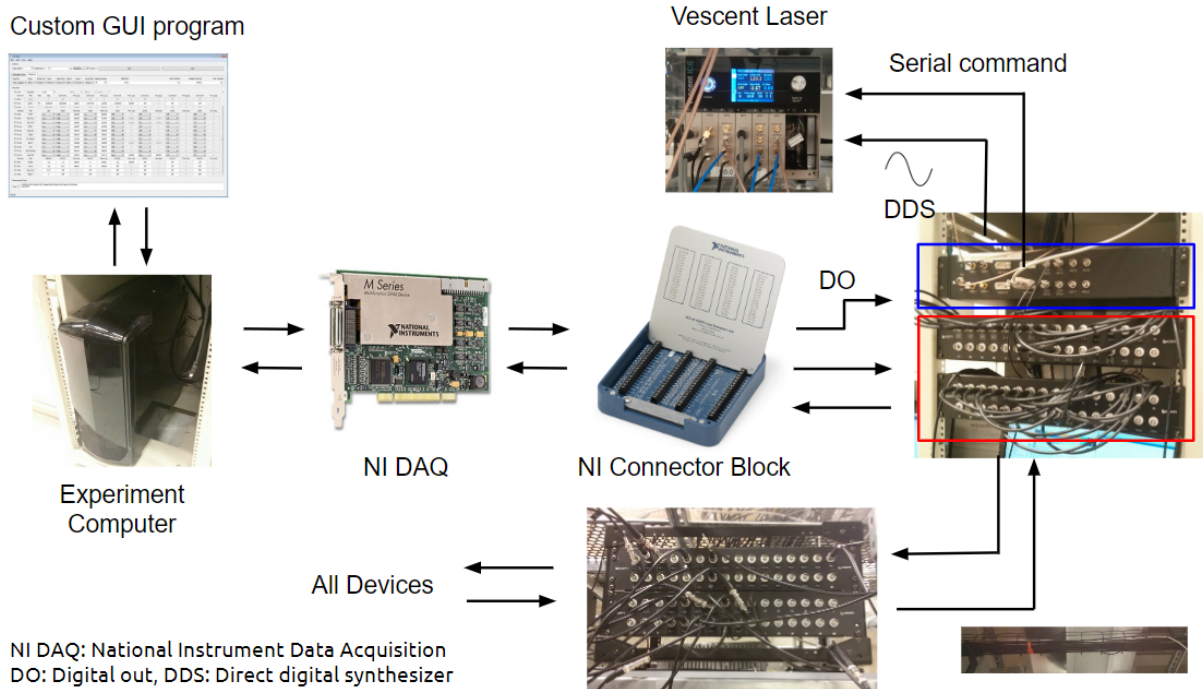


Figure 5.4: Connections between the control and the experimental apparatus

slave lasers are locked onto the master laser using offset locking. They are mainly used for cooling, control and probe beams in the experiment. The Ti:Sapphire laser has a tunable wavelength range from 690-1000 nm and a power of 2.0W. It is used as a dipole trap at 935 nm, which is the Cs magic wavelength. The AOM drivers and the AOMs will be discussed in the Appendix.

The magnetic field for the magneto-optic trap (MOT) is generated by a pair of Helmholtz coils sandwiching the Cs glass cell. It is controlled by the NI DAQ analog output and a proportional-integral-derivative (PID) controller which stabilizes the signal with a feedback loop. The PID controller would be discussed in greater detail in the appendix. The single-photon counting module (SPCM) is triggered by TTL signals generated by the NI DAQ card and is gathering signals from a single-mode fiber patch cable. [45]

5.3 Experimental procedure

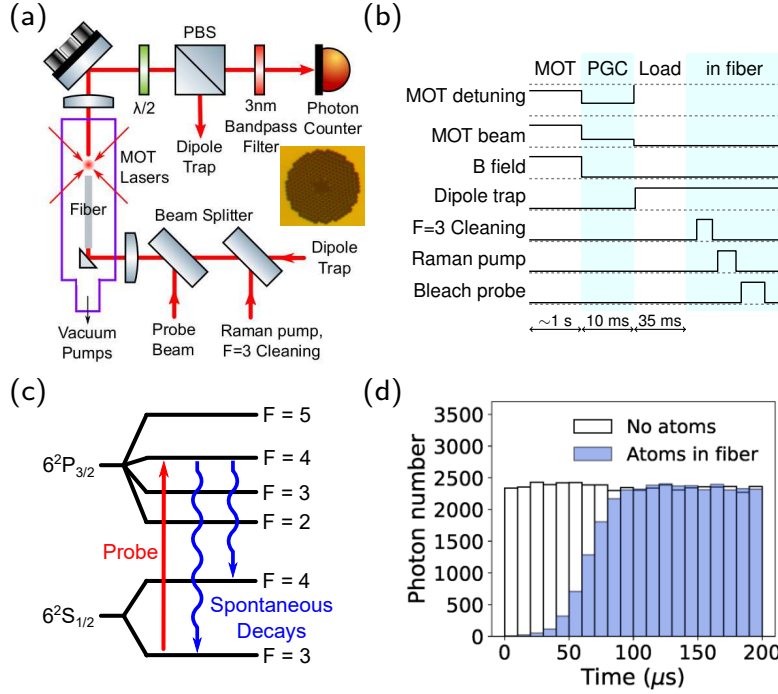


Figure 5.5: (a) Schematics of the experiment with an inset showing a microscope image of the cross section of the hollow-core fiber. (b) Time sequence of the experimental procedure. (c) Diagram of the cesium energy levels involved in detection of atoms. (d) Histograms of the probe photon counts with and without atoms inside the fiber. The figure is from Fig.2 of ref.[46].

We use the Cs D_2 transition ($6^2S_{1/2} \rightarrow 6^2P_{3/2}$, 532nm) for both the laser cooling and the Raman transition scheme. The control signals are shown in Fig.5.5. The trapping beam detuned from the cycling transition $|F = 4\rangle \rightarrow |F' = 5\rangle$ cool and trap $\sim 10^8$ atoms $\sim 5\text{mm}$ over the tip of the fiber, which is shown in Fig.5.3 [45]. A repumper laser, which is resonant on the transition $|F = 3\rangle \rightarrow |F' = 3\rangle$ recycles atoms from the dark state $|F = 3\rangle$ to the cycling transition [45]. The MOT beam will cool the atoms down to several hundred mK. Then the atoms are further cooled down to $12\mu\text{K}$ using polarization gradient cooling (PGC) for 10 ms [45]. After that, all the cooling beams and trapping fields are shut down

to let the atomic cloud free-falling into the fiber under the influence of gravity and the guidance of the dipole trap laser, which is turned on once all the other beams are shut off.

When the atoms are inside the fiber, we start sending the control and the probe beams into the fiber to perform the experiments. For the three-level superradiance, we chose $6^2S_{1/2}|F = 3\rangle$, $6^2S_{1/2}|F = 4\rangle$ and $6^2P_{3/2}$ as the $|g\rangle$, $|s\rangle$ and $|e\rangle$. When the atoms are first in the fiber, there is still some population left in the $6^2S_{1/2}|F = 3\rangle$ state and would be needed to clean up using the repumping beam $|F = 3\rangle \rightarrow |F' = 3\rangle$ for several microseconds [45] [46]. After that, the pump beam is on for certain duration, and subsequently turned off. The probe beam on resonance with the transition $|F = 3\rangle \rightarrow |F' = 4\rangle$ is then sent in to measure the population [46], which is shown in Fig.5.5. Now, $6^2S_{1/2}|F = 4\rangle$ is a dark states. As we are probing the atoms on $6^2S_{1/2}|F = 3\rangle$, we are losing population to $6^2S_{1/2}|F = 4\rangle$, resulting in an increasingly transparent ("bleached") atomic medium for the probe beam, which is shown in the histogram in Fig.5.5. The number of lost photons at the beginning of the novel measurement process is related to the population on $6^2S_{1/2}|F = 3\rangle$ by the ratio of the branching ratios between $|F' = 4\rangle \rightarrow |F = 3\rangle$ and $|F' = 4\rangle \rightarrow |F = 4\rangle$ [46].

5.4 Experimental results

The experimental results are shown in Fig.5.6. We extract the decay rate Γ_R from the population evolution curve shown in (a), which is constructed using the data yielded by the novel measurement technique described in the last section. The inset of (a) shows the original histograms that were used to create the evolution. For each Raman pump duration, the population is measured by extracting the total amount of missing photons from the histograms. As is shown in the inset, as time goes on, the population is gradually bleached by the incoming photons and eventually the transmitted photon number plateaus. In my program, I defined this plateau to be the saturation level. Specifically, I calculated the average amount of photons for the last few columns in the graph. Then I recovered the amount of missing photons from the unsaturated part of the histogram by subtracting the photon number in each column from the saturation level.

The branching ratio for $|F' = 4\rangle \rightarrow |F' = 3\rangle$ is 5/12, and the one for $|F' = 4\rangle \rightarrow |F' = 4\rangle$ is 7/12. This means that of 12 atoms decaying from $|F' = 4\rangle$, 5 will go to $|F = 3\rangle$ and 7 will go to $|F = 4\rangle$. The number of missing photons are only responsible for the ones that

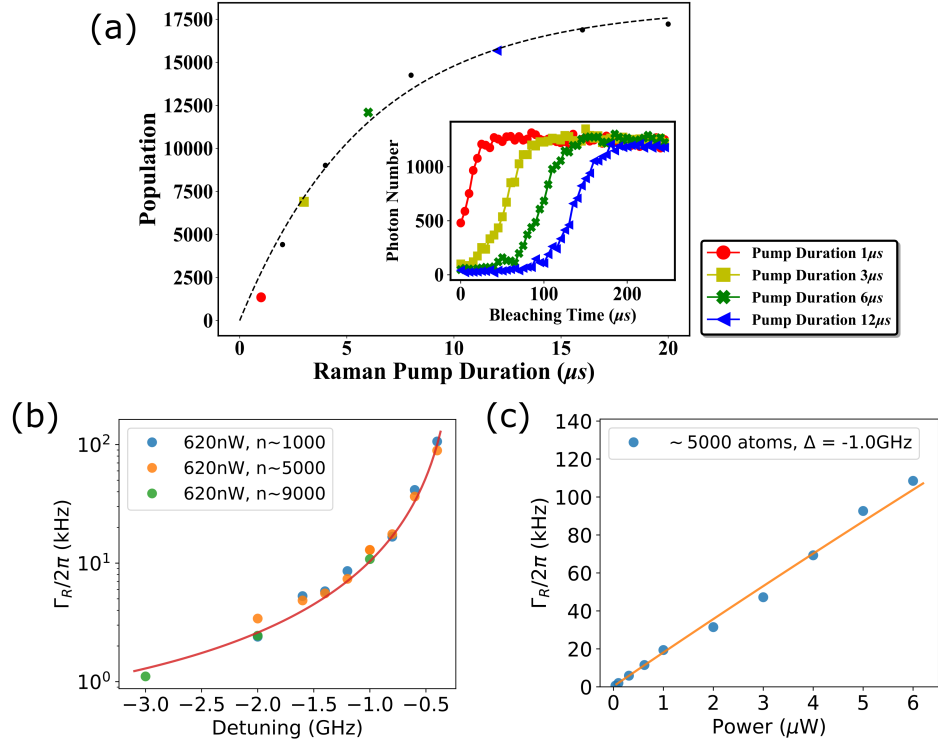


Figure 5.6: (a) Measured data on the ground state population versus the pump duration. The dashed line is a fit of Eq.5.2 with Γ_R as the fitting parameter found to be $2\pi \times 18.4$ kHz. The inset shows the counts of the transmitted probe photons vs. time during the measurement process. The colored markers indicate the atom numbers that are derived from each shape- and color-matched plot in the inset. The decay rates, Γ_R , obtained from the fits at (b) different pump powers and (c) different pump detunings. Solid lines in (b) and (c) are fits of Eq.5.4, with $\Gamma_S g$ and the atoms' distribution factor μ being the fitting parameters. This figure is from Fig.3 of ref.[46].

dropped onto $|F = 4\rangle$. As a result, when trying to extract the number of atoms on $|F = 3\rangle$, we need to multiple the photon loss by 12/5. Also, the SPCM detector has an efficiency of 55% at the wavelength of the probe, which is also taken into account in the analysis. The formula for the conversion between number of photons counted and the number of atoms on the ground state is shown below.

$$\text{number of atoms} = \text{number of photons} \times \frac{1}{\text{branching ratio}} \times \frac{1}{\text{detector efficiency}} \quad (5.1)$$

In the initial data analysis, we fitted the evolution of the ground state population with an exponential function, [46]

$$N_g = N_{\text{tot}}(1 - e^{-\Gamma_R t}), \quad (5.2)$$

and repeated the experiments with different pump powers and detunings, as well as different populations ranging from 1000 to 12000 atoms in the fiber [46]. The results are shown in Fig.5.6(b) and (c). In our system, the total effective decay rate, Γ_R can be seen as the sum of all the different decay rates.

$$\Gamma_R = \Gamma_{sg} + \Gamma_{eg} \quad (5.3)$$

The decay rate from $|e\rangle$ to $|g\rangle$ is proportional to $\Gamma_e \rho_{ee}$, where Γ_e is the decay rate of the D_2 transition line and ρ_{ee} is the population on $|e\rangle$, which is a function of the pump power and pump detuning [46]. Combining all the information above, the transition rate between $|s\rangle$ and $|g\rangle$ can be expressed as

$$\Gamma_R \approx \Gamma_{sg} + \Gamma_e \sum_{F'=3,4 \rightarrow F=3} a_{F' \rightarrow F=3} \frac{\Omega_{F'}^2}{4\Delta_{F'}^2 + 2\Omega_{F'}^2}. \quad (5.4)$$

where a is the branching ratio. There are some unknown parameters in this equation that are introducing difficulties into the theoretical prediction of the transition rate $|s\rangle \rightarrow |g\rangle$. For example, it is not quite clear what the actual value of the non-light induced transition rate Γ_{sg} would be [46]. Also, in order to determine the Rabi oscillation frequency in eq.5.4, we need to know the effective light intensity, which is a function of the radial distribution factor μ of the atomic cloud inside the fiber. From previous experiments on the AC-Stark shifts at different dipole trap wavelengths, it is measured that the radial distribution factor is $\mu = 1.61$. The fitting for different pump detunings gives us $\mu = 1.63$, and the fitting for different pump powers gives us $\mu = 1.72$. The change of the radial distribution factor may be caused by a change in the AC-Stark shift due to a higher pump power, but the results are close to each other within a reasonable range. [46]

However, it should be noted that the ground state population evolution curve in Fig.5.6(a) does show a slight deviation from the fitting. It shows a faster decay rate before $10\mu s$ and a slightly slower saturation rate at $t = 20\mu s$. They are possibly signs of a cooperative emission process, as they share the same geometrical properties as the simulation results obtained in the previous chapter. However, it is clear that the phenomenon is not very obvious in the current experimental results. If this experimental project were to be carried

on in the near future, people should try to increase the population density inside the fiber to make the cooperative effect more pronounced. Also, there is the need to come up with a more quantitative way of analyzing and evaluating the cooperative effects in the atomic ensemble for future experiments. The simulations and the analysis shown in this thesis are for building a solid understanding of superradiance, but they are not an ideal choice to be directly implemented in an actual experiment as a data-analysis method.

Chapter 6

Conclusion

The work presented in this thesis has three main parts. The first part is the derivation of the Hamiltonian describing the cooperative emission process. It is a more specific case of the master equation of open quantum systems. The second part consists of a series of computer simulations for free-space superradiance, waveguide superradiance and cavity superradiance for a 1-D lattice of atoms. The third part is an experimental paper that has been accepted for publication in *Optical Express* in May 2019. In the paper, we have developed a detection scheme for superradiance in our experimental setup, namely hollow-core photonic crystal fiber-based quantum optics. The main contribution of this thesis is to build up intuitive understanding of cooperative spontaneous emission processes through various computer simulations for multiple different physical settings, including ones that are tailored to our own experimental platform. This would provide insights for experimental work, such as looking for the experimental signatures of superradiance, the transition from cooperative spontaneous emission to uncorrelated spontaneous emission of the ensemble, and building a steady-state superradiant laser.

Though the formalism of superradiance has been well-established in the field, the contents of this thesis, especially the mathematical derivation of the superradiance Hamiltonian and the simulations are important to us as a research group and would make contributions to our future endeavor. When we started with the experimental investigation of superradiance with our setup in 2017 with the eventual goal of building a superradiant laser, we were mostly developing the detection schemes and looking for the signals without a very solid understanding of superradiance. Several important questions, including the experimental signatures, the physics of cooperative emission processes, the transition between superradiance and spontaneous emission and the difference between a normal laser and a

superradiance laser were largely unclear and poorly studied. Though the simulations in this thesis are not directly applicable to our actual experiments, as there is no computer in the world currently with the capability of running a fully quantum simulation effectively, the work presented in this thesis solved these aforementioned problems to a large extent and would greatly facilitate future studies of superradiance in our lab.

References

- [1] How does a pid controller work? - structure and tuning methods, Nov 2018.
- [2] Anatolii V Andreev, Vladimir I Emelyanov, and Yu A Ilinskii. Collective spontaneous emission (dicke superradiance). *Soviet Physics Uspekhi*, 23(8), 1980.
- [3] M G Benedict, A M Ermolaev, V A Malyshev, I V Sokolov, and E D Trifonov. *Superradiance: multiatomic coherent emission*. Institute of physics publ., 1996.
- [4] Justin G. Bohnet, Zilong Chen, Joshua M. Weiner, Dominic Meiser, Murray J. Holland, and James K. Thompson. A steady-state superradiant laser with less than one intracavity photon. *Nature*, 484(7392), 2012.
- [5] N.w. Carlson, D.j. Jackson, A.l. Schawlow, M. Gross, and S. Haroche. Superradiance triggering spectroscopy. *Optics Communications*, 32(2), 1980.
- [6] R. H. Dicke. Coherence in spontaneous radiation processes. *Physical Review*, 93(1), 1954.
- [7] Paul A.M. Dirac. Emission and absorption of radiation. *Proceedings of Royal Society*, 114(243), 1927.
- [8] A. Einstein. Über einen die erzeugung und verwandlung des lichtet betreffenden heuristischen gesichtspunkt. *Annalen der Physik*, 322(6):132–148, 1905.
- [9] A. Einstein. Strahlungs-emission und absorpition nach der quantentheorie. *Deutsche Physikalische Gesellschaft*, 18, 1916.
- [10] A. Einstein. Zur quantentheorie der strahlung. *Physikalische Zeitschrift*, 18, 1917.
- [11] Z. Ficek and R. Tanas. Entangled states and collective nonclassical effects in two-atom systems. *Physics Reports*, 372(5), 2002.

- [12] R. Florian, L.o. Schwan, and D. Schmid. Superradiance and high-gain mirrorless laser activity of o_2 centers in kcl. *Solid State Communications*, 42(1), 1982.
- [13] Reinhold Florian, Lothar O. Schwan, and Dankward Schmid. Time-resolving experiments on dicke superfluorescence of o_2 centers in kcl. two-color superfluorescence. *Physical Review A*, 29(5), 1984.
- [14] A. Flusberg, T. Mossberg, and S.r. Hartmann. Observation of dicke superradiance at $1.30 \mu\text{m}$ in atomic tl vapor. *Physics Letters A*, 58(6), 1976.
- [15] C. W. Gardiner and P. Zoller. *Quantum noise: a handbook of Markovian and non-Markovian quantum stochastic methods with applications to quantum optics*. Springer, 2010.
- [16] H. M. Gibbs, Q. H. F. Vrehen, and H. M. J. Hikspoors. Single-pulse superfluorescence in cesium. *Phys. Rev. Lett.*, 39, Aug 1977.
- [17] A. Goban, C.-L. Hung, J.D. Hood, S.-P. Yu, J.A. Muniz, O. Painter, and H.J. Kimble. Superradiance for atoms trapped along a photonic crystal waveguide. *Physical Review Letters*, 115(6), 2015.
- [18] P. Goy, L. Moi, M. Gross, J. M. Raimond, C. Fabre, and S. Haroche. Rydberg-atom masers. ii. triggering by external radiation and application to millimeter-wave detectors. *Physical Review A*, 27(4), 1983.
- [19] M. Gross, C. Fabre, P. Pillet, and S. Haroche. Observation of near-infrared dicke superradiance on cascading transitions in atomic sodium. *Physical Review Letters*, 36(17), 1976.
- [20] M. Gross and S. Haroche. Superradiance: An essay on the theory of collective spontaneous emission. *Physics Reports*, 93(5), 1982.
- [21] Fritz Haake, Mikhail I. Kolobov, Claude Fabre, Elisabeth Giacobino, and Serge Reynaud. Superradiant laser. *Physical Review Letters*, 71(7), 1993.
- [22] Christoph Hotter. *Superradiant cooling, trapping and lasing of dipole-interacting clock atoms*. PhD thesis, 2018.
- [23] Sebastian Kraemer, David Plankensteiner, Laurin Ostermann, and Helmut Ritsch. Quantumoptics.jl: A julia framework for simulating open quantum systems. *Computer Physics Communications*, 227, 2018.

- [24] J. C. Macgillivray and M. S. Feld. Theory of superradiance in an extended, optically thick medium. *Physical Review A*, 14(3), 1976.
- [25] Thomas Maier, Sebastian Kraemer, Laurin Ostermann, and Helmut Ritsch. A super-radiant clock laser on a magic wavelength optical lattice. *Optics Express*, 22(11):13269, 2014.
- [26] Michelle S. Malcuit, Jeffery J. Maki, David J. Simkin, Boyd, and Robert W. Transition from superfluorescence to amplified spontaneous emission. *Physical Review Letters*, 59(11), 1987.
- [27] D. Meiser, Jun Ye, D. R. Carlson, and M. J. Holland. Prospects for a millihertz-linewidth laser. *Physical Review Letters*, 102(16), 2009.
- [28] Matthew A. Norcia, Matthew N. Winchester, Julia R. K. Cline, and James K. Thompson. Superradiance on the millihertz linewidth strontium clock transition. *Science Advances*, 2(10), 2016.
- [29] Laurin Ostermann. *collective radiation of coupled atomic dipoles and the precise measurement of time*. PhD thesis, 2016.
- [30] Laurin Ostermann, Clement Meignant, Claudiu Genes, and Helmut Ritsch. Super- and subradiance of clock atoms in multimode optical waveguides. *New Journal of Physics*, 21(2):025004, 2019.
- [31] Ravinder R. Puri. *Mathematical methods of quantum optics*. Springer, 2011.
- [32] R. Rohlsberger, K. Schlage, B. Sahoo, S. Couet, and R. Ruffer. Collective lamb shift in single-photon superradiance. *Science*, 328(5983), 2010.
- [33] Jun John Sakurai and Jim Napolitano. *Modern quantum mechanics*. Pearson India Education Services, 2018.
- [34] Michael Scheibner, Thomas Schmidt, Lukas Worschech, Alfred Forchel, Gerd Bacher, Thorsten Passow, and Detlef Hommel. Superradiance of quantum dots. *Nature Physics*, 3(2), 2007.
- [35] Achim Schiller, Lothar O. Schwan, and Dankward Schmid. Large-sample effects in superfluorescence of o_2 centers in kcl. *Journal of Luminescence*, 38(1-6), 1987.

- [36] Achim Schiller, Lothar O. Schwan, and H.dankward Schmid. Spatial coherence in large-sample superfluorescence of o_2 centers in kcl. *Journal of Luminescence*, 40-41, 1988.
- [37] L. O. Schwan, P. Schwendimann, and E. Sigmund. Correlations in extended high-density superfluorescence: A self-organized distributed feedback laser. *Physical Review A*, 40(12), 1989.
- [38] M. O. Scully and A. A. Svidzinsky. The super of superradiance. *Science*, 325(5947), 2009.
- [39] Marlan O. Scully. Collective lamb shift in single photon dicke superradiance. *Physical Review Letters*, 102(14), 2009.
- [40] N. Skribanowitz, I. P. Herman, J. C. Macgillivray, and M. S. Feld. Observation of dicke superradiance in optically pumped hf gas. *Physical Review Letters*, 30(8), 1973.
- [41] Daniel Steck. *Quantum and atom optics*. 2019.
- [42] Haruka Tanji. *Few-photon nonlinearity with an atomic ensemble in an optical cavity*. PhD thesis, 2011.
- [43] E. Weisskopf, V.and Wigner. Berechnung der natuerlichen linienbreite auf grund der diracschen lichttheorie". *Zeitschrift für Physik*", 63(1), Jan 1930.
- [44] E. Weisskopf, V.and Wigner. Ueber die natuerliche linienbreite in der strahlung des harmonischen oszillators. *Zeitschrift für Physik*, 65(1), Nov 1930.
- [45] Taehyun Yoon and Michal Bajcsy. Laser-cooled cesium atoms confined with a magic-wavelength dipole trap inside a hollow-core photonic-bandgap fiber. *Physical Review A*, 99(2), 2019.
- [46] Taehyun Yoon, Zhenghao Ding, Jeremy Flannery, Fereshteh Rajabi, and Michal Bajcsy. From spontaneous to superradiant raman emission in cold atoms inside a hollow-core waveguide. *Optics Express*, accepted.

APPENDICES

Appendix A

Julia codes for the simulations

A.1 Two-level atoms in a 1-D lattice

A.1.1 Two-level atoms in a 1-D lattice in free space in the Lamb-Dicke regime

```
using PyPlot
using QuantumOptics

 $\Delta_a$  = 0.0 # detuned atom frequency

 $\Gamma$  = 1.0 # spontaneous loss rate
 $\gamma$  = 1.0 # dephasing loss rate

# atom ensemble parameters
L = 0.0 # atom ensemble length
Na = [2,3,4,5,6] # atom number

tspan = [0:0.01:4;]

population_ind_list = []
correlation_ind_list = []

population_list = []
correlation_list = []

for a in Na

    b_atom = SpinBasis(1//2) # single atom basis
    B = b_atoma # collective basis
```

```

# atom operator functions in atom basis
σ+(i) = embed(B,i,sigmap(b_atom))
σ-(i) = embed(B,i,sigman(b_atom))
σx(i) = embed(B,i,sigmax(b_atom)/2)
σy(i) = embed(B,i,sigmay(b_atom)/2)
σz(i) = embed(B,i,sigmaz(b_atom)/2)

# 1-D dipole-dipole interactions
F(ri, rj) = 1.5*Γ*(sin(2*π*abs(ri - rj))/(2*π*abs(ri - rj)) + cos(2*π*abs(ri - rj))
            /(2*π*abs(ri - rj))^2 - sin(2*π*abs(ri - rj))/(2*π*abs(ri - rj))^3)
G(ri, rj) = -3/4*Γ*(cos(2*π*abs(ri - rj))/(2*π*abs(ri - rj)) - sin(2*π*abs(ri - rj))
            /(2*π*abs(ri - rj))^2 + cos(2*π*abs(ri - rj))/(2*π*abs(ri - rj))^3)

# atomic position
d = L/a
pos = [d*(i-1) for i=1:a]
# pos = rand(N)
println("Atom position: $pos Å Ũ λ")

# building the Hamiltonians
H0 = Δa*sum(σz(i) for i=1:a)
Hdipole = sum(G(pos[i],pos[j])*σ+(i)*σ-(j) for i=1:a, j=1:a)
H = H0 + Hdipole

# decays
# J_col = [sum(σ-(i) for i=1:Na)]
J_col = [σ-(i) for i=1:a]
rates = [F(pos[i],pos[j]) for i=1:a, j=1:a]

ψ0 = tensor([spinup(b_atom) for i=1:a]...)
tout, ρt = timeevolution.master(tspan, ψ0, H, J_col; rates=rates)
tout, ρt_ind = timeevolution.master(tspan,ψ0,H0,J_col;rates=[Γ for i=1:a])

group_pop = sum(σ-(i)*σ+(i) for i=1:a)
dipoles = (sum(σ+(i) for i=1:a))*(sum(σ-(i) for i=1:a))

population = real(expect(group_pop, ρt))
correlation = real(expect(dipoles, ρt))

population_ind = real(expect(group_pop, ρt_ind))
correlation_ind = real(expect(dipoles, ρt_ind))

append!(population_list, population)
append!(correlation_list, correlation)

append!(population_ind_list, population_ind)
append!(correlation_ind_list, correlation_ind)

end

```

A.1.2 Two-level atoms in a 1-D lattice in free space in the extended ensemble regime

```

using PyPlot
using QuantumOptics

Δa = 0.0 # detuned atom frequency

Γ = 1.0 # spontaneous loss rate

# atom ensemble parameters
L = [0.1,0.2,0.3,0.5,1.0,2.0, 3.0] # atom ensemble length
a = 5 # atom number

tspan = [0:0.01:4;]

population_list = []
correlation_list = []

population_ind_list = []
correlation_ind_list = []

for i=1:length(L)

    b_atom = SpinBasis(1/2) # single atom basis
    B = b_atom^a # collective basis

    # atom operator functions in atom basis
    σ+(i) = embed(B,i,sigmap(b_atom))
    σ-(i) = embed(B,i,sigman(b_atom))
    σx(i) = embed(B,i,sigmax(b_atom)/2)
    σy(i) = embed(B,i,sigmay(b_atom)/2)
    σz(i) = embed(B,i,sigmaz(b_atom)/2)

    # 1-D dipole-dipole interactions
    F(ri, rj) = 1.5*Γ*(sin(2*π*abs(ri - rj))/(2*π*abs(ri - rj)) + cos(2*π*abs(ri - rj))
                / (2*π*abs(ri - rj))^2 - sin(2*π*abs(ri - rj))/(2*π*abs(ri - rj))^3)
    G(ri, rj) = -3/4*Γ*(cos(2*π*abs(ri - rj))/(2*π*abs(ri - rj)) - sin(2*π*abs(ri - rj))
                ) / (2*π*abs(ri - rj))^2 + cos(2*π*abs(ri - rj))/(2*π*abs(ri - rj))^3)

    # atomic position
    d = L[i]/a
    pos = [d*(i-1) for i=1:a]
    # pos = rand(N)
    println("Atom position: $pos Å λ")

    # building the Hamiltonians
    H0 = Δa*sum(σz(i) for i=1:a)

    Hdipole_dumb = sum(1*σ+(i)*σ-(j) for i=1:a, j=1:a)
    Hdipole = Hdipole_dumb*0
    for i=1:a
        for j=1:a
            if j!=i

```

```

        Hdipole = Hdipole + G(pos[i],pos[j])* $\sigma^+$ (i)* $\sigma^-$ (j)
    else
        Hdipole = Hdipole + 0* $\sigma^+$ (i)* $\sigma^-$ (j)
    end
end
end
H = H0 + Hdipole

# decays
# J_col = [sum( $\sigma^-$ (i) for i=1:Na)]
J_col = [ $\sigma^-$ (i) for i=1:a]

rates_0 = zeros(0)
for i=1:a
    for j=1:a
        if j!=i
            append!(rates_0,F(pos[i],pos[j]))
        else
            append!(rates_0,1)
        end
    end
end

rates = reshape(rates_0,a,:)

print(rates)

 $\psi_0$  = tensor([spinup(b_atom) for i=1:a]...)
tout,  $\rho_t$  = timeevolution.master(tspan,  $\psi_0$ , H, J_col; rates=rates)
tout,  $\rho_{t\_ind}$  = timeevolution.master(tspan, $\psi_0$ ,H0,J_col;rates=[ $\Gamma$  for i=1:a])

group_pop = sum( $\sigma^-$ (i)* $\sigma^+$ (i) for i=1:a)
dipoles = (sum( $\sigma^+$ (i) for i=1:a))*(sum( $\sigma^-$ (i) for i=1:a))

population = real(expect(group_pop,  $\rho_t$ ))
correlation = real(expect(dipoles,  $\rho_t$ ))

population_ind = real(expect(group_pop,  $\rho_{t\_ind}$ ))
correlation_ind = real(expect(dipoles,  $\rho_{t\_ind}$ ))

append!(population_list, population)
append!(correlation_list, correlation)

append!(population_ind_list, population_ind)
append!(correlation_ind_list, correlation_ind)

end

```

A.1.3 Two-level atoms in a 1-D lattice in an ideal single-mode fiber

```

using PyPlot
using QuantumOptics

 $\Delta a$  = 0.0 # detuned atom frequency

 $\Gamma$  = 1.0 # spontaneous loss rate

# atom ensemble parameters
L = [0,0.1,0.2,0.3,0.5,1.0,2.0] # atom ensemble length
a = 5 # atom number

tspan = [0:0.01:4;]

population_list = []
correlation_list = []

population_ind_list = []
correlation_ind_list = []

for k in L

    b_atom = SpinBasis(1//2) # single atom basis
    B = b_atom^a # collective basis

    # atom operator functions in atom basis
     $\sigma^+$ (i) = embed(B,i,sigmap(b_atom))
     $\sigma^-$ (i) = embed(B,i,sigmam(b_atom))
     $\sigma^x$ (i) = embed(B,i,sigmax(b_atom)/2)
     $\sigma^y$ (i) = embed(B,i,sigmay(b_atom)/2)
     $\sigma^z$ (i) = embed(B,i,sigmaz(b_atom)/2)

    # 1-D dipole-dipole interactions
    G( $r_i$ ,  $r_j$ ) = 0.5 $\gamma$ *sin(2* $\pi$ *abs( $r_i$  -  $r_j$ ))
    F( $r_i$ ,  $r_j$ ) =  $\gamma$ *cos(2* $\pi$ *abs( $r_i$  -  $r_j$ ))

    # atomic position
    d = k/a
    pos = [d*(i-1) for i=1:a]
    # pos = rand(N)
    println("Atom position: $pos Å  $\lambda$ ")

    # building the Hamiltonians
    H0 =  $\Delta a$ *sum( $\sigma^z$ (i) for i=1:a)
    Hdipole = sum(G(pos[i],pos[j])* $\sigma^+$ (i)* $\sigma^-$ (j) for i=1:a, j=1:a)
    H = H0 + Hdipole

    # decays
    # J_col = [sum( $\sigma^-$ (i) for i=1:Na)]
    J_col = [ $\sigma^-$ (i) for i=1:a]
    rates = [F(pos[i],pos[j]) for i=1:a, j=1:a]

     $\psi_0$  = tensor([spinup(b_atom) for i=1:a]...)
    tout,  $\rho_t$  = timeevolution.master(tspan,  $\psi_0$ , H, J_col; rates=rates)
    tout,  $\rho_t$ _ind = timeevolution.master(tspan, $\psi_0$ ,H0,J_col;rates=[ $\Gamma$  for i=1:a])

    group_pop = sum( $\sigma^-$ (i)* $\sigma^+$ (i) for i=1:a)

```

```

dipoles = (sum( $\sigma^+(i)$  for i=1:a))*(sum( $\sigma^-(i)$  for i=1:a))

population = real(expect(group_pop,  $\rho t$ ))
correlation = real(expect(dipoles,  $\rho t$ ))

population_ind = real(expect(group_pop,  $\rho t_{ind}$ ))
correlation_ind = real(expect(dipoles,  $\rho t_{ind}$ ))

append!(population_list, population)
append!(correlation_list, correlation)

append!(population_ind_list, population_ind)
append!(correlation_ind_list, correlation_ind)

end

```

A.1.4 Two-level atoms in a 1-D lattice in a leaky single-mode fiber

```

using PyPlot
using QuantumOptics

 $\Delta a$  = 0.0 # detuned atom frequency

 $\Gamma$  = 1.0 # spontaneous loss rate

# atom ensemble parameters
L = [0.2,0.3,0.4,0.5,0.6,0.7]# atom ensemble length
a = 3 # atom number

tspan = [0:0.01:4;]

population_list = []
correlation_list = []

population_ind_list = []
correlation_ind_list = []

for i=1:length(L)

    b_atom = SpinBasis(1/2) # single atom basis
    B = b_atom^a # collective basis

    # atom operator functions in atom basis
     $\sigma^+(i)$  = embed(B,i,sigmap(b_atom))
     $\sigma^-(i)$  = embed(B,i,sigman(b_atom))
     $\sigma^x(i)$  = embed(B,i,sigmax(b_atom)/2)
     $\sigma^y(i)$  = embed(B,i,sigmay(b_atom)/2)
     $\sigma^z(i)$  = embed(B,i,sigmaz(b_atom)/2)

    # 1-D dipole-dipole interactions

```



```

F3(r_i, r_j) = 1.5*Γ*(sin(2*π*abs(r_i - r_j))/(2*π*abs(r_i - r_j)) + cos(2*π*abs(r_i - r_j))
/(2*π*abs(r_i - r_j))^2 - sin(2*π*abs(r_i - r_j))/(2*π*abs(r_i - r_j))^3)
G3(r_i, r_j) = -3/4*Γ*(cos(2*π*abs(r_i - r_j))/(2*π*abs(r_i - r_j)) - sin(2*π*abs(r_i - r_j))
/(2*π*abs(r_i - r_j))^2 + cos(2*π*abs(r_i - r_j))/(2*π*abs(r_i - r_j))^3)
# 1-D dipole-dipole interactions in an ideal single-mode fiber
G1(r_i, r_j) = 0.5Γ*sin(2*π*abs(r_i - r_j))
F1(r_i, r_j) = Γ*cos(2*π*abs(r_i - r_j))

# atomic position
d = L[i]/a
pos = [d*(i-1) for i=1:a]
# pos = rand(N)
println("Atom position: $pos Å λ")

# building the Hamiltonians
H0 = Δa*sum(σz(i) for i=1:a)

Hdipole_dumb = sum(1*σ+(i)*σ-(j) for i=1:a, j=1:a)
Hdipole = Hdipole_dumb*0
for i=1:a
    for j=1:a
        if j!=i
            Hdipole = Hdipole + 0.5*G1(pos[i],pos[j])*σ+(i)*σ-(j) + 0.5*G3(pos[i],pos[j])*σ+(i)*σ-(j)
        else
            Hdipole = Hdipole + 0*σ+(i)*σ-(j)
        end
    end
end
end
H = H0 + Hdipole

# decays
# J_col = [sum(σ-(i) for i=1:Na)]
J_col = [σ-(i) for i=1:a]

rates_0 = zeros(0)
for i=1:a
    for j=1:a
        if j!=i
            append!(rates_0,(0.5*F1(pos[i],pos[j])+0.5*F3(pos[i],pos[j])))
        else
            append!(rates_0,1)
        end
    end
end
end

rates = reshape(rates_0,a,:)

print(rates)

ψ0 = tensor([spinup(b_atom) for i=1:a]...)
tout, ρt = timeevolution.master(tspan, ψ0, H, J_col; rates=rates)
tout, ρt_ind = timeevolution.master(tspan,ψ0,H0,J_col;rates=[Γ for i=1:a])

group_pop = sum(σ-(i)*σ+(i) for i=1:a)
dipoles = (sum(σ+(i) for i=1:a))*(sum(σ-(i) for i=1:a))

```

```

population = real(expect(group_pop,  $\rho t$ ))
correlation = real(expect(dipoles,  $\rho t$ ))

population_ind = real(expect(group_pop,  $\rho t_{ind}$ ))
correlation_ind = real(expect(dipoles,  $\rho t_{ind}$ ))

append!(population_list, population)
append!(correlation_list, correlation)

append!(population_ind_list, population_ind)
append!(correlation_ind_list, correlation_ind)

end

```

A.2 Three-level atoms in a 1-D lattice

A.2.1 Three-level atoms in a 1-D lattice in free space

```

 $\Delta a$  = 0.0 # detuned atom frequency

 $\Gamma$  = 1.0 # spontaneous loss rate

# atom ensemble parameters
L = [0.2,0.3,0.4,0.5,0.6,0.7] # atom ensemble length
a = 3 # atom number

tspan = [0:0.01:4;]

population_list = []
correlation_list = []

population_ind_list = []
correlation_ind_list = []

for i=1:length(L)

    b_atom = SpinBasis(1/2) # single atom basis
    B = b_atom^a # collective basis

    # atom operator functions in atom basis
     $\sigma^+$ (i) = embed(B,i,sigmap(b_atom))
     $\sigma^-$ (i) = embed(B,i,sigman(b_atom))
     $\sigma^x$ (i) = embed(B,i,sigmax(b_atom)/2)
     $\sigma^y$ (i) = embed(B,i,sigmay(b_atom)/2)
     $\sigma^z$ (i) = embed(B,i,sigmaz(b_atom)/2)

```

```

# 1-D dipole-dipole interactions
F(r_i, r_j) = 1.5*I*(sin(2*pi*abs(r_i - r_j))/(2*pi*abs(r_i - r_j)) + cos(2*pi*abs(r_i - r_j))
              /(2*pi*abs(r_i - r_j))^2 - sin(2*pi*abs(r_i - r_j))/(2*pi*abs(r_i - r_j))^3)
G(r_i, r_j) = -3/4*I*(cos(2*pi*abs(r_i - r_j))/(2*pi*abs(r_i - r_j)) - sin(2*pi*abs(r_i - r_j))
              /(2*pi*abs(r_i - r_j))^2 + cos(2*pi*abs(r_i - r_j))/(2*pi*abs(r_i - r_j))^3)

# atomic position
d = L[i]/a
pos = [d*(i-1) for i=1:a]
# pos = rand(N)
println("Atom position: $pos Å λ")

# building the Hamiltonians
H_0 = Δa*sum(σ^z(i) for i=1:a)

Hdipole_dumb = sum(1*σ^+(i)*σ^-(j) for i=1:a, j=1:a)
Hdipole = Hdipole_dumb*0
for i=1:a
    for j=1:a
        if j!=i
            Hdipole = Hdipole + G(pos[i],pos[j])*σ^+(i)*σ^-(j)
        else
            Hdipole = Hdipole + 0*σ^+(i)*σ^-(j)
        end
    end
end
H = H_0 + Hdipole

# decays
# J_col = [sum(σ^-(i) for i=1:N_a)]
J_col = [σ^-(i) for i=1:a]

rates_0 = zeros(0)
for i=1:a
    for j=1:a
        if j!=i
            append!(rates_0,F(pos[i],pos[j]))
        else
            append!(rates_0,1)
        end
    end
end

rates = reshape(rates_0,a,:)

print(rates)

ψ0 = tensor([spinup(b_atom) for i=1:a]...)
tout, ρt = timeevolution.master(tspan, ψ0, H, J_col; rates=rates)
tout, ρt_ind = timeevolution.master(tspan,ψ0,H_0,J_col;rates=[Γ for i=1:a])

group_pop = sum(σ^-(i)*σ^+(i) for i=1:a)
dipoles = (sum(σ^+(i) for i=1:a))*(sum(σ^-(i) for i=1:a))

population = real(expect(group_pop, ρt))
correlation = real(expect(dipoles, ρt))

```

```

population_ind = real(expect(group_pop,  $\rho$ t_ind))
correlation_ind = real(expect(dipoles,  $\rho$ t_ind))

append!(population_list, population)
append!(correlation_list, correlation)

append!(population_ind_list, population_ind)
append!(correlation_ind_list, correlation_ind)

end

```

A.2.2 Three-level atoms in a 1-D lattice in an ideal single-mode fiber

```

 $\Delta$ a = 0.0 # detuned atom frequency

 $\Gamma$  = 1.0 # spontaneous loss rate

# atom ensemble parameters
L = [0.2,0.3,0.4,0.5,0.6,0.7] # atom ensemble length
a = 3 # atom number

tspan = [0:0.01:4;]

population_list = []
correlation_list = []

population_ind_list = []
correlation_ind_list = []

for i=1:length(L)

    b_atom = SpinBasis(1/2) # single atom basis
    B = b_atom^a # collective basis

    # atom operator functions in atom basis
     $\sigma^+$ (i) = embed(B,i,sigmap(b_atom))
     $\sigma^-$ (i) = embed(B,i,sigman(b_atom))
     $\sigma^x$ (i) = embed(B,i,sigmax(b_atom)/2)
     $\sigma^y$ (i) = embed(B,i,sigmay(b_atom)/2)
     $\sigma^z$ (i) = embed(B,i,sigmaz(b_atom)/2)

    # 1-D dipole-dipole interactions
    G( $r_i$ ,  $r_j$ ) = 0.5 $\gamma_3$ *sin(2* $\pi$ *abs( $r_i$  -  $r_j$ ))
    F( $r_i$ ,  $r_j$ ) =  $\gamma_3$ *cos(2* $\pi$ *abs( $r_i$  -  $r_j$ ))
    # atomic position
    d = L[i]/a
    pos = [d*(i-1) for i=1:a]
    # pos = rand(N)

```

```

println("Atom position: $pos x λ")

# building the Hamiltonians
H0 = Δa*sum(σz(i) for i=1:a)

Hdipole_dumb = sum(1*σ+(i)*σ-(j) for i=1:a, j=1:a)
Hdipole = Hdipole_dumb*0
for i=1:a
    for j=1:a
        if j!=i
            Hdipole = Hdipole + G(pos[i],pos[j])*σ+(i)*σ-(j)
        else
            Hdipole = Hdipole + 0*σ+(i)*σ-(j)
        end
    end
end
H = H0 + Hdipole

# decays
# J_col = [sum(σ-(i) for i=1:Na)]
J_col = [σ-(i) for i=1:a]

rates_0 = zeros(0)
for i=1:a
    for j=1:a
        if j!=i
            append!(rates_0,F(pos[i],pos[j]))
        else
            append!(rates_0,1)
        end
    end
end
rates = reshape(rates_0,a,:)

print(rates)

ψ0 = tensor([spinup(b_atom) for i=1:a]...)
tout, ρt = timeevolution.master(tspan, ψ0, H, J_col; rates=rates)
tout, ρt_ind = timeevolution.master(tspan,ψ0,H0,J_col;rates=[Γ for i=1:a])

group_pop = sum(σ-(i)*σ+(i) for i=1:a)
dipoles = (sum(σ+(i) for i=1:a))*(sum(σ-(i) for i=1:a))

population = real(expect(group_pop, ρt))
correlation = real(expect(dipoles, ρt))

population_ind = real(expect(group_pop, ρt_ind))
correlation_ind = real(expect(dipoles, ρt_ind))

append!(population_list, population)
append!(correlation_list, correlation)

append!(population_ind_list, population_ind)
append!(correlation_ind_list, correlation_ind)

```

```
end
```

A.2.3 Three-level atoms in a 1-D lattice in a leaky single-mode fiber

```
Na = 3 # atom number
γ3 = 1.0
Ω = 0.5*γ3
Δ2 = 3*γ3
Δ3 = 0.0
L = [0.3,0.4,0.5,0.6,1.0] # atom ensemble length

tspan = [0:2:200;]

population_list = []
correlation_list = []

population_ind_list = []
correlation_ind_list = []

for i=1:length(L)

    b = NLevelBasis(3)
    B = b^Na

    # atom operator functions in atom basis
    σ(i, s, e) = embed(B,i,transition(b,s,e))

    # 1-D dipole-dipole interactions
    F3(ri, rj) = 1.5*γ3*(sin(2*π*abs(ri - rj))/(2*π*abs(ri - rj)) + cos(2*π*abs(ri - rj))
        / (2*π*abs(ri - rj))^2 - sin(2*π*abs(ri - rj))/(2*π*abs(ri - rj))^3)
    G3(ri, rj) = -3/4*γ3*(cos(2*π*abs(ri - rj))/(2*π*abs(ri - rj)) - sin(2*π*abs(ri - rj))
        / (2*π*abs(ri - rj))^2 + cos(2*π*abs(ri - rj))/(2*π*abs(ri - rj))^3)
    # 1-D dipole-dipole interactions in an ideal single-mode fiber
    G1(ri, rj) = 0.5*γ3*sin(2*π*abs(ri - rj))
    F1(ri, rj) = γ3*cos(2*π*abs(ri - rj))

    # atomic position
    d = L[i]/Na
    pos = [d*(i-1) for i=1:Na]
    # pos = rand(N)
    println("Atom position: $pos Å λ")

    # The Hamiltonians
    H0 = Δ2*sum(σ(i,2,2) for i=1:Na) + Δ3*sum(σ(i,3,3) for i=1:Na)
    Hpump = Ω*sum(σ(i,1,2)*exp(2.0im*π*pos[i]) + σ(i,2,1)*exp(-2.0im*π*pos[i]) for i=1:Na)

    Hdipole_dumb = sum(1*σ(i,2,3)*σ(j,3,2) for i=1:Na, j=1:Na)
    Hdipole = Hdipole_dumb*0
    for i=1:Na
```

```

    for j=1:Na
        if j!=i
            Hdipole = Hdipole + 0.5*G3(pos[i],pos[j])*σ(i,2,3)*σ(j,3,2)
                + 0.5*G1(pos[i],pos[j])*σ(i,2,3)*σ(j,3,2)
        else
            Hdipole = Hdipole + 0*σ(i,2,3)*σ(j,3,2)
        end
    end
end
H = H0 + Hpump + Hdipole

# decays
# J_col = [sum(σ-(i) for i=1:Na)]
J_col = [σ(i, 3, 2) for i=1:Na]
rates_0 = zeros(0)
for i=1:Na
    for j=1:Na
        if j!=i
            append!(rates_0,(0.5*F1(pos[i],pos[j])+0.5*F3(pos[i],pos[j])))
        else
            append!(rates_0,1)
        end
    end
end
end

rates = reshape(rates_0,Na,:)

ψ0 = tensor([nlevelstate(b, 1) for i=1:Na]...)
tout, ρt = timeevolution.master(tspan, ψ0, H, J_col; rates=rates)
tout, ρt_ind = timeevolution.master(tspan,ψ0,H0 + Hpump,J_col;rates=[γ3 for i=1:Na])

group_pop = sum(σ(i,3,3) for i=1:Na)
dipoles = sum(σ(i,1,3)*σ(j,3,1) for i=1:Na, j=1:Na)

population = real(expect(group_pop, ρt))
correlation = real(expect(dipoles, ρt))

population_ind = real(expect(group_pop, ρt_ind))
correlation_ind = real(expect(dipoles, ρt_ind))

append!(population_list, population)
append!(correlation_list, correlation)

append!(population_ind_list, population_ind)
append!(correlation_ind_list, correlation_ind)

end

```

A.3 Superradiant laser simulation

```

# atom parameters
Na = [2,3,4,5]
Δa = 0.0 # atom detuning
Γ = 1.0 # atom spontaneous loss rate
g = 5*Γ # cavity-atom coupling rate
Ω = 0*Γ # coherent pumping rate
L = 0.0 # length of the ensemble
R = 8*Γ

# cavity parameters
Nphoton = 10 # cutoff photon number
Δc = 1.0 # cavity detuning
κ = 30*Γ # cavity loss rate
n = 1 # cavity initial photon number

freq = zeros
spec_c = zeros

figure(figsize=(6, 4))

for N in Na
  # cavity operators
  bfield = FockBasis(Nphoton)
  a = destroy(bfield)
  a+ = create(bfield)

  # atom operators
  batom = SpinBasis(1//2)
  Batom = batomN
  B = bfield ⊗ Batom
  σ(i) = embed(B,i+1,sigmap(batom))
  σ+(i) = embed(B,i+1,sigmap(batom))
  a = embed(B,1,destroy(bfield))
  a+ = embed(B,1,create(bfield))
  as = destroy(bfield)
  a+s = create(bfield)

  # 1-D dipole-dipole interactions
  G(ri, rj) = 0.5Γ*sin(2*π*abs(ri - rj))
  F(ri, rj) = Γ*cos(2*π*abs(ri - rj))

  # atomic position
  d = L/N
  pos = [d*(i-1) for i=1:N]
  # pos = rand(N)
  println("Atom position: $pos Å λ")

  # Hamiltonian
  Hc = -Δc*a+s*as
  H0 = -Δa*a+*a + Δa*sum(σ+(i)*σ(i) for i=1:N)
  Hi = g*sqrt(N)*(sum((a+ * σ(i) + a * σ+(i)) for i=1:N))
  Hd = sum(G(pos[i], pos[j])*σ+(i)*σ(j) for i=1:N, j=1:N)
  #Hp = Ω*one(bfield) ⊗ sum((σ+(i) + σ(i)) for i=1:Na)
  H = H0 + Hi + Hd #+ Hp

  # loss rate matrix

```



```

rates = zeros(2*N+1, 2*N+1)
for i=2:N+1,j=2:N+1
    rates[i,j] = F(pos[i-1],pos[j-1])
end

for i=N+2:N*2+1
    rates[i,i] = R
end
rates[1,1] =  $\kappa$ 

J = [a,[ $\sigma(i)$  for i=1:N]...,[ $\sigma^+(i)$  for i=1:N]...]
Jc = [sqrt( $\kappa$ )*a_s]

# initial state of the cavity
 $\varphi_0$  = fockstate(b_field,0)  $\otimes$  tensor([spinup(b_atom) for i=1:N]...)
 $\varphi_C$  = fockstate(b_field,n)
 $\rho_0$  = dm( $\varphi_0$ )
 $\rho_C$  = dm( $\varphi_C$ )

d $\tau$  = 0.05
 $\tau_m$  = 100
 $\tau$  = [0:d $\tau$ : $\tau_m$ ;]
tout,  $\rho$  = timeevolution.master( $\tau$ ,  $\rho_0$ , H, J; rates=rates)
corr = timecorrelations.correlation( $\tau$ , $\rho$ [end],H,J,a+,a; rates=rates)
corr_em = timecorrelations.correlation( $\tau$ , $\rho_C$ ,Hc,Jc,a+s,as)
 $\omega$ ,spec = timecorrelations.correlation2spectrum( $\tau$ ,corr; normalize_spec=true)
 $\omega$ ,spec_em = timecorrelations.correlation2spectrum( $\tau$ ,corr_em; normalize_spec=true)

plot( $\omega$ , spec, label="with $N atoms")

freq =  $\omega$ 
spec_c = spec_em

end
plot(freq, spec_c, label="with no atoms", ls="dotted")
xlabel("freq.")
ylabel("spectrum")
axvline(x=0,color="k",ls="dashed")
legend()

```

Appendix B

AOM setup

B.1 AOM principle

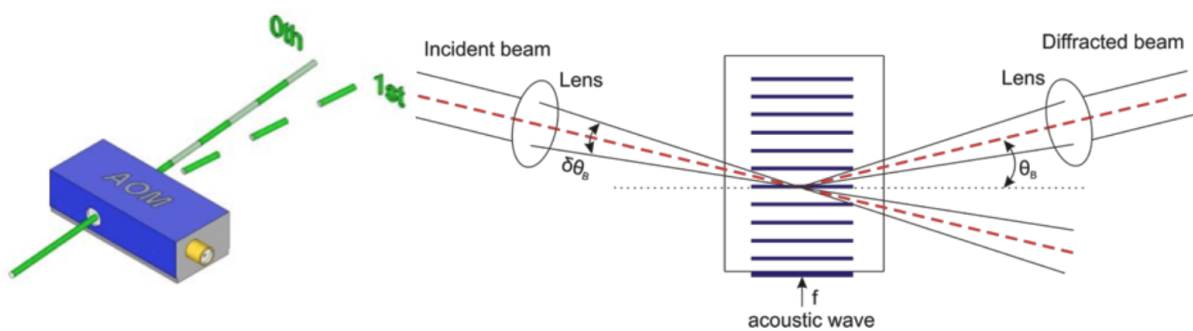


Figure B.1: AOM principle

The acousto-optic modulators (AOMs) are used as optical shutters in the experiments. They could operate at a time scale of microseconds with an efficiency over 70% if properly aligned. The principle is as follows: when a radio frequency acoustic wave is propagating across the crystal inside the AOM, it stretches and compresses the crystal so that it periodically modulates the index of refraction, which is essentially a grating capable of diffracting an incident laser beam. A diagram is shown in Fig.B.1 to demonstrate the mechanism of AOM.

As the acoustic wave travels across the material, the diffracted beam picks up a Doppler shift by the amount that equals to the frequency of the acoustic wave. It could be red-shifted or blue-shifted, depending on the angle of the incident beam with respect of the acoustic wave.

B.2 AOM driver

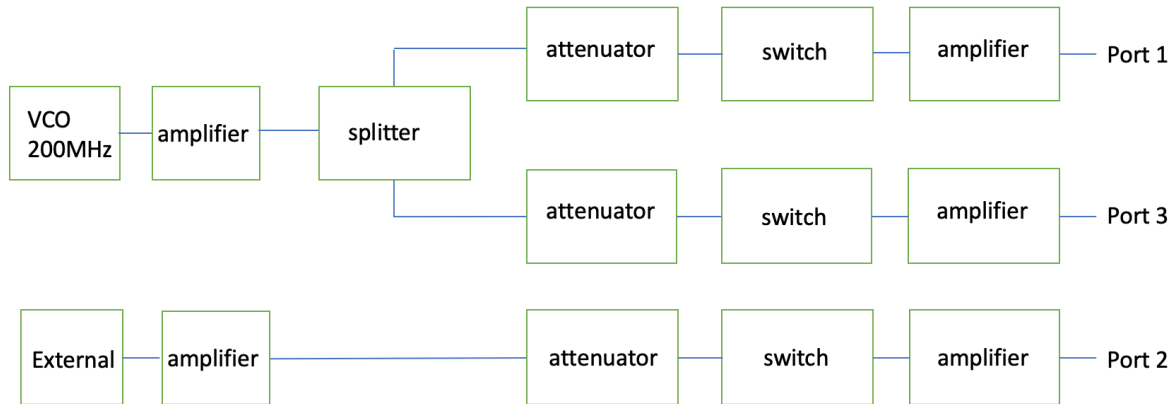


Figure B.2: AOM driver structure

The AOM driver is used for generating the RF acoustic wave for the diffraction. Fig.B.2 shows the structure of one of the AOM drivers in our lab that I modified for our 200MHz AOM. There are three output ports on the control panel: two for 200MHz output and one for external frequency signal. All the RF circuit components are from Mini Circuit with an output impedance of 50Ω . The voltage controlled oscillator (VCO, MiniCircuit ZX95-200+) has a linear tuning range from 100-200MHz. The wideband amplifier (MiniCircuit

ZX60-V62+) has a gain of $15.98dB$ at 200MHz. The power splitter/combiner (MiniCircuit ZFSC-3-1) has three input ports and one output sum port. It is bypassed in the modified external branch in the driver. The attenuator (MiniCircuit ZMAS-3) is bi-phase and capable of handling frequencies from 1 to 200MHz. Its maximum attenuation at 200MHz is around $41.7dB$. The high isolation wideband switch (MiniCircuit ZASWA-2-50DR+) could be triggered using TTL pulses, which will be generated by the NI DAQ card. It could switch at 5000MHz frequency. The amplifier (MiniCircuit ZHL-1A) can operate at the range from 2 to 500MHz with a maximum gain of $16dB$.

B.3 AOM testing

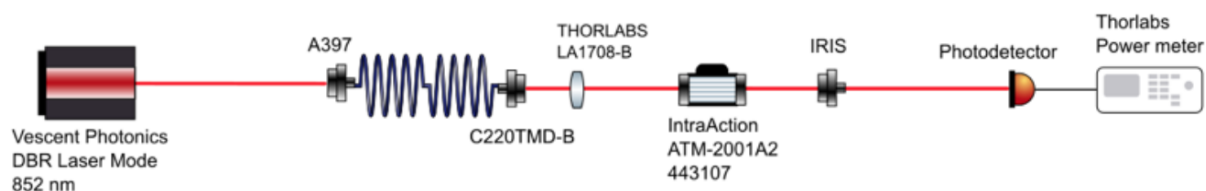


Figure B.3: AOM efficiency testing optical layout

AOM	frequency	1 st order power	Original beam power	efficiency
200 MHz	200 MHz	1.73 mW	6.31 mW	27.42%
80 MHz	80 MHz	3.45 mW	6.30 mW	54.76%
80 MHz	125 MHz	0.47 mW	6.32 mW	7.45%

Figure B.4: AOM efficiency test result

Appendix C

935 nm laser setup

The 935 nm laser was built by me with help from Taehyun and will be used as the second dipole trap laser. The optical layout is shown in Fig.C.1.

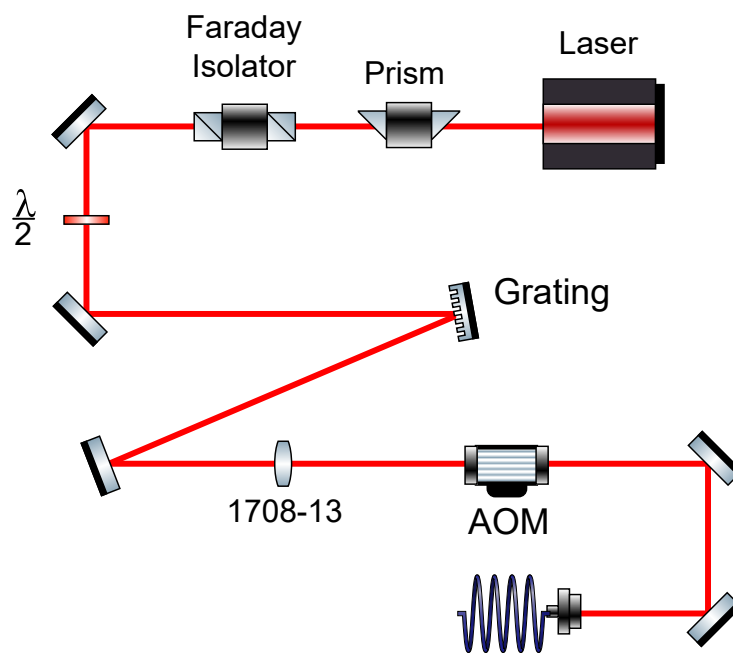


Figure C.1: 935 nm laser optical scheme

Appendix D

PID circuit design

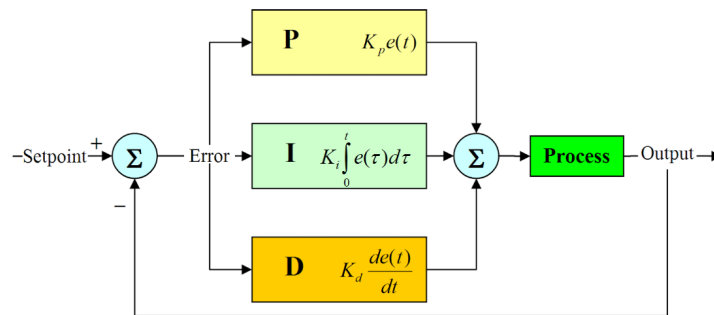


Figure D.1: PID conceptual diagram

The PID controller is used to stabilize the output so that there is no difference, or error between the setpoint and the output signal. The structure of a typical PID loop is shown in Fig.D.1. The P stands for proportional, which means that one part of the circuit gives a signal that is proportional to the size of the error signal. The I stands for integral, meaning that one part of the circuit is integrating the error signal over time until it reaches zero. This process is needed to eliminate the steady state error. However, the integral process also limits the response time of the circuit. The D stands for derivative. It outputs a signal that is proportional to the rate of change of the error, which could give a kick start of the stabilization process [1].

The PID circuit I designed for the lab is shown in Fig.D.2.

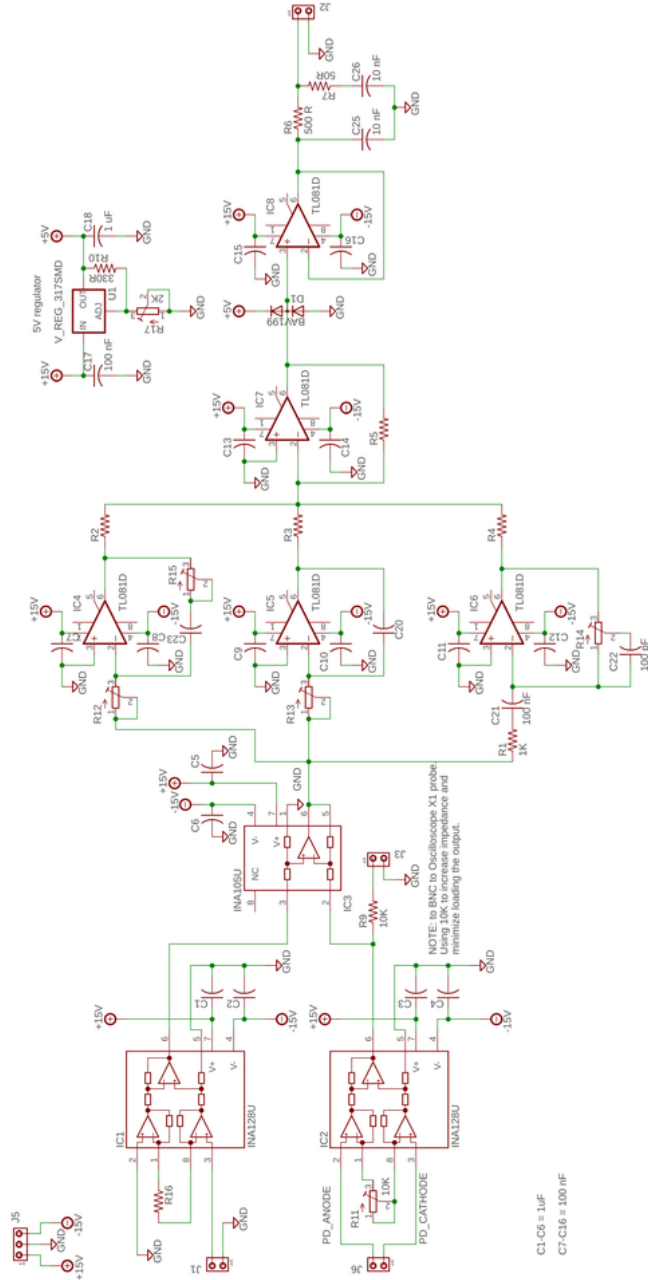


Figure D.2: PID circuit design layout